VNiVERSiDAD D SALAMANCA
CAMPUS DE EXCELENCIA INTERNACIONAL
DEPARTAMENTO DE INGENIERÍA CARTOGRÁFICA
Y DEL TERRENO

Tesis Doctoral

HERRAMIENTAS GEOMÁTICAS APLICADAS A LA OPTIMIZACIÓN DE RECURSOS ENERGÉTICOS

Programa de Doctorado:
Geotecnologías aplicadas a la Construcción, Energía e Industria.

Luis López Fernández

2017

Departamento de Ingeniería Cartográfica y del Terreno

Escuela Politécnica Superior de Ávila

Universidad de Salamanca

AUTOR:

Luis López Fernández

DIRECTORES:

Dr. Diego González Aguilera

Dra. Susana Lagüela López

2017

Herramientas geomáticas aplicadas a la optimización de recursos energéticos

Tesis doctoral presentada por
Luis López Fernández

Informe de los directores de Tesis

La Tesis Doctoral "*Herramientas geomáticas aplicadas a la optimización de recursos energéticos*", presentada por Luis López Fernández, se inserta en las líneas de investigación de procesado de imagen y visión por computador; fotogrametría UAV y láser escáner aplicadas a ingeniería y arquitectura, así como de cámaras termográficas: caracterización y calibración.

Los resultados obtenidos con todas y cada una de las metodologías presentadas dieron lugar a la publicación de uno o varios artículos científicos, en función de si la metodología sufrió mejoras durante el desarrollo de la tesis o se trataba de técnicas más consolidadas.

Todos los artículos fueron publicados en revistas internacionales de prestigio sometidas a un proceso de revisión anónimo por pares. Éstos, por orden de calidad de la publicación, se distribuyen del siguiente modo:

- Dos artículos en la revista "Remote Sensing", indexada en el Journal Citation Report y colocada en la posición 7 del ranking de un total de 29 revistas dedicadas al ámbito de Teledetección (1º cuartil).
- Un artículo publicado en la revista internacional "Indoor and Built Environment", indexada en Journal Citation Report en la posición 32, de 61 revistas dedicadas al campo de la Tecnología de Construcción y Edificación.

Dadas las condiciones presentadas, se considera que la presente tesis se ajusta, de modo óptimo, a las condiciones requeridas para la presentación de la misma por la modalidad de "compendio de publicaciones", conforme los requisitos expuestos en el Reglamento de Doctorado de la Universidad de Salamanca. La calidad de las metodologías desarrolladas, así como su validación de uso mediante su aplicación a casos de estudio reales queda irrefutablemente reconocida después de su aceptación en los ámbitos internacionales de la ingeniería civil, tecnologías de la construcción, así como de las ciencias termográficas y geodésicas.

La presente tesis presenta una propuesta pionera sobre la explotación conjunta de la termografía y la geometría asociada, así como la automatización del proceso de detección de defectos superficiales y subsuperficiales en aplicaciones energéticas, tanto de utilización (edificación) como de generación (granja fotovoltaica). Además, se

desarrollan y verifican una serie de metodologías para la consecución de los objetivos propuestos, basados en la aplicación de principios de fotogrametría, visión por computador y termografía a información procedente tanto de imagen visible como termográfica.

Los resultados de la presente tesis abren nuevas líneas de investigación de cara al estudio y extrapolación del método a más tipologías de defectos, tanto en elementos constructivos como en instalaciones generadoras de energía, de modo que se posibilite la cuantificación del efecto de dichos defectos en la energía generada y/o consumida. Se plantea la posibilidad de automatización de este proceso, de modo que se posibilite la inspección de elementos constructivos e instalaciones energéticas a personal con formación no específica en termografía o fenómenos de transferencia de calor. Asimismo, se abren líneas de investigación para la profundización en el desarrollo de plataformas móviles de inspección incorporando sensores LíDAR, con los que la generación de la geometría quede simplificada de manera importante; así como la evaluación de la aplicación de diferentes bandas espectrales a la detección de diferentes tipos de defectos.

Finalmente, dadas las características cuantitativas aportadas por estas metodologías, así como el alto nivel de detalle de la información aportada, junto con el desarrollo de aplicaciones informáticas que permiten su uso por personal no experto así como la obtención de productos que proporcionan toda la información necesaria para el desempeño del trabajo de expertos tanto en inspección de edificación como de instalaciones energéticas, estas modernas herramientas se llegarán a convertir en herramientas fundamentales para el abordaje de este tipo de inspecciones.

Dada la participación de coautores en los artículos presentados, se relaciona a continuación la aportación de cada autor, en orden cronológico de publicación:

Artículo 1: *Thermographic and mobile indoor mapping for the computation of energy losses in buildings,* publicado en la revista internacional *Indoor and Built Environment.* Cabe destacar que este artículo es resultado de un Proyecto de Investigación entre las Universidades de Salamanca y Vigo: ENERBIUS. ENE2013-48015-C3-3-R, financiado por el Ministerio de Economía y Competitividad.

Luis López Fernández: procesado de datos geométricos y termográficos, así como de cuantificación energética; interpretación de resultados.

Susana Lagüela López: formación en termografía infrarroja, diseño y adquisición de imágenes y datos geométricos, asesoramiento en la realización de tareas de procesado e interpretación, así como de explotación de resultados.

Diego González Aguilera: formación en estrategias de procesado fotogramétrico, asesoramiento en la realización de tareas de procesado, así como de explotación de resultados.

Henrique Lorenzo Cimadevila: gestión de la adquisición de datos, asesoramiento de explotación de resultados.

Artículo 2: *Large scale automatic analysis and classification of roof surfaces for the installation of solar panels using a multi-sensor aerial platform,* publicado en la revista internacional *Remote Sensing.* Destacar que los resultados preliminaries de este trabajo han sido presentados en el Congreso Internacional *3D ARCH 2015. 3D Virtual Reconstruction and Visualization of Complex Architectures,* organizado en Ávila (Febrero 2015).

Luis López Fernández: adquisición y procesado de datos geométricos y termográficos para la clasificación de tejados en función de su idoneidad para albergar paneles solares.

Susana Lagüela López: diseño de la adquisición de imagen, asesoramiento en la realización de tareas de adquisición y procesado, así como de explotación de resultados.

Inmaculada Picón Cabrera: colaboración en la búsqueda de fuentes, revisión de resultados.

Diego González Aguilera: asesoramiento en la realización de tareas de procesado, así como de explotación de resultados.

Artículo 3: *Automatic evaluation of photovoltaic power stations from high-density RGB-T 3D point clouds,* publicado en la revista internacional *Remote Sensing.*

Luis López Fernández: diseño y adquisición de datos, procesado y programación de la metodología.

Susana Lagüela López: formación en el procesado termográfico, supervisión y asesoramiento en la interpretación de resultados.

Jesús Fernández Fernández: gestión de la adquisición de datos, asesoramiento de explotación de resultados.

Diego González Aguilera: formación y tutorización de los trabajos desarrollados por el doctorando, supervisión y asesoramiento en la interpretación de resultados.

La Tesis concluye con el correspondiente apartado de Conclusiones en el que de forma precisa y concreta se especifican las principales aportaciones realizadas de tal manera que puedan ser objeto de crítica y de proyección hacia el desarrollo de futuros trabajos integrados en línea de investigación.

Lo que firman, a todos los efectos oportunos, en Ávila, a 14 de Julio de 2017.

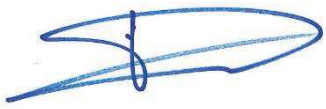

Dr. Diego González Aguilera

Dra. Susana Lagüela López

Listado de artículos publicados

La presente Tesis Doctoral está constituida por un compendio de tres artículos científicos, publicados en revistas internacionales de alto impacto. A continuación, se enumeran estas publicaciones.

1. **Thermographic and mobile indoor mapping for the computation of energy losses in buildings**

   Luis López-Fernández[1], Susana Lagüela[1,2], Diego González-Aguilera[1] and Henrique Lorenzo[2]

   [1]Department of Cartographic and Land Engineering, University of Salamanca, Hornos Caleros, Ávila 05003, Spain
   [2]Applied Geotechnologies Research Group, University of Vigo, Rúa Maxwell s/n, Campus Lagoas-Marcosende, Vigo 36310, Spain

   Indoor and Built Environment, Marzo 2016.

   DOI: 10.1177/1420326X16638912

2. **Large scale automatic analysis and classification of roof surfaces for the installation of solar panels using a multi-sensor aerial platform**

   Luis López-Fernández[1], Susana Lagüela[1,2], Inmaculada Picón[1] and Diego González-Aguilera[1]

   [1]Department of Cartographic and Land Engineering, University of Salamanca, Hornos Caleros, Ávila 05003, Spain
   [2]Applied Geotechnologies Research Group, University of Vigo, Rúa Maxwell s/n, Campus Lagoas-Marcosende, Vigo 36310, Spain

   Remote Sensing, Septiembre 2015.

   DOI: 10.3390/rs70911226

3. Automatic evaluation of photovoltaic power stations from high-density RGB-T 3D point clouds

Luis López-Fernández[1], Susana Lagüela[1,2], Jesús Fernández[1] and Diego González-Aguilera[1]

[1]Department of Cartographic and Land Engineering, University of Salamanca, Hornos Caleros, Ávila 05003, Spain
[2]Applied Geotechnologies Research Group, University of Vigo, Rúa Maxwell s/n, Campus Lagoas-Marcosende, Vigo 36310, Spain

Remote Sensing, Junio 2015.

DOI: 10.3390/rs9060631

A la memoria de D. Francisco José López García,

por hacer crecer en mí la semilla de la curiosidad.

"Rememos todos en la misma dirección."

Resumen

En la presente Tesis Doctoral se plantea el uso de herramientas geomáticas complementadas con mediciones termográficas para el desarrollo y automatización de procedimientos que permitan la optimización de la explotación de los recursos energéticos. Las técnicas geomáticas de captura de información son estrategias asentadas en el ámbito científico y ampliamente utilizadas en el ámbito metrológico de la ingeniería. Estas técnicas posibilitan la digitalización precisa de entornos complejos mediante la captura masiva de información geométrica y radiométrica no estructurada. La información geométrica resultante se representa como un conjunto de puntos tridimensionales sobre el que es posible realizar mediciones geométricas e incluso consultas de la información radiométrica asociada. No obstante, esta información geométrica y radiométrica se presenta como un conjunto de valores discretos, carentes de semántica que los caracterice o los relacione entre sí. La generación de procesos que automaticen el análisis de esta información, dotándola de semántica que enriquezca el producto, posibilitando análisis expertos en diferentes ámbitos profesionales, representa una línea de investigación muy activa en el siglo XXI. En la presente Tesis Doctoral se pretende proporcionar al experto en análisis energético de herramientas que le permitan, a partir de esta información geomática, optimizar el aprovechamiento de los recursos energéticos. Por un lado, se pretende estudiar la integración de información procedente de técnicas tan distintas como la geomática, donde el producto se representará en un espacio tridimensional, y la termografía, donde el producto se representará en un formato de imagen bidimensional o malla de temperaturas. Por otro lado, se pretende abordar el desarrollo de algoritmos de análisis que automaticen los procesos de inspección, enfocados tanto a la determinación de las posibilidades de explotación de recursos energéticos, en concreto solar, como a la optimización energética de instalaciones existentes.

Para ello se plantea un proceso de análisis de las tecnologías más adecuadas para cada estudio, atendiendo principalmente a aspectos referentes a la precisión, resolución y alcance de cada metodología. Se utilizan productos geomáticos procedentes tanto de sensores activos como

pasivos. Dentro de los primeros, planteamos el uso de sistemas LiDAR (Light Detection And Ranging) móvil (Mobile LiDAR System - MLS) para la digitalización de escenarios interiores complejos. En estos sistemas, un equipo de medición láser, complementado con sensores y estrategias software de posicionamiento, posibilita la adquisición de datos dinámica para la documentación geométrica de escenarios complejos. Dentro de los segundos, planteamos el uso de diferentes plataformas aéreas de captura, tanto tripuladas como no tripuladas. Estas plataformas son capaces de portar sistemas de percepción de bajo formato, cuyas dimensiones y peso estará limitado por las características técnicas de la plataforma de transporte. De esta forma, se embarcan sistemas de captura RGB, cuyas imágenes son incorporadas a procesos fotogramétricos y de visión computacional de última generación para la reconstrucción 3D implementados en el software GRAPHOS® (inteGRAted PHOtogrammetric Suite) (ver Apéndice B), desarrollado por los autores durante esta Tesis Doctoral. Estas plataformas de adquisición de información geomática son complementadas con la integración de sistemas de captura termográficos, cuya radiometría es transferida al producto geomático.

El producto multidimensional resultante de la integración de los productos geomáticos con radiometría termográfica alimenta los algoritmos de segmentación y clasificación de elementos de interés. Los trabajos comienzan alineados con el novedoso concepto de "Smart city", en busca de un desarrollo urbano basado en la sostenibilidad energética y el aprovechamiento de fuentes de energía renovables. Dentro de este marco podemos identificar tres puntos clave para avanzar hacia el concepto de comunidad autosuficiente energéticamente:

- Optimización de la eficiencia energética de las instalaciones consumidoras.
- Identificación del recurso de energía renovable disponible.
- Optimización de productividad energética de las instalaciones productoras.

Siguiendo estas tres premisas, analizadas en función de las capacidades técnicas del equipamiento y las metodologías a nuestra disposición, la presente Tesis Doctoral trata de dar una respuesta integral a la

implantación y optimización de recursos energéticos, con especial énfasis al recurso solar.

Inicialmente se presenta una metodología para la inspección de envolventes de edificaciones capaz de detectar y evaluar el efecto de patologías que comprometan la eficiencia energética de la construcción como fallos en aislamiento, humedades o filtraciones de aire. A mayores, la metodología propuesta dota al inspector de una herramienta capaz de realizar una simulación del impacto energético de acciones de rehabilitación. La segunda premisa se aborda con el desarrollo de una metodología de captura y procesamiento de datos para la identificación automática y a gran escala de coberturas urbanas candidatas a albergar instalaciones solares. La metodología propuesta presenta una captura de datos utilizando una plataforma aérea tripulada, dotada de sensores pasivos de imagen RGB y termográficos. El algoritmo de procesamiento de la información, implementado en el software SOLEMAP® (SOLar Energy MAPping) desarrollado durante esta Tesis Doctoral para tal fin (ver Apéndice B), consigue la detección y clasificación automática de superficies candidatas a albergar paneles solares en función de su área, inclinación, orientación y existencia de obstáculos. Por último, la tercera premisa se aborda dando solución a la optimización de plantas fotovoltaicas mediante la detección automática de patologías que limiten su productividad. De este modo, se presenta una metodología de captura de datos utilizando una plataforma aérea no tripulada dotada de nuevo de sensores pasivos RGB y termográficos. El algoritmo de procesamiento de la información, implementado en el software SOLFIN® (SOLar Farm INspection) desarrollado durante esta Tesis Doctoral (ver Apéndice B), consigue la detección y clasificación automática de patologías en superficies fotovoltaicas según su gravedad, en función de sus características geométricas y análisis estadísticos de la información termográfica transferida al producto geomático.

Abstract

This research work proposes the use of geomatic tools complemented with thermographic surveys for the development of automatic processes applied to the optimization of energy resources. These geomatic surveying techniques are currently being used both in scientific and engineering metrological field. They make possible the accurate scanning of complex scenarios through the massive capture of unstructured geometric and radiometric information. The information acquired is represented as a set of three-dimensional points where the performance of geometric measurements and queries of associated radiometric information is possible. However, this geometric information is presented as discrete values, without the semantics that characterizes or relates them. The development of processes that automate the analysis of this information represents very active research lines in the 21st century. The main purpose of these developments is to generate semantic information that enriches the product, enabling expert analysis in different professional fields. This Doctoral Thesis aims at providing novel techniques that are useful to carry out inspections for optimizing the use of available energy resources. On one hand, we intend to study the integration of information from such different techniques such as geomatics, where the product is represented in the three-dimensional space, and thermography, where the product is represented in a bidimensional image format or temperatures grid. On the other hand, the development of analytical algorithms that automate inspection processes is performed, focused both on the detection of possible untapped energy resources and on the energy optimization of existing facilities.

To this end, a process of analysis of the most suitable technologies for each study is carried out focusing on aspects related to the accuracy, resolution and scope of each methodology. Geomatic products from both active and passive sensors are used. Within the first, we propose the use of mobile LiDAR (MLS) systems for the digitization of complex interior scenarios. In these systems, a laser measuring device, complemented with navigation sensors and software positioning strategies, enables the dynamic acquisition of data for the geometric documentation of complex scenarios.

Within seconds, we propose the use of different aerial acquisition platforms, both manned and unmanned. These platforms are able to carry low format perception systems, which dimensions and weight will be limited by the technical characteristics of the transport platform. In this way, RGB acquisition systems are embarked, which images will be incorporated into the latest generation photogrammetric and computer vision processes for 3D reconstruction implemented in the GRAPHOS® software (see Appendix B), developed by the authors during this work. These platforms, equipped with geomatic acquisition systems, will be complemented by the integration of thermographic systems, which acquired radiometry that is transferred to the geomatic product.

The multidimensional product resulting from the integration of the geomatic products with thermographic radiometry feeds the segmentation and classification algorithms for elements of interest. The works are aligned with the new concept of "Smart city", in the line of an urban development based on energy sustainability and the use of renewable energy sources. Within this framework we can identify three key points to move towards an energy self-sufficient community:

- Energy efficiency optimization of consumer installations.
- Identification of available renewable energy resource.
- Energy productivity optimization of production facilities.

Following these three premises, analyzed in terms of the technical capabilities of the geomatic equipment and methodologies available, this Doctoral Thesis tries to give a comprehensive response to the implementation and optimization of energy resources, with special emphasis on the solar resource.

Initially, a methodology for the inspection of building envelopes is presented. The methodology is capable of detecting and evaluating the effect of pathologies that compromise the energy efficiency of the construction, such as insulation defects, moisture or air leaks. As a complement, the proposed methodology provides the inspector with a tool capable of performing an energy simulation of the energy impact of rehabilitation actions. The second premise is addressed through a methodology for large-scale data acquisition and processing towards the automatic identification of urban coverage candidates for photovoltaic

installations. The proposed methodology presents a data survey using a manned aerial platform equipped with RGB and thermographic sensors. The developed processing algorithm, implemented in the SOLEMAP® software developed during this work for this purpose (see Appendix B), performs the automatic detection and classification of surfaces that are candidate to place solar panels according to their area, inclination, orientation and existence of obstacles. Finally, the third premise is addressed by providing a solution to the optimization of photovoltaic facilities by means of automatic detection of pathologies that reduce their productivity. In this way, a methodology for data surveying is presented using an unmanned aerial platform equipped again with RGB and thermographic sensors. The processing algorithm developed, which is implemented in SOLFIN® software developed during this work for this purpose (see Appendix B), achieves automatic detection and classification of pathologies on photovoltaic surfaces according to their severity, which is calculated based on geometric characteristics and statistical analysis of the thermographic information transferred to the geomatic product.

Agradecimientos

Este documento supone el alcance de un hito. Un objetivo fijado hace ya cinco años pero iniciado mucho tiempo atrás. De esta forma, no puedo evitar acordarme de todos los compañeros y personal docente que me han acompañado y ayudado hasta llegar a este punto. Han sido numerosas las personas que han sentado las bases de este camino y me han dotado de capacidades para recorrerlo de forma satisfactoria, a todos ellos quiero expresarles todo mi agradecimiento.

Para empezar, quiero agradecer encarecidamente a los directores de la presente Tesis Doctoral, el Doctor Diego González-Aguilera y la Doctora Susana Lagüela López, la confianza depositada en mí para alcanzar los objetivos fijados en la línea de investigación, su continuo apoyo y soporte. Su confianza ha supuesto para mí un giro radical tanto en lo personal como en lo profesional y, por lo tanto, quiero hacerles partícipes no solo de este éxito sino de todos los que están por venir. Por suerte, nuestra relación en este periodo ha superado la barrera de lo docente, convirtiéndoos en compañeros ejemplares en lo que a esfuerzo y dedicación se refiere.

Agradecer también a mis compañeros de trabajo y amigos del grupo de investigación TIDOP de la Universidad de Salamanca la oportunidad de trabajar con ellos y de compartir conocimientos, experiencias y ocio. Vosotros habéis sido mi familia durante mi estancia en Ávila, haciendo que me sintiese como en casa desde el primer momento.

Finalmente, ya en un ámbito más personal, quiero dirigir mis más sinceros agradecimientos a mis padres, Luis y Mª Antonia, por haberme proporcionado una formación completa y extensa, sin ningún condicionante y acompañada de independencia en la toma de decisiones que hoy se representa en una autonomía que me caracteriza y de la que me siento muy orgulloso. Agradecer del mismo modo a mis tíos, Pepe y Pilar, por su intenso cariño y sus certeros y sabios consejos. Al resto de mi familia, que por extensión no podré reflejar en este documento, por el apoyo y afecto incondicional pese al escaso tiempo que podemos compartir. Este camino solo supondría un fracaso si no se materializase en un orgullo para todos vosotros. Sé que no es así.

Del mismo modo quiero agradecer a Rocío su apoyo incondicional durante todo este tiempo. Tú mejor que nadie conoces el duro camino recorrido hasta aquí. Las distancias, las esperas, el tiempo escaso, las vacaciones pegado al ordenador…

Este trabajo es vuestro.

Gracias a todos.

Contenido

Capitulo I

Introducción

1. Introducción

El análisis de eficiencia energética es una técnica que persigue no solo la optimización de los recursos energéticos disponibles, sino la reducción de emisiones contaminantes a la atmosfera, en un intento de avanzar hacia un estadio ideal de consumo energético responsable, sostenible y respetuoso con el medio ambiente. En marzo del 2007, los líderes de los países miembros de la Unión Europea acordaron, a través del "Paquete Europeo de Energía y Cambio Climático" [1], un acuerdo que establece objetivos concretos a alcanzar en el año 2020 en materia de energía renovable, eficiencia energética y reducción de emisiones de gases de efecto invernadero. En concreto, las emisiones del conjunto de la Unión Europea deben reducirse en un 20% respecto a los niveles del año 1990. Con el fin de dotar de continuidad a este acuerdo, en octubre del 2014 fue aprobado el "Marco de Políticas de Energía y Cambio Climático 2021-2030" ("Marco 2030") [2], estableciendo un objetivo de reducción de al menos un 40% en las emisiones de gases de efecto invernadero; un 27% de energía consumida procedente de recursos renovables y una mejora del 27% en la eficiencia energética. Más recientemente, en el año 2016, se formaliza el Acuerdo de París, en el que los países pertenecientes a las Naciones Unidas se comprometieron a reducir el aumento de la temperatura global a 1.5ºC, reforzando el límite de aumento de 2ºC anterior [3]. El avance hacia un consumo energético eficiente y respetuoso con el medio ambiente, que posibilite además esta desaceleración del calentamiento global, implica afrontar un proceso de descarbonización, que reduzca de manera radical la cantidad de combustibles fósiles, en cualquiera de sus formatos, empleados como fuente de energía [4]. Estos recursos energéticos, a pesar de ser limitados y los principales causantes de la contaminación, el calentamiento global o el agujero de la capa de ozono, representan los fuentes energéticas más utilizadas, siendo el origen de un porcentaje superior al 81% de la energía consumida a nivel global en lo que va de año 2017 [5]. De un modo similar, la energía de origen nuclear, pese a no suponer la emisión directa de sustancias contaminantes durante los procesos de creación y ser poseedora de una muy elevada productividad energética, no supone un avance hacia un modelo energético responsable y respetuoso con el medio ambiente [6]. El impacto negativo

de esta fuente de energía en nuestro ecosistema viene derivado de su inestabilidad, el gran espacio necesario para la instalación de las centrales de producción y el almacenamiento de los residuos generados, la peligrosidad de estos residuos o las catastróficas consecuencias que supondrían cualquier incidencia en las instalaciones de producción energética [7–9] o almacenamiento de combustibles.

De este modo, la principal alternativa energética al uso de carbón y otros combustibles fósiles se encuentra en la potenciación de las energías renovables [10]. Las fuentes renovables, además de contribuir al descenso de las emisiones de gases de efecto invernadero, contribuyen al establecimiento de redes energéticas menos centralizadas y más distribuidas, en las que la producción energética se encuentra más próxima al consumidor, de modo que se reducen el coste y las pérdidas por el transporte. El nivel de integración de las fuentes renovables en la red eléctrica presenta diferencias en Europa, con países que planifican importantes reestructuraciones como Alemania [11] y otros cuyo consumo energético renovable implica la práctica totalidad de su demanda como Noruega e Irlanda [12]. De este modo, maximizar el aprovechamiento de las fuentes de energía renovables a nuestra disposición, que a día de hoy solo representa menos del 4% de la energía consumida a nivel global [13], parece ser la única alternativa que garantiza una producción y consumo energético sostenible.

1.1. Sistemas de cartografiado móviles

Tradicionalmente, los sistemas de cartografiado móviles estaban comandados por una unidad de control, capaz de integrar datos procedentes de equipos de percepción de diferente índole con la información de posicionamiento, procedente de un sistema de navegación inercial (Inertial Measurement Unit – IMU) en combinación con indicadores de medición de distancia (Distance Measurement Idicators - DMI) y un sistema de navegación global por satélite (Global Navigaton Satellite System - GNSS). La tecnología inicial limitaba la aplicabilidad de estos equipos al cartografiado de escenarios exteriores dada la gran dependencia del sistema de navegación global para su posicionamiento.

En la actualidad, los sistemas de cartografiado móviles incluyen sistemas de medición LiDAR (Light Detection and Ranging) como unidad principal de cartografiado, complementados por otros sistemas de percepción que adapten el equipo a los requisitos técnicos del trabajo para el que se diseña la plataforma de captura. Estos equipos de percepción complementarios abarcan desde sensores de imagen pasivos, capaces de capturar información radiométrica en diferentes bandas del espectro electromagnético; sensores pasivos de captación de intensidad lumínica como luxómetros o sensores activos como el georradar, entre muchos otros. Los sistemas de medición LiDAR se consideran sensores activos al estar dotados de un sensor capaz de medir la distancia recorrida por un pulso láser, emitido por el propio equipo, hasta incidir con un objeto o superficie de estudio. El sistema LiDAR es complementado con un espejo que permite direccionar el pulso láser, convirtiendo el equipo en un sistema de medición bidimensional capaz de registrar medidas automatizadas de ángulos y distancias. La combinación de la dupla formada por una medición síncrona de ángulo y distancia del sistema LiDAR, complementada por la integración del sistema de posicionamiento GNSS-IMU-DMI, permite la transformación de las coordenadas polares (ángulo-α y distancia-d) procedentes del sistema de referencia local del sensor LiDAR, a coordenadas cartesianas 3D (X,Y,Z) representadas en el sistema de referencia global [14].

En un intento de emular estos sistemas de cartografiado móvil en escenarios interiores, algunos autores [15] han avanzado en el desarrollo de sistemas de cartografiado de interiores mediante la integración de un sistema complejo de sensores pasivos RGB. Pese a que estos sensores pasivos destacan por su bajo coste, se requiere de un gran número de sensores que den cobertura a la escena en su totalidad al paso de la plataforma de transporte. A mayores, es necesario considerar el alcance de la metodología propuesta dada la dependencia de complejos algoritmos de procesamiento fotogramétrico [16] que deben hacer frente a factores externos como la iluminación o la calidad/homogeneidad textural del entorno a cartografiar y la posible debilidad en el establecimiento de una red fotogramétrica (ubicación espacial y angular de las cámaras). Otros autores, en cambio, han trabajado en la implementación de sistemas híbridos integrando sensores activos y pasivos [17], tratando de conciliar

las ventajas de ambos con la contrapartida de tener que afrontar complejos procesos de registro.

En la actualidad, la evolución de los sistemas de posicionamiento, principalmente en cuanto a los sistemas IMU y DMI se refiere, tanto a nivel hardware como a nivel software mediante la implementación de filtros predictivos para la modelización y eliminación del ruido pseudoaleatorio intrínseco a este tipo de dispositivos [18], junto con las estrategias de posicionamiento y mapeado simultaneo a partir de datos LíDAR (Simultaneous Location And Mapping - SLAM) [19], están posibilitando la adaptación exitosa de estos sistemas de cartografiado móvil para la medición de escenarios interiores. Estas nuevas tecnologías permiten prescindir de sistemas de posicionamiento global para el cálculo de la trayectoria de la plataforma, sin condicionar la precisión o calidad del producto final. Este nuevo alcance de la tecnología supone una solución óptima y eficiente para el cartografiado de escenarios interiores complejos, donde los sistemas de escaneado LiDAR estáticos no aportan la solución idónea al requerir diversos estacionamientos y una etapa crítica de registro a posteriori en gabinete.

1.2. Fotogrametría aérea

En los últimos años, la hibridación de la fotogrametría digital con las más novedosas técnicas de visión computacional, complementada por los grandes avances en la capacidad de cómputo de los equipos informáticos de última generación, representa una de las técnicas más eficientes y de menor coste para la obtención de datos espaciales de alta resolución y precisión. Este flujo de trabajo, conocido como "Structure from Motion" (SfM), garantiza un alto nivel de automatización, resultados de calidad, gran eficiencia y facilidad de uso incluso para operarios no especializados. Este flujo de trabajo es derivado de los últimos avances en cuanto a técnicas de pre-procesamiento de imágenes [20,21]; detección y emparejamiento automático de puntos homólogos [22,23]; autocalibración, orientación y ajuste de bloques fotogramétricos [24,25] y la densificación de nubes de puntos de alta precisión [26].

Estas técnicas, complementadas con los grandes avances de la ingeniería aeroespacial en cuanto a capacidad de carga, estabilidad y autonomía de las plataformas aéreas de transporte, tanto tripuladas como no tripuladas, así como el aumento de la disponibilidad de estas plataformas dada la gran reducción de su coste, han superado la barrera de lo científico, incorporándose satisfactoriamente tanto en procesos de producción cartográfica como en otros ámbitos de la ingeniería. De esta forma, la metodología combinada de técnicas fotogramétricas y de visión computacional, aplicadas a imágenes procedentes de cámaras embarcadas en plataformas aéreas de bajo coste, permite la reconstrucción 3D de escenarios de gran escala de forma automática, sencilla y rentable, sin renunciar a la calidad y precisión geométrica de los resultados, obteniendo un producto de gran valor para el análisis dimensional de la escena.

1.3. Técnicas termográficas

La termografía es una técnica multidisciplinar aplicada a innumerables campos de la ciencia. Esta técnica se caracteriza por el uso de sensores pasivos formadores de imagen, capaces de cuantificar valores térmicos en función de un proceso de captación de radiación en la banda espectral del infrarrojo térmico (longitud de onda de 8 – 14 μm). Se trata de una técnica que proporciona resultados de una forma no intrusiva o destructiva, sin contacto directo con el objeto de estudio, permitiendo la evaluación "in-situ" dada la posibilidad de portabilidad de los equipos de medición.

La técnica termográfica se puede clasificar [27] según el objetivo de la metodología aplicada. De esta forma, denominaremos *termografía cualitativa* cuando se pretenda realizar un análisis de los gradientes o las diferencias relativas de la intensidad de la radiación infrarroja capturada por el sensor y representada en la imagen térmica. La técnica suele ser aplicada a escenarios complejos, compuestos por objetos de diferente naturaleza, principalmente con fines de detección e identificación de elementos de interés. En este caso, no suele ser crucial una modelización precisa y la consecuente corrección de los agentes externos, físicos o ambientales, influyentes en la captura termográfica. De hecho, la técnica se beneficia de las diferencias en las propiedades físicas de los elementos

presentes en la escena dado que la intensidad de la radiación en el espectro infrarrojo captada por el sensor, para dos objetos de idéntica temperatura, será diferente si sus emisividades no coinciden. Una aplicación capaz de clarificar esta técnica, en contraposición con la técnica ilustrada a continuación, es la detección de personas, aplicable a cualquier ser vivo de sangre caliente, independientemente de las condiciones lumínicas e la escena [28]. Por otro lado, denominaremos *termografía cuantitativa* cuando el objetivo persigue el análisis o cuantificación de las propiedades termofísicas de un objeto de estudio, un análisis de precisión de la temperatura, enfriamiento, calentamiento o respuesta ante una secuencia térmica. Las metodologías con este enfoque presentan una dependencia crítica de la correcta modelización de todos los factores externos que condicionan las observaciones termográficas, siendo crucial una correcta modelización de los factores físicos y ambientales influyentes en el proceso. Un ejemplo de esta tecnología, aplicada al mismo objeto de estudio presentado para la termografía cualitativa para una mejor comprensión de las diferencias, es la medición de la temperatura corporal de seres humanos [29] para el control epidemiológico en aeropuertos [30]. Para este objetivo resulta crucial la medición del valor térmico con precisión, siendo imprescindible el ajuste de la medición en base a la emisividad de la piel humana y las condiciones ambientales del escenario de estudio.

Por otro lado, la técnica termográfica puede ser clasificada también según las características de la metodología aplicada, con arreglo a la existencia o no de una fuente de estimulación externa actuante sobre el objeto de estudio. De este modo, podemos identificar como *termografía pasiva* aquellos estudios en los que la captura termográfica es utilizada como un proceso de monitorización directa de un elemento de estudio sin actuar sobre el estado térmico del mismo o del ecosistema en el que habitualmente se encuentra. Esta técnica es ampliamente utilizada, pudiendo encontrar ejemplos significativos de su aplicación como el análisis de la envolvente térmica de una construcción [31] o la detección y diagnóstico de patologías en instalaciones eléctricas [32]. También se considera *termografía pasiva* cuando se recurre al calentamiento ocasionado por la radiación solar sobre el cuerpo, de manera natural, dado que no involucra el uso de fuentes artificiales ni el control de la aplicación del pulso térmico. Por el contrario, podemos identificar la *termografía*

activa como un método de ensayo no destructivo mediante la monitorización termográfica de un elemento de estudio sobre el que se aplica una estimulación externa, ya sea térmica, eléctrica, ultrasónica o vibro-mecánica, con el fin de estimular y provocar una reacción en los átomos del material. Esta técnica, utilizada de forma habitual en numerosos ámbitos de la ingeniería e industria, es aplicada principalmente a la detección de imperfecciones o defectos superficiales, subsuperficiales o internos. Un ejemplo de la aplicación de esta metodología es la detección y evaluación de defectos e imperfecciones en uniones soldadas [33].

De este modo, la termografía cualitativa pasiva representa un método no intrusivo de medición remota, útil no solo para la detección de elementos de interés en una escena, sino capaz de detectar anomalías térmicas producidas por agentes externos como humedades, flujos de aire o tensiones eléctricas. Si bien la técnica termográfica descrita, tal y como se concretará en los siguientes capítulos, se viene aplicando al aprovechamiento de recursos energéticos de diferentes formas, su uso se limita a labores de inspección supervisadas por operarios expertos, con una gran componente de subjetividad y carente de la componente geométrica necesaria para un análisis dimensional de precisión.

1.4. Estructura de la Tesis Doctoral

Esta Tesis Doctoral es presentada de acuerdo a la regulación vigente para programas de doctorado de la Universidad de Salamanca, siendo objeto de transferencia científica, a través de tres artículos publicados en revistas científicas internacionales de alto impacto, y tecnológica, representada por 4 registros de propiedad intelectual del software desarrollado para tal fin. Su estructura consiste en un total de 6 capítulos acordes al desarrollo de las labores de investigación llevadas a cabo para la materialización de los objetivos fijados en la Tesis Doctoral.

Se han incluido un total de dos apéndices al final del documento, con el fin de complementar el documento con información y documentación de interés.

Capítulo I. Introducción: Proporciona una visión general de marco en el que se desarrolla la presente Tesis Doctoral, complementada con una presentación de las principales tecnologías utilizadas durante su desarrollo y finalizando, en esta sección, con una descripción de la estructura del presente documento.

Capítulo II. Hipótesis de trabajo y objetivos: Describe de forma detallada los planteamientos iniciales y objetivos que motivaron en su inicio el desarrollo de esta línea de investigación.

Capítulo III. Automatización de procesos de evaluación energética para la optimización de recursos energéticos: Recoge el contenido de la primera publicación científica, titulada "*Thermographic and mobile indoor mapping for the computation of energy losses in buildings*", presentando un proceso automatizado de evaluación de la eficiencia energética de construcciones, capaz de cuantificar el efecto de patologías como humedades o puentes térmicos que comprometan la eficiencia energética de las envolventes.

Capítulo IV. Automatización de procesos de evaluación de cobertura urbana para la instalación de paneles solares: Recoge el contenido de la segunda publicación científica, titulada "*Large scale automatic analysis and classification of roof surfaces for the installation of solar panels using a multi-sensor aerial platform*", presentando un proceso automatizado para la detección de superficies de cobertura urbana con las características adecuadas para alojar paneles solares, así como una clasificación de las mismas de acuerdo a su potencial en función de la radiación solar incidente.

Capítulo V. Automatización de procesos de inspección en plantas fotovoltaicas: Recoge el contenido de la tercera publicación científica, titulada "*Automatic evaluation of photovoltaic power stations from high-density RGB-T 3D point clouds*", presentando un proceso automatizado de inspección de superficies fotovoltaicas para la detección y cuantificación de patologías que afecten la productividad energética de la instalación

Capítulo VI. Conclusiones y perspectivas futuras: Como capítulo final, se proporciona una discusión técnica basada en las conclusiones y resultados alcanzados durante el desarrollo de la presente Tesis Doctoral,

complementada con las líneas de trabajo derivadas o abiertas a partir de la misma y que podrán dar continuidad a este trabajo.

Apéndice A. Indexación y factor de impacto de las publicaciones: Proporciona información referente a parámetros de interés sobre las revistas científicas donde han sido realizadas las publicaciones.

Apéndice B. Software: Recoge información y documentación relacionada con los registros de propiedad intelectual referentes al software desarrollado durante este trabajo.

Capitulo II

Hipótesis de trabajo y objetivos

2. Hipótesis de trabajo y objetivos

En el apartado anterior se ha mostrado una visión general de las principales técnicas geomáticas aplicadas a la reconstrucción de escenarios complejos de gran escala, junto con una introducción a las diferentes técnicas y metodologías de captura termográfica. El contexto de aplicación de las metodologías y herramientas desarrolladas en la presente Tesis Doctoral es el **aprovechamiento de los recursos energéticos renovables** a nuestra disposición, avanzando hacia el **modelo comunitario de eficiencia energética sostenible**. En la etapa inicial, donde se ha evaluado la viabilidad de la línea de investigación, se han recogido una serie de hipótesis de trabajo y objetivos, que marcarían la hoja de ruta a seguir de esta Tesis Doctoral.

2.1. Hipótesis de trabajo

La base de la línea de investigación es el desarrollo de estrategias que permitan la automatización de procesos de inspección relacionados con el aprovechamiento de recursos energéticos. Las nubes de puntos 3D de alta precisión, derivadas de las herramientas geomáticas descritas en apartados anteriores, son utilizadas en diferentes campos como soporte para la representación tridimensional de los elementos capturados por sensores formadores de imágenes bidimensionales, mediante la resolución de la transformación proyectiva que los relaciona. De esta forma, la información contenida en cada pixel del producto bidimensional es proyectada y asociada a la nube de puntos 3D. Sin embargo, la automatización de procesos que aporten semántica a estos productos híbridos resulta un campo de investigación muy activo en la actualidad, no habiéndose mostrado avances significativos en su aplicabilidad al aprovechamiento de recursos energéticos. La presente Tesis Doctoral se centra en la definición de la metodología adecuada para la generación del producto termográfico 3D, según diferentes escenarios y objetivos, y el desarrollo de procesos para la generación de un producto dotado de semántica que aporte valor añadido a los protocolos de inspección.

Para dar respuesta a esta investigación, se plantean las siguientes **hipótesis**:

- Las herramientas geomáticas modernas presentan alternativas potentes para la digitalización y modelado tridimensional de escenarios complejos, de una forma rápida y eficaz y con unos costes contenidos, posibilitando su implementación en el ámbito profesional.
- La capacidad de cómputo de los equipos informáticos de última generación permite el desarrollo de técnicas de procesamiento automático de esta información espacial masiva no estructurada, derivada del uso de herramientas geomáticas.
- Es posible diseñar técnicas de detección de elementos de interés, capaces de identificar y extraer automáticamente de la nube de puntos tanto primitivas básicas como entidades complejas.
- Es posible identificar comportamientos térmicos anómalos sobre una superficie teóricamente homogénea mediante el uso de sensores termográficos.
- Es posible identificar diferentes materiales utilizando sensores termográficos, incluso si estos se encuentran a la misma temperatura, si sus propiedades físicas superficiales, en especial sus emisividades, no son coincidentes.
- Es posible cuantificar la irradiación solar recibida por un objeto a partir de unas características geométricas básicas del mismo y de su entorno.

2.2. Objetivos

Enmarcados en el contexto presentado en los apartados anteriores, se plantean los objetivos de la línea de investigación materializada en esta Tesis Doctoral, clasificados en un objetivo general y varios objetivos específicos.

El **objetivo general** de la línea de investigación es el desarrollo y puesta en ejecución de procesos automáticos que aporten valor añadido a los

procesos de inspección relacionados con el aprovechamiento de recursos energéticos.

Los **objetivos específicos** de la línea de investigación son:

- Identificar las herramientas geomáticas adecuadas para la digitalización de diferentes escenarios de interés.
- Optimizar los recursos energéticos empleados en labores de climatización de espacios cerrados mediante nuevas metodologías de auditoría energética.
- Implementar una metodología de detección de patologías constructivas asociadas a presencia de fluidos (agua y aire) en los elementos constructivos.
- Cuantificar el efecto energético de la presencia de las diferentes patologías térmicas detectadas, tanto como incremento del consumo como reducción de la generación energética.
- Desarrollar estrategias de extracción y matching de características que seas robustas a cambios en geometría y radiometría.
- Desarrollar una estrategia de identificación automática y caracterización geométrica de tejados en nubes de puntos 3D de escenarios urbanos.
- Diseñar e implementar una metodología para la detección de obstáculos en tejados que impidan la instalación de paneles solares.
- Desarrollar una metodología que permita clasificar las superficies de los tejados en función de la irradiación solar recibida y estimar así la productividad energética de paneles solares.
- Crear una metodología de inspección automática de plantas fotovoltaicas que permita un mantenimiento activo de las instalaciones y la consecuente optimización de la producción energética.
- Diseñar estrategias de automatización de la detección y clasificación de patologías térmicas en superficies receptoras de radiación solar.

De esta forma, la línea de investigación se presenta completamente alineada con dos de los retos establecidos en el programa “Horizon 2020”, más concretamente:

- Reto 3: "Energía segura, eficiente y limpia" [34] concibiendo la sostenibilidad energética y medioambiental como un "elemento de competitividad y de calidad que debe ser considerado en todas las etapas del proceso de edificación, así como de la innovación para la eficiencia y el mejor aprovechamiento de los recursos energéticos".
- Reto 5: "Reto en acción sobre cambio climático y eficiencia en la utilización de recursos y materias primas" [35].

Capítulo III

Automatización de procesos de evaluación energética para la optimización de recursos energéticos

3. Thermographic and mobile indoor mapping for the computation of energy losses in buildings

Este capítulo contiene el artículo "*Thermographic and mobile indoor mapping for the computation of energy losses in buildings RGB-T 3D point clouds*" publicado en la revista de alto impacto *Indoor and Built Environment* en Marzo de 2016.

3.1. Resumen

La publicación científica recogida en este capítulo representa el primer hito establecido en la hoja de ruta de la línea de investigación. El objetivo principal es el desarrollo de una metodología que permita realizar una evaluación del estado real de la envolvente de una construcción en cuanto a consumo energético, incluyendo en el cálculo no solo el estado idealizado de la envolvente reflejado en la documentación del proyecto, sino complementado con la detección y medición de patologías que supongan un incremento en el consumo energético de la construcción. En particular en este caso, el trabajo se centra en la detección de variaciones en la envolvente, debidas a fallos en el aislamiento y presencia de agua (humedades). La propuesta proporciona además una herramienta válida para la simulación de proyectos de rehabilitación, permitiendo calcular las reducciones resultantes en cuanto al consumo energético que se obtendrían con la aplicación de diferentes medidas. En particular, el enfoque desarrollado tiene cuatro componentes secuenciales: (1) definición de las técnicas geomáticas más adecuadas para la digitalización de escenarios interiores complejos; (2) generación de ortotermogramas como producto geomático métrico; (3) detección y segmentación de elementos constructivos de interés y patologías que afecten al consumo energético en labores de climatización y (4) parametrización de las propiedades termofísicas y geométricas de los elementos constructivos de interés para el cálculo de la demanda energética de la construcción.

Dado que se propone la digitalización de escenarios interiores complejos, se ha elegido una plataforma de cartografíado móvil, desarrollada por el "Applied Geotechnologies Research Group" de la Universidad de Vigo, dotada de sistemas de posicionamiento IMU-DMI y sensores de medición LiDAR, obteniendo directamente la nube de puntos 3D. En este caso, la adquisición termográfica se realiza de manera independiente de la adquisición geométrica, siendo la cámara portada por el operario, con el objetivo de garantizar la adquisición de la totalidad de las superficies y desde los ángulos que permiten una captura válida de valores de temperatura.

Palabras clave: termografía infrarroja; nube de puntos; mosaico; pérdidas de calor; envolvente constructiva; indoor mapping.

Original Paper

Indoor and Built Environment

Indoor and Built Environment
2017, Vol. 26(6) 771–784

DOI: 10.1177/1420326X16638912
journals.sagepub.com/home/ibe
SAGE

Thermographic and mobile indoor mapping for the computation of energy losses in buildings

L. López-Fernández[1], S. Lagüela[1,2], D. González-Aguilera[1] and H. Lorenzo[2]

Abstract
A mobile indoor mapping system combined with infrared thermography was used for the acquisition of data needed for the quantification of heat loss through a building envelope by conduction; that is, temperature values and building geometry. The methodology presented orthothermograms to provide measurement of heat loss and thermographic images with geometric information. This way, not only the energy loss through the building envelope is provided, but also thermographic information regarding the existence of thermal pathologies, their location and their impact on the building can also be evaluated.

Keywords
Infrared thermography, Thermal pathology, Point cloud, Mosaic, Heat losses, Building envelope, Indoor mapping

Accepted: 23 February 2016

Introduction

The use of infrared thermography as a widely tested technique for building inspection and location of pathologies such as air leakage and moisture[1–3] allows the performance of quality, quick, effective and non-destructive 'in-situ' inspections without direct contact with the object under study. This qualitative measurement technique has been used for detecting and localizing thermal and physical pathologies by some authors to perform in-situ studies, mainly in historical buildings or cultural heritage elements.[4,5] On the other hand, quantitative approaches have been performed mainly in laboratories with limited sample size.[6,7] In those cases where these quantitative thermography studies were performed in-situ,[8,9] temperature values were accurately measured in order to be used for the computation of the real thermophysical properties (thermal conductivity) of the building envelope, but their spatial distribution has not been considered. If the constituent materials are taken into account, infrared thermography should also be used for the determination of thermophysical properties such as diffusivity and thermal transmittance.[10,11]

Regarding geometry, the complex geometry of building indoors and the common presence of furniture and other elements, the use of static terrestrial laser scanning systems would entail a time-consuming data acquisition, since a high number of measuring positions would be needed to provide a full coverage of the scene. In this sense, the use of a mobile 'indoor mapping' laser scanning system is considered as the ideal technique for data recording, ensuring enough quality and speed.

In order to fill these gaps and obtain a thermographic-metric result, an approach combining both qualitative and quantitative measurement techniques was applied in our present study. Qualitative thermography was used for the automatic classification of the

[1]Department of Cartographic and Land Engineering, University of Salamanca, Hornos Caleros, Ávila, Spain
[2]Applied Geotechnologies Research Group, University of Vigo, Vigo, Spain

Corresponding author:
L. López-Fernández, Department of Cartographic and Land Engineering, University of Salamanca, Hornos Caleros, Ávila, Spain.
Email: luisloez89@usal.es

façade elements, while quantitative techniques were used for the measurement of temperatures of the wall and the pathologies, and the subsequent computation of heat loss. In addition, the spatial distribution of the pathologies was accurately assessed through the combination of thermographic images with the point cloud acquired with an indoor mapping system. The registration of the thermographic images with the point clouds was performed through the identification of homologous points between the thermograms and the point clouds allowing the computation of the spatial resection parameters.[12] What is more, the computation of the heat loss by conduction through the building envelope was automated, based on the temperatures measured with a thermographic camera and the geometry measured by an indoor mapping system through the automated generation of orthothermograms. In this way, thermography was used to represent the state of the wall, and to quantify the energy loss through it.[13–15] In addition, the generated orthothermograms can be used for the determination of energy losses in buildings.

Materials and methods

Equipment

Data acquisition was performed with two different systems. The geometric information was acquired with an indoor mapping system to generate point clouds of building interiors simultaneously to the displacement of the platform. Temperatures were measured with a thermographic camera, acquiring thermographic images of every wall. Both systems were used separately in this study.

Indoor mapping unit. The indoor mapping unit (Figure 1) was equipped with positioning systems and geomatics sensors for the generation of 3D point clouds of the buildings inspected.

In particular, the positioning systems used, were an inertial measurement unit (IMU) 'spatial' from 'advanced navigation' (Table 1) and two dual channel 'Kübler' odometers able to register a total of 128 counts per channel. These sensors were used to perform the computation of the trajectory followed by the mapping unit from the measurements of the rotation in the three axes and the longitudinal displacement in the plane.[16]

Regarding the geomatics sensors, the indoor mapping unit was equipped with a time of flight laser scanner, 'Hokuyo UTM-30LX', with a measuring range of 30 m and an angular resolution of 0.25°, with 30 mm precision.[17]

The laser sensor has a measurement frequency of 25 ms^{-1}. During this time the laser emits rays sweeping an arc of 270°. Given this fact, the sensor was positioned in the indoor mapping system in a horizontal position, measuring profiles perpendicular to the trajectory, and the coordinates measured for each point were (y, z). The 90° angle where no measurements were performed was oriented towards the floor, in such a way that no information would be missed from the walls and the ceiling of the building inspected, as shown in Figure 1.

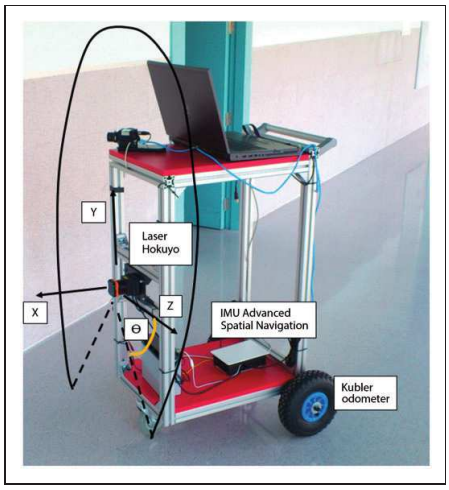

Figure 1. Diagram of the indoor mapping unit, the position of the different sensors and the axes assigned to the different components of movement.

Measurements of the laser and the positioning sensors were simultaneously acquired. Each 2D profile (y, z) from the laser has a time stamp for its association with the position data of the mobile unit during acquisition. Because of this time stamp, the position of each laser profile in the trajectory was used for the generation of a complete 3D point cloud of the building inspected[18] but without GPS data. The position was assumed as the x coordinate, therefore each point would be assigned its (x, y, z) coordinates.

Thermographic camera. Thermographic data acquisition was performed with a camera NEC TH9260 (Figure 2, left), measuring temperatures in a range from −20°C to 60°C, with a thermal resolution of 0.006°C at 30°C (30 Hz). The sensor was an Uncooled Focal Plane Array (UFPA), 640 × 480 size, capturing radiation between 7 and 14 μm wavelength. The instant field of view (IFOV) of the camera was 0.6 mrad, and its field of view with the current lens of 20 mm focal length was 21.7° (Horizontal – H) and 16.4° (Vertical – V). The IFOV (typically described in milliradians)

Table 1. 'Spatial' IMU specifications.

Sensor	Accelerometers	Gyroscopes	Magnetometers	Pressure
Range (dynamic)	2 g	250°/s	2 G	10 to 120 KPa
	4 g	500°/s	4 G	
	16 g	200°/s	8 G	
Bias Instability	20 μg	3°/h	–	10 Pa
Initial bias	< 5 mg	< 0.2°/s	–	< 100 Pa
Initial scaling error	< 0.06%	< 0.04%	< 0.07%	–
Scale factor stability	< 0.06%	< 0.05%	< 0.09%	–
Non-linearity	< 0.06%	< 0.05%	< 0.08%	–
Cross-axis Alignment Error	< 0.05 °	< 0.05 °	< 0.05 °	–
Noise density	150 μg/√Hz	0.005°/s/√Hz	210 μG/√Hz	0.56 Pa/√Hz
Bandwidth	400 Hz	400 Hz	110 Hz	50 Hz

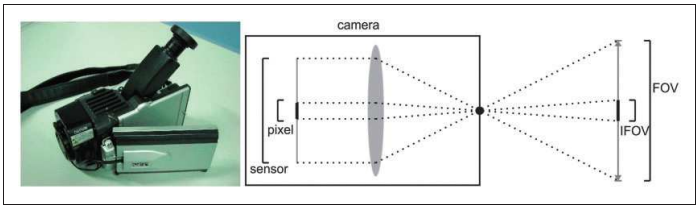

Figure 2. Thermographic camera used in this study (left). FOV and IFOV diagram of the thermographic camera (right).

corresponds to the two dimensional (H and V) angular area which was viewed by a single pixel of the detector through the optics of the camera. This defines the spatial resolution, or the size of the smallest object that can be viewed or resolved at a specific distance from the camera. The FOV (typically described in horizontal degrees by vertical degrees) can be defined as the largest area that an imaging sensor can capture at a set distance (Figure 2, right).

The main advantage of this camera for its use in the presented methodology is the availability of its geometric calibration, so that its inner orientation parameters are known, such as the principal point, sensor size and lens distortion coefficients. This calibration was previously performed using a specially designed calibration field.[19]

In addition to the thermographic camera, the acquisition of thermal data was complemented with a contact thermometer TESTO 720 (Table 2), which was used for the measurement of the inner and outer ambient temperature to perform the energy consumption analysis, and the temperature of the walls in certain points was measured to perform an emissivity correction of each thermography. This way, all data needed for the energy analysis, and for the emissivity correction of the values which were measured in the thermographic images, were recorded.

Table 2. Testo 720 specifications.

Parameter	Value
Range	−50°C to 150°C
Accuracy	±0.2°C (−25°C to +40°C)
	±0.3°C (+40.1°C to +80°C)
	±0.4°C (+80.1°C to +125°C)
	±0.5°C (<25°C and >125°C)
Resolution	0.1°C

There are three different sources of infrared (IR) radiation that can be captured by the thermographic camera if we assume that the object under study is opaque, implying that the transmission of IR radiation is null. These are the emission from the object under study; the reflected radiation from the surroundings (both attenuated by the atmospheric transmission) and the emission from the atmosphere[20] (Figure 3).

The emissivity correction was based on Stefan-Boltzmann's law (1), assuming that a real body with a surface temperature measured by a thermometer can be considered as a real body, whereas they can be considered as black bodies when temperature values are measured with a thermographic camera (with no emissivity

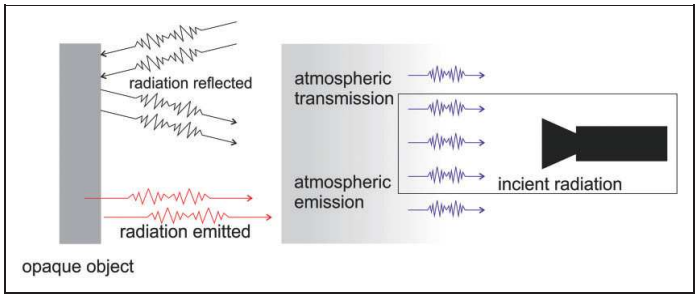

Figure 3. Components of incident IR radiation acquired by the thermographic camera.

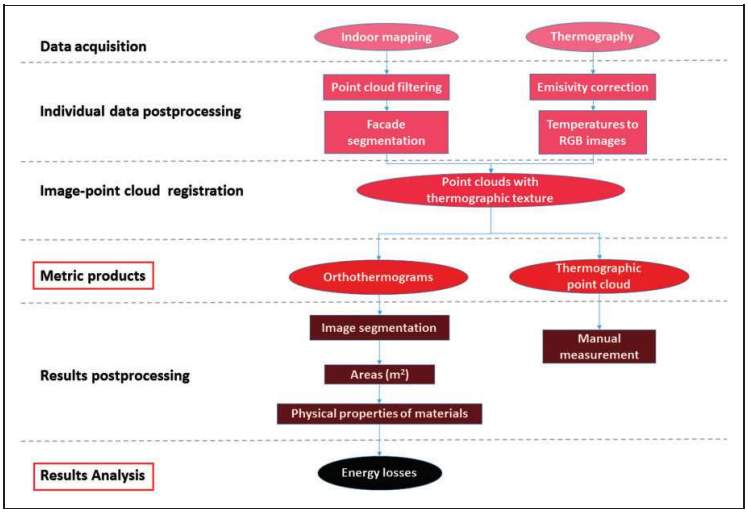

Figure 4. Workflow representing the methodology developed for the automatic quantification of energy losses and pathologies assessment in buildings using data acquired with a mobile indoor mapping unit and a thermographic camera.

correction introduced in the camera parameters). This way, emissivity can be defined by equation (1) as

$$\varepsilon_{rb} = \frac{T_{rb}^4}{T_{bb}^4} \quad (1)$$

where 'T_{bb}' is the temperature measured with the thermographic camera, and 'T_{rb}' is the temperature measured by the contact thermometer.

The correction of the atmospheric effect was directly performed by the thermographic camera through the configuration of the ambient parameters (temperature and humidity) and the camera–object distance.

Methodology

The proposed methodology (Figure 4) consists of three steps, and these are defined as follows:

- Data acquisition and pre-processing.
- Data processing and registration.
- Result interpretation

Data acquisition. This procedure involves the acquisition of both thermographic images and 3D point clouds.

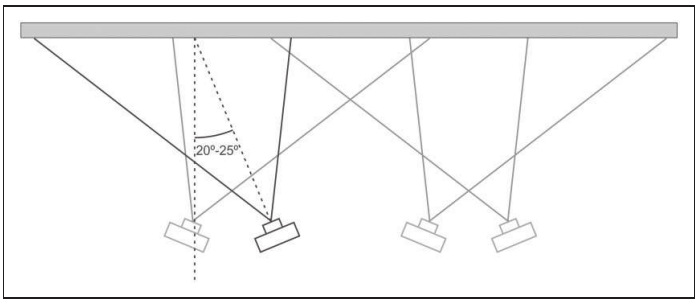

Figure 5. Overlapping between images and angle of incidence between the camera optical axis and the evaluated surface.

Thermographic images: Given the influence of the external parameters in the measurements performed with thermographic cameras, the establishment of a protocol for data acquisition was required for the minimization of these effects and the acquisition of valid products for their processing and analysis.

The *first rule* in the protocol is the existence of an approximate 10°C difference between the indoor-to-outdoor average temperature difference of the building (standard temperature difference considered for these studies) for maximizing the detection of the existing pathologies, like insulation deficiencies or moisture.[21] For example, the type of construction and location of the insulation layer within the building envelope could influence the temperature conditions under which pathologies may be detected. A minimum indoor-to-outdoor average temperature difference could mean inaccuracies in the pathologies detection, and this process could even become unapproachable. Although precipitation would be a significant issue for external surveys and less relevant to the type of internal survey reported in this study, prior building inspection is recommended to ensure no precipitation occurs for at least 24 h.

The *second rule* is the acquisition of thermographic images with an angle of incidence of 20° or 25° between the normal of the wall under study and the optical axis of the camera (Figure 5), therefore, avoiding the influence of the infrared radiation that would be emitted by the operator and reflected from other surfaces on the recorded thermal pattern.

The *third rule* is the adjustment of the ambient parameters in the camera; that is, distance camera–object, ambient temperature and humidity, prior data acquisition.

The *fourth rule* is the preparation of the survey in order to achieve an approximate steady-state heat transfer through the building envelope conditions. In particular, this would require a historical study of the temperatures of the building location in order to perform the survey in a time slot where the variation of the exterior temperature could be minimized. The survey should be conducted in winter as recommended, with overcast skies and at night, some hours after sunset if possible, in order to minimize the solar gain effect over the façades.

Given the limited field of view of the thermographic camera used, several acquisitions were required for the inspection of the total surface under study. This would require the maintenance of a minimum 10% overlap between consecutive images for the posterior generation of one product to represent completely the surface under study.

Point clouds: Planning data acquisition with the indoor mapping unit was required for the optimization of the quality of the data acquired.

The main error source of these devices comes from the Inertial Measurement Unit. In order to minimize the drift, the trajectory should avoid sharp turns that imply unnecessary drift accumulations, as well as avoiding every obstacle that could block or modify the trajectory of the indoor mapping unit. The displacement over sliding surfaces should be avoided, in order to minimize the risk of having inconsistent readings in the odometers that imply great deviations in the posterior computation of the trajectory, as well as incoherent data between these sensors and the inertial unit.

The IMU could be affected by external electromagnetic sources, such as metallic material, wiring, magnets and electrical transformers, to produce unacceptable variations in the measurement. For this reason, the presence of these objects should be considered and avoided if possible.

Finally, the measurement range of the laser scanner in the indoor mapping unit was taken into account for the definition of the trajectory with the aim of guaranteeing a continuous data acquisition for these scenes under study.

Image-point cloud registration. The transmission of the thermographic texture to the point

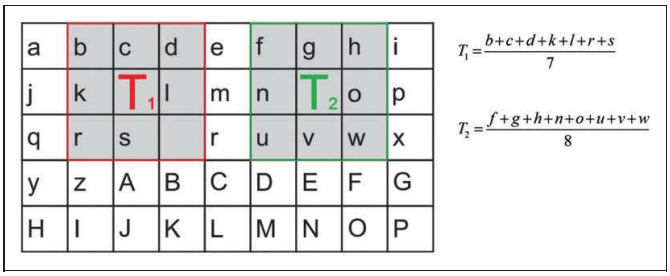

Figure 6. Convolution mask for solving the resampling of those pixels without thermographic texture. The different examples show that the mask ignores no-texture pixels for the computation.

cloud obtained with the indoor mapping unit was developed through the computation of the spatial resection[12] of the thermographic images using the laser scanning point cloud as reference and the identification of homologous entities (interest points) between each image and the point cloud by a human operator. The spatial resection would make use of image coordinates and their homologous object coordinates to determine the position and orientation of the camera.[22]

Once the exterior orientation of each thermography was calculated, the thermographic texture was transmitted to the point cloud. The result obtained was a thermographic point cloud where each point would have a temperature value associated and represented by the RGB conversion to the defined colour map.

The next step involved the orthogonal projection of each wall of the scene to their corresponding parallel planes, in a procedure where an image called orthothermogram was generated. Orthothermograms are images with geometric scale and no distortion, in such way that the measurement of a distance on the image, multiplied by the scale, would result in the measurement in the reality. Given that the procedure of projecting the thermographic point clouds into a plane would result in an image with occlusions or areas with missing information, an adaptive resampling algorithm was applied in order to cover the existing gaps between pixels. This algorithm would require the implementation of a convolution mask size 3×3 to work on the pixels that was lacking in thermographic texture by evaluating the surrounding pixels and using only those pixels with thermographic texture for the computation of the mean temperature (Figure 6).

Orthothermogram segmentation. The thermographic-metric results generated permit the performance of accurate analysis of the energy consumption of the building under study. The point cloud with thermographic texture allows analysis of the 3D model of the building directly and to extract accurate information of the elements of interest. However, the energy study was focused on the analysis of the orthothermograms.

According to the Spanish Technical Code for Buildings (Código Técnico de Edificación, CTE),[23] the computation of heat losses through a building envelope requires the location of the areas corresponding to the walls, openings (windows) and thermal bridges reflected in the orthothermograms. The different values of thermal emissivity of the principal construction elements (walls, windows and thermal bridges) allow the segmentation process through the study of the reflected temperatures and the thermal gradients.

The segmentation of the zones of interest was performed in two steps. (i) First, identify the critical points on the envelope (pathologies, differentiating between moisture and thermal bridges) and (ii) Second, recognize the openings. For this purpose, each orthothermogram was divided into two different orthothermograms in grey scale: one for the high-temperature areas, and another for the low-temperature areas, using as cutting point the mean value of the temperatures appearing in the image. The result to this segmentation was an orthothermogram with the openings (high-temperature), and an orthothermogram with the existing pathologies (low-temperature): from thermal bridges to damp areas.

The next step consisted the binarization of each image, for the identification of the areas of interest and the elimination of wrongly classified surfaces. This process required the user interaction for the choice of a binarization coefficient that guarantees the expected results. The resultant Boolean image was subjected to a supervised selection of areas of interest allowing the elimination of the noise introduced in the resampling step (pixels without neighbours), as well as the elimination of false positive clusters that did not correspond to elements of interest (these being pathologies and openings).

Once the Boolean image was generated with the zones of interest, the area of each zone was computed thanks to the knowledge of the GSD (Ground Sample

Distance)[24] of the orthothermogram. In particular, the areas corresponding to openings and critical points of the façade were obtained through the multiplication of the number of pixels overpassing the process of feature extraction by the GSD of the orthothermogram. Areas corresponding to walls were obtained through the difference between the total area of the façade and the openings' area.

At this point, the characteristic elements were accurately measured with minimum user interaction.

Heat loss computation. The computation of the energy loss of a building façade entails the study of the thickness, area and thermal properties of the materials used in the building construction. The thermal properties of the materials were determined by their thermal transmittance, U (W/m^{2}K), which represents the rate of heat transfer through 1 m^2 of a structure divided by the temperature difference across the structure. The study was based on an approximate steady-state heat transfer, as an acceptable approximation for conditioned buildings in climates with small solar gains and small outdoor temperature oscillation amplitude as compared with the indoor-to-outdoor average temperature difference. For the sake of simplification, U-values were considered as constant with temperature[25] omitting the effect of solar gain on heat transmission through the fabric, minimized by the implementation of the survey under guidelines described above. This parameter is defined by equation (2)

$$U = {}^{1}/_{R_t} \tag{2}$$

where 'U' represents the thermal transmittance and 'R_t' is the total thermal resistance of the construction element (m^{2}K/W).

Given that the wall of the building under study was composed of several layers of different materials, the total thermal resistance was calculated as the sum of the thermal resistance of each layer and the superficial thermal resistances of the inner and outer air.

The effect of the thermal bridges was considered through the computation of the heat transfer by transmission coefficient of the surface 'H_T', calculated by equation (3).

$$H_T = \sum_i A_i U_i + \sum_i l_k \psi_k \tag{3}$$

where 'U' is the thermal transmittance of the wall analysed (W/m^{2}K), 'A' is the area of the wall under study (m^2), 'ψ_k' is the lineal thermal transmittance of the thermal bridge (W/mK) and 'l' is the length of the thermal bridge (m).

After the computation of the heat transfer by transmission coefficient of the wall, the computation of the energy loss can be determined. The heat loss by conduction through the envelope of a building due to the thermophysical properties of the constructive materials can be determined by equation (4).

$$Q = H_T \cdot (T_{int} - T_{ext}) \tag{4}$$

where 'Q' is the heat loss through the wall analysed (W), 'H_T' is the heat transfer by transmission coefficient (W/K) and 'T_{int}' and 'T_{ext}' are the interior and exterior temperatures, respectively (K).

The thermal transmittance of the openings was computed using the knowledge of the materials composing these elements and their corresponding thermal transmittances, as well as the percentage of opening occupied per material.

From these data and following the standard established by the CTE, the total thermal transmittance of the openings, U_H, was computed with equation (5).

$$U_H = (1 - FM) \cdot U_{H,v} + FM \cdot U_{H,m} \tag{5}$$

where 'U_H' is the total thermal transmittance of the opening, '$U_{H,v}$' is the thermal transmittance of the semi-transparent surface, and '$U_{H,m}$' is the thermal transmittance of the window frame; all of them in W/m^{2}K. Finally, 'FM' is the opening percentage occupied by the frame (%).

In this case, the evaluation of the effect of any thermal bridge is not necessary, as it is possible to calculate directly the heat loss through the openings using the equation (6)

$$Q_H = U_H \cdot A \cdot (T_{int} - T_{ext}) \tag{6}$$

where 'Q_H' is the heat loss through the opening analysed (W).

The heat losses were computed following the protocol described in the CTE which would reflect the energy loss assuming an 'ideal' condition of the envelope. However, reality shows the presence of thermal pathologies in the building envelopes, directly affecting the energy consumption.

As a result, the additional heat loss through the building envelope on the critical surfaces was computed using equations (3) and (4), but considering only the area of those surfaces with pathologies without the thermal bridging effect, and the temperature difference between the surface with pathologies and the undamaged wall. For the sake of simplification, the increase of heat loss through the critical surfaces can be calculated using equation (7):

$$Q_c = U \cdot A_c \cdot (T_m - T_c) \tag{7}$$

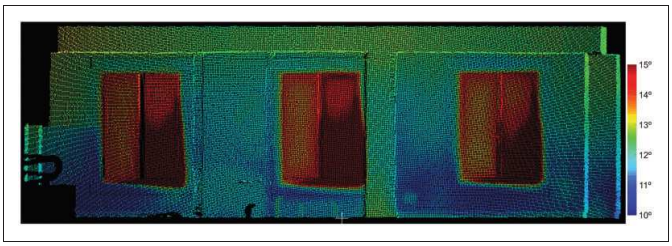

Figure 7. Point cloud with thermographic texture (south façade).

where Q_c is the additional energy loss through the critical surfaces (W) in addition to the heat loss as a function of the building composition; U is the total thermal transmittance of the wall (W/m^{2}K) and A_c is the total critical area (m^2). T_m is the mean temperature of the wall in good conditions (K), and T_c is the mean temperature of the critical surface in the wall (K).

Experimental results

Case study

The proposed methodology was validated in a building chosen by its architectural importance, in the town of Baiona (Northwest Spain). Currently, the building has been dedicated to music education so, the study must be performed during the day in order to measure the energy demand in the time slot when the infrastructure was being used and the HVAC (Heating, Ventilation and Air Conditioning) instruments should be working to maintain the adequate thermal comfort. The survey was performed on March 2013 under partly cloudy sky conditions in order to minimize the outside temperature variations during the survey process and the effect of direct solar irradiation incidence. After the historical temperature analysis, the optimum time slot to perform the survey was defined between 11:00 and 13:00 hours. The study was undertaken prior to the refurbishment of the building. The conservation condition of the inner face of the façades was evaluated and the existence of any thermal pathology was determined and detected to minimize any would be increase in energy consumption for heating the building.

Thus, the proposed methodology was applied to each façade of the building under study. Both the structure of each façade and the thermophysical properties of the thermal bridges was obtained from the technical documentation included in the building construction project. Walls of the building were composed of homogeneous layers of granite and bricks, also with a non-ventilated cavity wall and a thermal insulation of mineral wool. The openings are windows with aluminum frames with single-pane glazing.

Atmospheric conditions during data acquisition were 6°C exterior air temperature, while the interior air temperature was 13°C measured with the contact thermometer.

Data combination

The first step for the combination of the dataset was the computation of the orientation of each thermographic image regarding the point cloud of the building. For this purpose, the maximum number of significant features in each thermographic image was identified by a human operator, consequently minimizing the error in the computation of the external orientation parameters. Once the orientation parameters were computed per thermographic image, and the thermographic texture was transferred to the point cloud, the product was a point cloud with thermographic texture (Figure 7).

Metric thermographic images

The thermographic point cloud was subjected to the generation of an orthothermogram per wall (Figure 8), and a re-sampling process for the minimization of areas with no information.

Orthothermogram segmentation

The orthothermogram of each wall was subjected to an operation of automatic segmentation of the zones of interest so that they can be used for the quantification of the heat loss through the wall. This process requires a classification of the pixels into two groups: one for highest temperatures, where openings are; another for lowest temperatures, where the critical surfaces of the façade can be identified (Figure 9). Consequently, two orthothermograms were obtained: one for the openings, one for the pathologies. In this case study, consisting of a room with closed shutters at the moment of

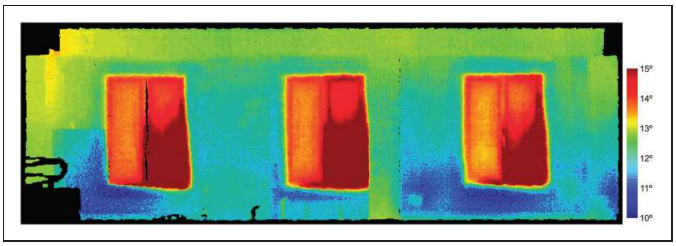

Figure 8. South façade: Orthothermogram after resampling with a GSD of 1 cm.

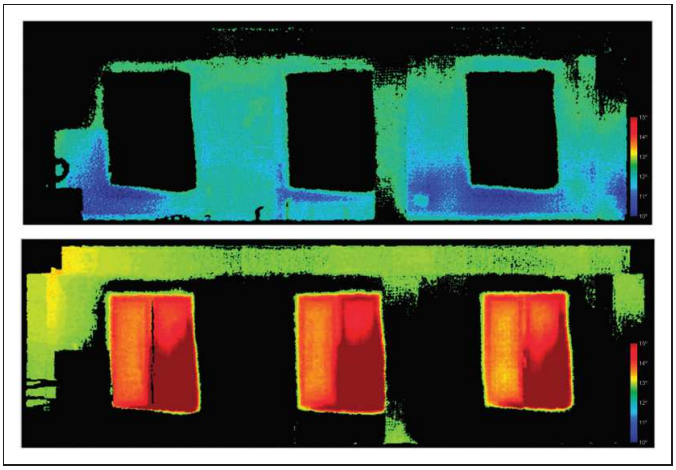

Figure 9. South façade: (top) Low-temperature group. (bottom) High-temperature group.

the inspection, the Sun was radiating on the windows, leading to their overheating. This is the reason for the presence of windows in the high-temperature group. What is more, the main pathology of the building was moisture, presenting low temperature due to the cooling of the surface caused by evaporation. Moisture was easily differentiated in the thermal images by its geometry, location and temperature difference with the undamaged wall. In addition, some zones with pathologies related with air leakage were characterized by larger temperature variations than those produced by moisture and being located in junctions between different elements of the façade.

Group images were segmented in the different zones of interest corresponding to the windows and critical surfaces, resulting in a binary image for each element.

Finally, a visual inspection by a human operator was required with the aim of eliminating the noise introduced in the orthothermograms during the re-sampling step, as well as to overcome the binarization process within the zones that do not represent any element of interest (Figure 10).

Energy analysis

Walls. The segmented orthothermograms provide information of the area of the different elements of interest. Consequently, only the thermophysical parameters of the materials obtained directly from the syllabus of construction solution of the CTE[26] and their thickness in the wall (Table 3), were needed for the determination of the energy requirements of each façade, following the indications of the CTE and the methodology presented in section 'Heat loss computation'.

Each wall of the scene under study was composed by one layer of granite with 0.2 m of thickness, 0.05 m of

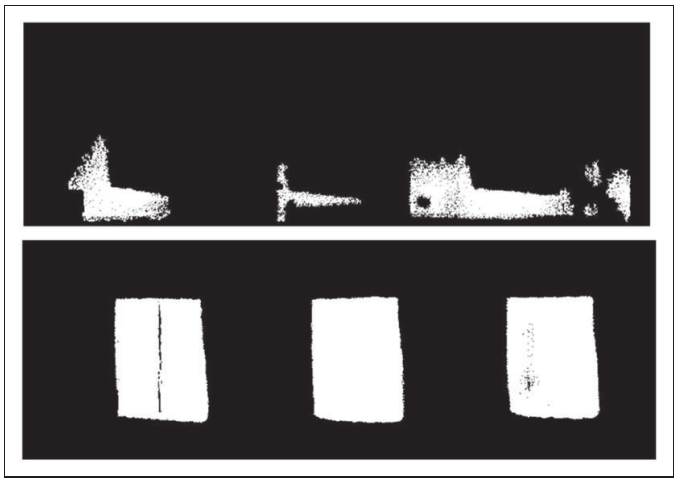

Figure 10. South façade: (top) Final binary image with critical surfaces (pathologies). (bottom) Final binary image with windows.

Table 3. Thermal resistance, thermal conductivity and thickness of the elements involved in the calculation of the thermal transmittance of the wall.

Material	Thickness (m)	Thermal conductivity (W/m·K)	Thermal resistance (m^2K/W)
Granite	0.2	2.8	0.071
Bricks	0.045	0.214	0.210
Non-ventilated cavity wall	0.05	–	0.180
Thermal insulation (Mineral wool)	0.02	0.031	0.645
Plastering	0.015	0.57	0.026
Inner air 'R_{SI}'	n/a	n/a	0.130
Outer air 'R_{SE}'	n/a	n/a	0.040
Total thermal resistance of the wall			1.302

Source: CTE.[26] *Openings*. n/a: not applicable

non-ventilated cavity wall with 0.02 m of thermal insulation made of mineral wool and 0.045 m of bricks finished with 0.015 m of plastering (Figure 11). The thermal resistance for this composition was 1.302 m^2K/W giving a total thermal transmittance value 'U' of 0.768 W/m^2K.

All window openings (Table 4) were composed with a simple insulated glass (4–6–4 mm) within an aluminum frame covering 20% of the opening.

Thermal bridges. The thermal bridging effect produced by junctions between walls with the floor, windows and other walls, as well as in the pillars where the uniformity of the façade is broken was evaluated by the study. The linear thermal transmittances of the thermal bridges were obtained from the catalog included in the building construction project. The length of the thermal bridges was obtained directly from the geometric information in the orthothermograms (Table 5).

The effect of the thermal bridges was applied to the calculation of the thermal transmittance based on the area of the walls to provide a heat transfer with a transmission coefficient 'H_T' of 135.052 W/K.

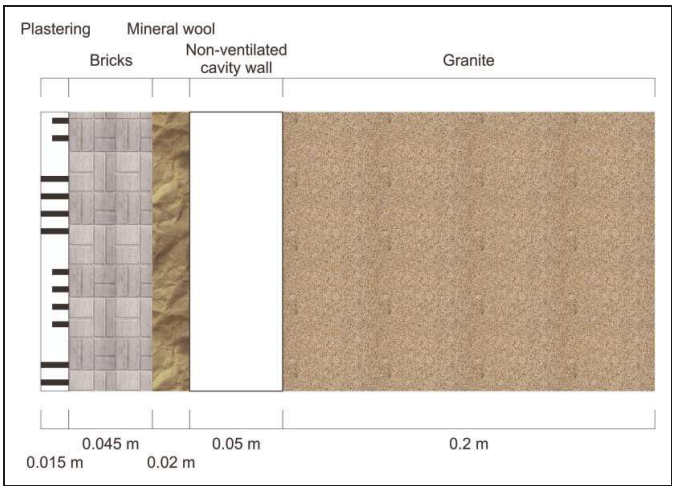

Figure 11. Composition diagram of the wall.

Table 4. Thermal transmittance and percentage per material in the openings.

Material	Thermal transmittance (W/m^2K)	% in the opening
Glass (4 + 6 + 4) mm	3.6	80
Aluminium frame	7.2	20

Source: CTE.[26]

Table 5. Linear thermal transmittance and length of the thermal bridges.

Thermal bridge	Linear thermal transmittance (W/mK)	Total length of the thermal bridge (m)
Junction between walls	0.09	13
Junction between wall and floor	0.96	44.4
Junction between wall and window	0.25	50
Junction between wall and pillar	0.27	41.6

Final results

The application of the proposed methodology had generated two different output results:

- Thermographic point cloud and orthothermograms: 3D point cloud with thermographic texture, allowing the visual inspection of the scene under study, and the preliminary geometric analysis directly measuring the point cloud (Figure 12). The complementary result is the orthothermogram of each façade, used for the automatic determination of the energy requirements of the building. Orthothermograms can also be imported in CAD software for further analysis.
- Heat loss computation per façade as a function of the temperature of the construction element and the area of the wall. Software has been developed for the generation of a file with data of the area occupied per element of interest. This was determined after a semi-automatic segmentation process and the computation of the total thermal transmittance. The knowledge of the specific heat loss through each construction element would allow the identification of the most critical elements towards the refurbishment of the building, and the effect of refurbishment in the total energy consumption of the building under study (Table 6).

Discussion

The first decision to be taken for the development of the present procedure is the configuration of the data acquisition system. In this case, the integration of the

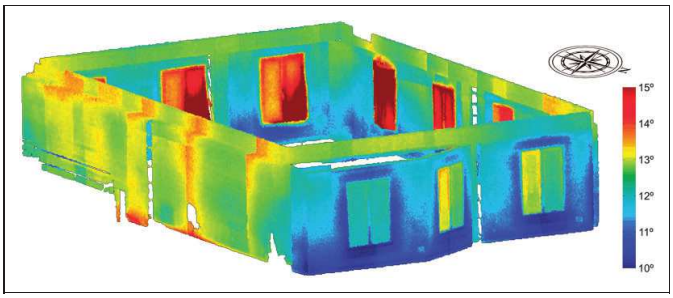

Figure 12. External view of the point cloud with thermographic texture. Holes created by obstacles as well as the side of columns that have not been caught due to the path followed by the indoor mapping unit, were also captured. However, these areas should also be taken into account for the energy analysis.

Table 6. Results obtained after the application of the algorithm developed in this study to the building under study.

	Façade				
	North	South	East	West	Total
Total area (m^2)	24.959	23.018	35.149	34.435	117.561
Wall area (m^2)	19.958	17.331	29.024	34.435	100.748
Window area (m^2)	5.001	5.687	6.125	0	16.813
Pathologies area (m^2)	4.183	0.940	1.599	0	6.722
Total thermal transmittance, wall ($W/(m^2\ K)$)			1.302		
Heat transfer by transmission coefficient of the wall (W/K)			135.052		
Total thermal transmittance, opening ($W/m^2\ K$)			4.320		
Heat loss through the wall in good condition (W)					945.364
Heat loss through the critical surfaces (W)	35.503	9.035	15.378	0	59.916
Total heat loss in the wall (W)					1005.280
Total heat loss in the openings (W)	151.233	171.972	185.217	0	508.422
Total heat loss through the façade (walls + openings) (W)					1513.702

camera in the indoor mapping system would remove the flexibility in data acquisition, both spatial and temporally.[27] Regarding spatial flexibility, the angle for image acquisition would be limited by the position of the camera in the indoor mapping system and the displacement direction, preventing the acquisition of images from other angles of interest. This fact is especially critical for the upper and lower parts of the walls, not visible from the height of the indoor mapping system (Figure 13).

Furthermore, the performance of an optimal thermographic inspection would imply the modification of the trajectory of the indoor mapping system, distorting the geometric data acquisition.

Regarding temporal flexibility, the possibility of completing the thermographic inspection at night separately from the laser scanning to reduce the influence of solar gains would be lost.

With respect to the error caused in temperature measurement and, consequently, in the computation of the energy loss, the accuracy of the thermographic camera and the contact thermometer were 2°C and 0.5°C, respectively. The uncertainty associated to each emissivity correction value can be calculated through the simplified uncertainty propagation method for a non-linear combination of independent variables. Through this uncertainty evaluation method for the least favourable case within the range of measured temperature values, the uncertainty associated to each emissivity correction value was lower than 0.6°C.

Considering that, for this study, only the relative values along the surfaces were evaluated in order to

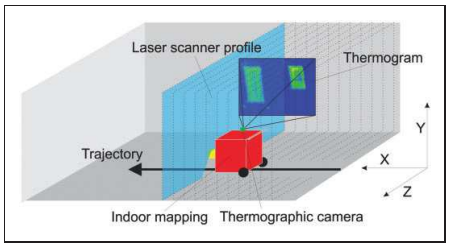

Figure 13. Limitations of using a thermographic camera mounted onboard the indoor mapping system. Due to the limited field of view of the thermographic camera, walls are not fully covered if images are acquired from the indoor mapping system.

segment the façades in their different components, the correction of the reflected temperatures was not necessary, assuming that their effect would be uniform over the whole surface and would not affect the relative difference between temperatures.

The use of infrared thermography would allow the estimation of these energy losses due to the accurate identification of the critical points and the thermal differences existing between these and non-critical surfaces. A similar analysis was performed by Asdrubali et al.[28] for the characterization of thermal bridges, and by González-Aguilera[29] through the classification of the building envelope using isotherms.

Conclusions

This article presents a methodology for the generation of thermographic point clouds and orthothermograms, as well as the computation of heat losses through walls based on the semi-automatic integration of thermographic images and indoor point clouds which were applied to indoor building scenes. The results obtained have provided complete thermographic and metric information of the different elements, to enable a better detection, spatial location and interpretation of thermal pathologies than a single thermal image. The geometric information embedded on the orthothermograms enables the measurement of areas and distances for the quantification of energy losses and thus allows the determination of any increase in the energy consumption that could be caused by the existence of pathologies.

The methodology could provide a suitable routine method to accurately evaluate the state of buildings prior to refurbishment in order to assess the need to invest in the partial or total refurbishment of the façade and calculate an approximation of the refurbishment effect on the heat loss transmission resulting in energy savings.

The main problem of the presented methodology is the complexity of the automation of the detection of thermal pathologies mainly due to the high number of factors to consider in the thermal imaging interpretation, such as environmental conditions, solar impact, surface state of the element under study and emissivity. This problem can be solved by specifying an appropriate temperature interval for the representation of temperature differences for the object analysed, so that the detection of areas affected by pathologies is maximized, allowing the performance of appropriate binarization of the orthothermograms.

Authors' contribution

All authors contributed equally in the preparation of this manuscript. SLL performed the data acquisition, LLF developed data processing and analysis; data interpretation was made by LLF, SLL and DGA.

Declaration of conflicting interests

The author(s) declared no potential conflicts of interest with respect to the research, authorship, and/or publication of this article.

Funding

The author(s) disclosed receipt of the following financial support for the research, authorship, and/or publication of this article: The authors would like to thank the Ministerio de Educación. Cultura y Deporte (Gobierno de España) for the financial support given through human resources programs (FPDI-2013-17516). Also, they thank the support given by the Ministerio de Economía y Competitividad through projects ENE2013-48015-C3-1-R.

References

1. Grinzato E, Vavilov V and Kauppinen T. Quantitative infrared thermography in buildings. *Energ Build* 1998; 29: 1–9.
2. Rosina E and Spodek J. Using infrared thermography to detect moisture in historic masonry: a case study in Indiana. *APT Bull* 2003; 34: 11–16.
3. Li H, Gong G, Xu C, Su H, Cao Z, Zhou M and Yu CWF. Thermal and humid environment and moisture condensation characteristics of cold surfaces. *Ind Built Environ* 2014; 23: 474–484.
4. Avdelidis N and Moropoulou A. Applications of infrared thermography for the investigation of historic structures. *J Cult Herit* 2004; 5: 119–127.
5. Tavukcuoglu A, Duzgunes A, Demirci S and Caner-Saltık EN. The assessment of a roof drainage system for an historical building. *Building Environ* 2007; 42: 2699–2709.
6. Bison P and Grinzato E. IR thermography applied to the assessment of thermal conductivity of building materials. SPIE Defense, Security, and Sensing. *Int Soc Opt Photon* 2010; 7661: 76610G–G-9.
7. Barreira E and de Freitas VP. Evaluation of building materials using infrared thermography. *Constr Build Mater* 2007; 21: 218–224.

8. Lagüela S, Díaz-Vilariño L, Armesto J and Arias P. Non-destructive approach for the generation and thermal characterization of an as-built BIM. *Constr Build Mater* 2014; 51: 55–61.
9. Fokaides PA and Kalogirou SA. Application of infrared thermography for the determination of the overall heat transfer coefficient (U-Value) in building envelopes. *Appl Energ* 2011; 88: 4358–4365.
10. Mercuri F, Zammit U, Orazi N, Paoloni S, Marinelli M and Scudieri F. Active infrared thermography applied to the investigation of art and historic artefacts. *J Therm Anal Calorimetr* 2011; 104: 475–485.
11. Vavilov V, Kauppinen T and Grinzato E. Thermal characterization of defects in building envelopes using long square pulse and slow thermal wave techniques. *J Res Nondestr Eval* 1997; 9: 181–200.
12. Kraus K. Advanced methods and applications. Vol. 2. *Fundamentals and Estándar processes. Vol.* 1. Institute for Photogrammetry Vienna University of Technology, Ferd Dummler Verlag Bonn. Bonn, Germany, 1993..
13. Lagüela S, Díaz-Vilariño L, Martínez J and Armesto J. Automatic thermographic and RGB texture of as-built BIM for energy rehabilitation purposes. *Automat Constr* 2013; 31: 230–240.
14. Hoegner L and Stilla U. Automatic generation of façade textures from terrestrial thermal infrared image sequences. In: *CNRS-ENSAM*, Bordeaux (France), 7–11 July 2014.
15. Previtali M, Barazzetti L, Redaelli V, Scaioni M and Rosina E. Rigorous procedure for mapping thermal infrared images on three-dimensional models of building façades. *J Appl Remot Sens* 2013; 7: 073503–073503.
16. Borenstein J, Everett H and Feng L. *Where am I? Sensors and methods for mobile robot positioning: Vol. 119*. Michigan, Ann Arbor: University of Michigan, 1996, p.27.
17. Riveiro B, Morer P, Arias P and De Arteaga I. Terrestrial laser scanning and limit analysis of masonry arch bridges. *Constr Build Mater* 2011; 25: 1726–1735.
18. Puente I, González-Jorge H, Martínez-Sánchez J and Arias P. Review of mobile mapping and surveying technologies. *Measurement* 2013; 46: 2127–2145.
19. Lagüela S, González-Jorge H, Armesto J and Herráez J. High performance grid for the metric calibration of thermographic cameras. *Meas Sci Technol* 2012; 23: 015402.
20. Taylor T, Counsell J and Gill S. Combining thermography and computer simulation to identify and assess insulation defects in the construction of building façades. *Energ Build* 2014; 76: 130–142.
21. ISO 6781:1983. *Thermal insulation, qualitative detection of thermal irregularities in building envelopes, infrared method*. Geneva: International Organization for Standardization, 1983.
22. Shih T and Faig W. A solution for space resection in closed form. *Int Arch Photogramm Remot Sens* 1988; 27: 547–56.
23. Ministerio de Fomento. Código Técnico de la Edificación, http://www.codigotecnico.org/images/stories/pdf/ahorroEnergia/DA-DB-HE-1-Calculo_de_parametros_caracteristicos.pdf (accessed 15 February 2016).
24. Pierrot-Deseilligny M, De Luca L and Remondino F. Automated image-based procedures for accurate artifacts 3D modeling and orthoimage generation. *Geoinform FCE CTU J* 2011; 6: 291–299.
25. Barrios G, Huelsz G, Rojas J, Ochoa JM and Marincic I. Envelope wall/roof thermal performance parameters for non air-conditioned buildings. *Energ Build* 2012; 50: 120–127.
26. Ministerio de Fomento. CTE. Syllabus of construction solution, http://cte-web.iccl.es/materiales.php (accessed 18 February 2014).
27. Liu L and Stamos I. Automatic 3D to 2D registration for the photorealistic rendering of urban scenes. In: *Proceedings of the 2005 IEEE computer society conference on computer vision and pattern recognition*, IEEE, San Diego, CA, December 2005; Vol. 2: pp.137–143.
28. Asdrubali F, Baldinelli G and Bianchi F. A quantitative methodology to evaluate thermal bridges in buildings. *Appl Energ* 2012; 97: 365–373.
29. González-Aguilera D, Rodriguez-Gonzalvez P, Armesto J and Lagüela S. Novel approach to 3D thermography and energy efficiency evaluation. *Energ Build* 2012; 54: 436–443.

Capítulo IV

Automatización de procesos de evaluación de cobertura urbana para la instalación de paneles solares

4. Large scale automatic analysis and classification of roof surfaces for the installation of solar panels using a multi-sensor aerial platform

Este capítulo contiene el artículo "*Large scale automatic analysis and classification of roof surfaces for the installation of solar panels using a multi-sensor aerial platform"* publicado en la revista de alto impacto *Remote Sensing* en Septiembre del 2015.

4.1. Resumen

La publicación científica recogida en este capítulo representa el segundo hito establecido en la hoja de ruta de la línea de investigación. El objetivo principal es el desarrollo de una metodología que permita realizar la detección automática de las superficies de cobertura urbana que, por sus condiciones geométricas de área, orientación e inclinación, complementadas con la identificación de obstáculos si existiesen, sean candidatas a la instalación de superficies de paneles solares. La detección de estas superficies se complementa con la clasificación de las mismas en función de su potencial fotovoltaico dada la irradiación solar incidente sobre la misma. En particular, el enfoque desarrollado tiene cuatro componentes: (1) definición de las técnicas geomáticas más adecuadas para la digitalización de escenarios urbanos a gran escala desde un punto de vista cenital; (2) desarrollo de estrategias de detección, segmentación y parametrización de superficies candidatas a la instalación de paneles solares; (3) identificación de obstáculos que impidan la instalación de paneles solares o generen sombras limitando su productividad y (4) cuantificación del potencial solar de la superficie en función de la irradiación solar incidente.

Dado que se propone la evaluación de zonas urbanas a gran escala, se ha elegido una plataforma aérea tripulada (paramotor) que garantiza la autonomía, alcance y capacidad de carga necesaria para la captura de todos

los datos necesarios. Se ha incluido una plataforma giroestabilizada (MUSAS- MUltiSpectral Airborne Sensor), desarrollada por el Instituto de Desarrollo Regional (IDR) de la Universidad de Castilla-La Mancha, capaz de albergar un sensor fotográfico comercial de medio formato DSLR (Digital Single Lens Reflex) y el sensor termográfico. El producto geomático, en forma de nube de puntos 3D, se ha obtenido utilizando los procesos fotogramétricos a partir de las imágenes capturadas por el sensor DSLR.

El proceso desarrollado ha sido validado con datos reales, sobre los que se ha generado una verdad-terreno a través de una inspección visual detallada y la correspondiente clasificación manual de los tejados del caso de estudio.

Palabras clave: reconstrucción 3D, paramotor, fotogrametría, termografía infrarroja, nube de puntos, edificios, irradiación solar, panel solar.

Remote Sens. **2015**, *7*, 11226-11248; doi:10.3390/rs70911226

OPEN ACCESS

remote sensing

ISSN 2072-4292

www.mdpi.com/journal/remotesensing

Technical Note

Large Scale Automatic Analysis and Classification of Roof Surfaces for the Installation of Solar Panels Using a Multi-Sensor Aerial Platform

Luis López-Fernández [1,*], Susana Lagüela [1,2], Inmaculada Picón [1] and Diego González-Aguilera [1]

[1] Department of Cartographic and Land Engineering, University of Salamanca, Hornos Caleros, 50, Ávila 05003, Spain; E-Mails: susiminas@uvigo.es (S.L.); ipicon@usal.es (I.P.); daguilera@usal.es (D.G.-A.)

[2] Applied Geotechnologies Research Group, University of Vigo. Rúa Maxwell s/n, Campus Lagoas-Marcosende, Vigo 36310, Spain

* Author to whom correspondence should be addressed; E-Mail: luisloez89@usal.es; Tel.: +34-920-353-500 (ext. 3820); Fax: +34-920-353-505.

Academic Editors: Fabio Remondino, Richard Müller and Prasad S. Thenkabail

Received: 3 July 2015 / Accepted: 25 August 2015 / Published: 1 September 2015

Abstract: A low-cost multi-sensor aerial platform, aerial trike, equipped with visible and thermographic sensors is used for the acquisition of all the data needed for the automatic analysis and classification of roof surfaces regarding their suitability to harbor solar panels. The geometry of a georeferenced 3D point cloud generated from visible images using photogrammetric and computer vision algorithms, and the temperatures measured on thermographic images are decisive to evaluate the areas, tilts, orientations and the existence of obstacles to locate the optimal zones inside each roof surface for the installation of solar panels. This information is complemented with the estimation of the solar irradiation received by each surface. This way, large areas may be efficiently analyzed obtaining as final result the optimal locations for the placement of solar panels as well as the information necessary (location, orientation, tilt, area and solar irradiation) to estimate the productivity of a solar panel from its technical characteristics.

Keywords: 3D reconstruction; aerial trike; photogrammetry; infrared thermography; point cloud; buildings; solar influence; solar irradiation; solar panel

1. Introduction

Several techniques have been applied so far for the calculation of the solar incidence on roofs trying to find the most suitable roof surfaces for the installation of solar panels with optimal performance without assessing the possible obstacles that can prevent their installation. In most cases the analysis is done from Geographical Information Systems (GIS) fed with low-resolution raster or vector cadastral data sources [1–4], GML (Geography Markup Language) systems with simplified LOD (Level Of Detail) [5] or topologically consistent 3D city models obtained through the extrusion of building footprints to a stimated average building height [6]. These techniques, that generally use simplified models and approximations of the positions and orientations of the roofs, could imply errors in the calculation of the solar incidence on the surfaces of the roofs and thus cause large variations in their productivity [7]. In order to avoid these limitations, we developed a methodology able to identify the optimal location for the installation of solar panels [8] and the estimation of their solar irradiation from a precise dataset obtained with a low cost aerial platform equipped with RGB and thermographic cameras. The data processing methodology is scalable to any other aerial data sources like LiDAR (Light Detection and Ranging), acquired from piloted aerial vehicles or UAV's (Unmanned Aerial Vehicles). The use of geo-referenced 3D dense point clouds of roofs will allow the performance of accurate analysis of areas, orientations and tilts of the roofs. Furthermore, if these data are complemented with qualitative thermal information, which provides direct knowledge about the relative temperature difference between roofs and consequently about the influence of the solar radiation on them, the removal of surfaces that could present ideal geometric conditions to install solar panels will be possible. The thermal values recorded by the thermographic camera cannot be considered as the rigorous temperature values of the object due to the difficulty to perform an accurate emissivity correction on the measurement. However, these values provide useful information for the detection of differences in solar incidence over the object surface. For instance, those surfaces containing elements that could prevent the installation of solar panels such as skylights or chimneys will be automatically detected.

This work proposes and tests a methodology useful for the performance of the automatic classification of roofs regarding their suitability to harbor solar panels, the detection of the optimal location inside these surfaces and the estimation of the solar irradiation received. The methodology consists on the processing of visible and thermographic images acquired from a low-cost aerial trike equipped with a multi-sensor platform (MUSAS, which stands for MUltiSpectral Airborne Sensors) towards the generation of 3D point clouds of roofs.

The paper has been structured as follows: after this introduction, Section 2 includes a detailed explanation of the materials and methods used for data acquisition and processing towards the automatic segmentation and classification of the roof surfaces for the installation of solar panels. Section 3 is devoted to be an explanation of the methodology presented through its application to an urban area selected as case study; finally, Section 4 establishes the most relevant conclusions of the proposed approach. The procedure is presented through its application to a real case study, based on the classification of the roofs in a neighborhood in Ávila, located near the center of Spain (coordinates 40°38'27.6"N, 4°41'27.8"W). The location of the case study determines the restrictions applied for the installation of solar panels following the Spanish Regulation for Construction [9].

2. Materials and Methods

2.1. Equipment

2.1.1. Aerial Trike

The aerial trike is a driven low-cost aerial system equipped with a MUSAS platform able to accommodate different types of remote sensors, from imaging sensors (RGB and thermographic cameras) to navigation systems (GNSS/IMU). The use of these kind of aerial vehicles shall be regulated by the local legislation on air navigation as long as it does not conflict with the general air navigation law of the DGAC (General Guidance of Civil Aviation). The aerial trike is an experimental "Tandem Trike AIRGES" (Table 1), with a weight capacity up to 220 kg and flying altitudes up to 300 m, which is the limit established by the current Spanish legislation for this type of aerial vehicles [10]. The main advantages of this platform over the usual driven aerial vehicles are its low cost, ease of use and the possibility of flying below 300 m, consequently obtaining better GSD (Ground Sample Distance) with the imaging sensors. This increase in the spatial resolution of the RGB images regarding usual aerial photogrammetric flights allows the generation of dense point clouds, as well as improves the use of thermographic images, given that the thermographic sensor presents very limited resolution implying a high GSD that, for altitudes over 300 m could prevent the differentiation of characteristic elements of roofs. Regarding UAV platforms, the aerial trike is able to transport greater weights, which implies the possibility of using more and higher quality sensors with longer autonomy than copter-type platforms. Thus, this aerial platform is used to obtain good quality georeferenced images from a zenithal point of view, allowing for a better spatial perception given the absence of obstacles between the camera and the object.

Table 1. Technical specifications of the manned aerial platform, aerial trike.

Parameter	Value
Empty weight	110 kg
Maximum load	220 kg
Autonomy	3.5 h
Maximum speed	60 km/h
Motor	Rotax 503
Tandem paraglide	MACPARA Pasha 4
Emergency system	Ballistic parachutes GRS 350
Gimbal	Stabilized with 2 degrees of freedom (MUSAS)
Minimum sink rate	1.10
Maximum glide rate	8.60
Plant surface	42.23 m^2
Projected area	37.80 m^2
Wingspan	15.03 m
Plant elongation rate	5.35
Central string	3.51 m
Boxes	54 boxes
Zoom factor	100%

Sensors are supported by a specific gyro-stabilized platform (MUSAS) (Figure 1) allowing for a full coverage of the study area with an appropriate GSD. This device includes two servomotors arranged on the *x* and *y* axes to maintain the vertical position of the camera along the flight path with precision. The servomotors are controlled by an Arduino board, which incorporates an IMU with 6 degrees of freedom: 3 accelerometers with a range of ± 3.6 G m/s^2, a double-shaft gyroscope (for pitch and roll control) and an additional gyroscope for yaw control (both gyroscopes have a measurement range of ± 300°/s). The navigation devices allow the geolocation of each datum for the successive generation of geo-referenced point clouds with real and thermographic texture.

Last, the software developed for the control of the device was based on Quad1_mini V 20 software, with DCM (Direction Cosine Matrix) as the management algorithm for the IMU [11].

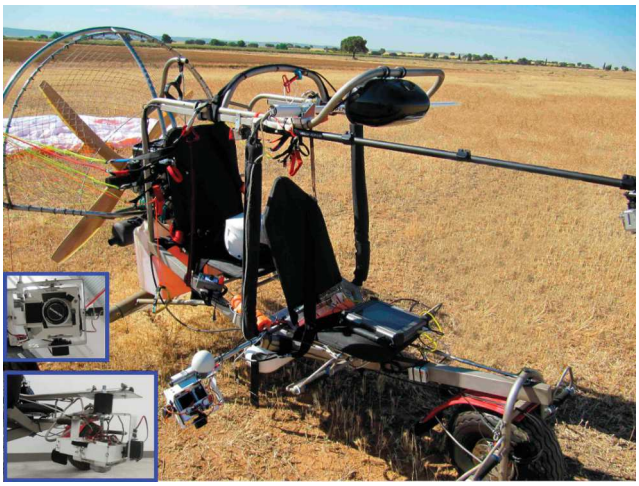

Figure 1. Aerial trike and MUSAS platform used in this study; bottom-left corner: detail of the gyro-stabilized platform for the installation of sensors.

2.1.2. RGB Camera

RGB cameras are used for the acquisition of images towards the reconstruction of 3D point clouds as well as to provide visual information of the state of the roofs. The visible camera selected for this work is a full frame reflex camera Canon 5D mkII. This camera has a CMOS sensor which size is 36 × 24 mm with a resolution of 21.1 megapixel and equipped with a 50 mm focal length lens. The size of the image captured with this sensor is 21 MP with a pixel size of 6.4 µm.

The camera is calibrated prior acquisition in order to allow the correction of the distortion and perspective effects from the data collected and the 3D reconstruction in the photogrammetric process. The calibration of cameras working in the visible band of the electromagnetic spectrum (Table 2) is performed through the acquisition of multiple convergent images of a geometric pattern (known as calibration grid) with different orientations of the camera. The adjustment of the rays ruling the position of the camera and the image in each acquisition allows the determination of the inner orientation

parameters of the camera (focal length, format size, principal point, radial lens distortion and decentering lens distortion). The camera calibration was processed in the commercial software ImageMaster which performs the automatic detection of the targets in each image and computes and adjusts the orientation of each image, resulting in the computation of the internal calibration parameters of the camera. Since the flight was performed at medium speed and low altitude, there should not be any change in the "camera-lens" system caused by sudden movements of the platform or major changes in the atmosphere. For this reason, the camera calibrations performed in the laboratory have been considered as fixed for both cameras.

Table 2. Interior orientation parameters of visible camera Canon 5D mkII, result of its geometric calibration.

Parameter	--	Value
Focal length (mm)	Value	50.1
Format size (mm)	Value	34.819 × 23.213
Principal point displacement (mm)	X value	−0.21
	Y value	−0.11
Radial lens distortion	K_1 value (mm^{-2})	6.035546×10^{-5}
	K_2 value (mm^{-4})	-1.266639×10^{-8}
Decentering lens distortion	P_1 value (mm^{-1})	1.585075×10^{-5}
	P_2 value (mm^{-1})	6.541129×10^{-5}
Point marking residuals	Overall RMSE (pixels)	0.244

2.1.3. Thermographic Camera

The thermographic camera selected for this study is the FLIR SC655. This device has been specially developed for scientific applications. It allows the capture and recording of thermal variations (Figure 2) in real time, enabling the measurement of heat dissipation or leakage. Its sensor is an Uncooled Focal Plane Array (UFPA) 0.3 MP, capturing radiation with 7.5 to 13.0 µm wavelengths and measuring temperatures in a range from −20 °C to 60 °C. The Instant Field of View (IFOV) of the camera is 0.69 mrad, and its Field of View (FOV) is 25° (Horizontal) and 18.8° (Vertical) with the current lens of 25 mm focal length.

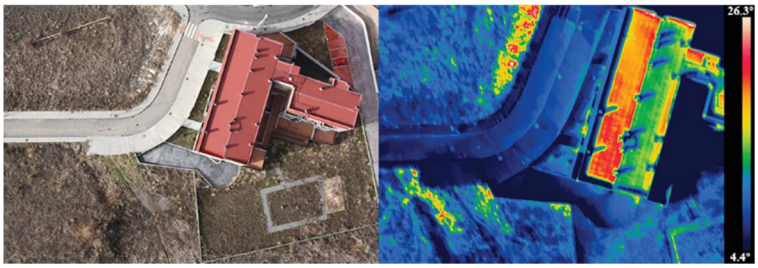

Figure 2. Comparison between the products generated by the different used imaging sensors. (**Left**) RGB image. (**Right**) Thermographic image with the thermal values represented using a color map.

Thermographic cameras capture radiation in the infrared range of the spectrum, in contrast to photographic cameras that work in the visible range. For this reason, the geometric calibration (Table 3) of the camera is performed using a specially designed calibration field, presented in [12], which is based on the capability of the thermographic cameras for the detection of objects being at different temperatures even if they are at the same temperature but with different emissivity values. This calibration field consists on a wooden plate with black background (high emissivity) on which foil targets are placed (low emissivity). In this case, the calibration was processed in the commercial photogrammetric station Photomodeler Pro5©, which not only computes the calibration parameters of the cameras in a procedure analogous to the one previously explained for ImageMaster, but it also provides the standard deviation of the calibration parameters as a value to test their quality.

Table 3. Interior orientation parameters of thermographic camera FLIR SC655, result of its geometric calibration.

Parameter	–	Value	Std. Deviation
Focal length (mm)	Value	25.063	0.022
Format size (mm)	Value	10.874 × 8.160	0.002
Principal point displacement (mm)	*X* value	−0.174	0.022
	Y value	0.024	0.026
Radial lens distortion	K_1 value (mm^{-2})	5.281×10^{-5}	2.4×10^{-5}
	K_2 value (mm^{-4})	7.798×10^{-7}	6.1×10^{-7}
Decentering lens distortion	P_1 value (mm^{-1})	1.023×10^{-4}	1.2×10^{-5}
	P_2 value (mm^{-1})	-3.401×10^{-5}	1.3×10^{-5}
Point marking residuals (pixels)	Overall RMSE	0.173	--

2.2. Methodology

2.2.1. Flight Planning and Data Acquisition

Proper flight planning is important to optimize available resources, ensuring a high quality of the images and minimizing capture time. The spatial information required for the flight planning can be obtained free of charge from the National Center of Geographic information in Spain (CNIG), from its National Aerial Orthoimage Plan (PNOA, 2009) with a GSD of 0.25 m and a Digital Terrain Model (DTM) with a 5 m grid resolution. The flight planning was carried out based on the classical aerial photogrammetric principles [13] but adapted to the new algorithms and structure from motion (SfM) strategies [14], ensuring image acquisition with forward and side overlaps of 70% and 30%, respectively. Given the format difference between the thermographic and RGB sensors, time between shots will be considered independently in order to ensure these overlaps.

The gyro-stabilized platform ensures the theoretical geometric setup of a photogrammetric aerial image capture in each shot, which stablishes that the optical axis of the camera should be zenithal. The theoretical definition of scale in digital aerial photogrammetry is related to the geometric resolution of the pixel size projected over the ground (GSD). This parameter can be calculated by considering the relationship between flight altitude over the ground, the GSD, the focal length of the sensor and the pixel size (Equation (1)). Considering that the objective of this study is not to identify small entities, and in

order to allow the procedure to be scalable to sparse 3D point clouds from other measurement systems, we fixed the target GSD for the lower resolution sensor between 10 and 15 cm.

$$\frac{f}{H} = \frac{pixel\ size}{GSD} \quad (1)$$

where f is the focal length of the sensor; H is the flight altitude over the ground and GSD is the Ground Sample Distance.

Due to the lower resolution of the thermographic images, the flight planning is performed according to the characteristics of this sensor (Figure 3), considering the planning completely valid also for the RGB sensor.

In order to locate the solar incidence deficiencies over the objects under study in the higher production time zone of the solar panels, the survey should be performed when the Sun is located at the highest point of the solar path.

2.2.2. 3D Point Cloud Reconstruction

The image-based modelling technique based on the combination of photogrammetry and computer vision algorithms allows the reconstruction of dense 3D point clouds. The absolute orientation (position and attitude) of each image is known because the position of the imaging sensors is registered with respect to the GNSS/IMU navigation devices of the aerial trike, and data acquisition is synchronized with the navigation. For this reason, using these absolute orientation as initial approximations, only an orientation refinement was required for the precise geolocation of the images.

The orientation refinement process starts with the automatic extraction and matching of image features through a SIFT [15] (Scale-Invariant Feature transform) algorithm which provides effectiveness against other feature detection algorithms. In addition, these features present optimal results for these type of aerial surveys where scale variations are minimal and perspective effects are almost nonexistent thanks to the gyro-stabilized platform. Next, taking as initial approximation the external orientation parameters provided by the GNSS system and as fixed the laboratory internal calibration parameters, an orientation refinement was performed through a global bundle adjustment between all images by means of the collinearity equations [16,17]. As a result, the spatial and angular geo-positioning of the RGB sensor was computed enabling the dense point cloud generation. Next, a dense matching method through the MicMac implementation [18] based on the semi global matching technique (SGM) [19,20] allows the generation of a dense and scaled 3D point cloud resulting from the determination of the 3D coordinates of each pixel. This process was performed using the RGB images because their higher resolution provides a 3D point cloud with higher point density than the point cloud generated from thermographic images. Regarding computation effort, the last step is the most expensive and time-consuming. All these photogrammetric tasks were performed using the Photogrammetry Workbench (PW) [21].

Last but not least, a dense 3D point cloud with thermographic information was obtained for the case study. This thermographic mapping was obtained thanks to the known baseline between both sensors which was previously calibrated in laboratory. In particular, this calibration consisted in solving the relative orientation of the thermographic camera regarding the RGB camera through the simultaneous visualization of a common pattern (the same used for the thermographic camera calibration). After the

identification of homologous entities between both sensors, the calculation of the baseline (*bx, by, bz*) and the boresight (*Rx, Ry, Rz*) values was performed.

2.2.3. Automatic Planes Segmentation

Once the 3D point cloud is generated from the RGB images and the thermographic texture is applied, the following procedure is the segmentation of the roofs. This is performed in different steps using the Point Cloud Library (PCL) [22], open source and licensed under BSD (Berkeley Software Distribution) terms, which includes a collection of state-of-the-art algorithms and tools useful for 3D processing, computer vision and robotic perception. First, ground and vegetation are removed using a pass through filter with a *Z* coordinate restriction. A pass through filter performs a simple filtering along a specified dimension removing the elements that are either inside or outside a given range. In this case, the filter gets the minimum *Z* value of the point cloud and removes all points with a *Z* value close to the minimum *Z*. The distance threshold is established as a parameter set for the user, being 5 m a recommendable value, established experimentally by the authors after the segmentation of several point clouds. In addition, although the presence of points belonging to the facades is minimal due to the vertical configuration of the capture, a conditional filter based on the angle between the normal vector of each point and the vertical axis is applied to remove these points. Then, the point cloud including the roofs is segmented using a Euclidean cluster segmentation, providing better and faster results for the subsequent extraction of the different planes of each roof [23,24] by dividing the point cloud in individual roofs. This way, RANSAC (Random Sample Consensus) algorithm [25] is applied to each roof individually for the extraction of the composing planes.

Once each roof is clustered in different planes, and the coefficients that describe each surface in a Cartesian coordinate system by the general equation of the plane are known (Equation (2)), the geometric evaluation is performed, resulting in the orientation and tilt values for each surface from which we can calculate the percentage of solar energy productivity regarding the maximum productivity of the installed solar panels.

$$Ax + By + Cz = D \tag{2}$$

where *A*, *B* and *C* are the components of the vector normal to the plane, whereas *D* is the independent term.

From the components *A*, *B* and *C* of the general equation of the plane that match with the values of the unit vector normal to the plane, denoted as $\vec{v}$ (Equation (3)) we can proceed to compute the orientation and tilt values for each roof. The orientation of the surface requires the computation of the angle between the projection of vector $\vec{v}$ on the horizontal plane and the cartesian *Y*-axis (Equation (4)). The quadrant to which the angle belongs, identified through the evaluation of the sign of *A* and *B* components of the unit vector (Figure 3 left), will allow us to get the orientation angle of the surface (Figure 3 right).

$$\vec{v} = (A, B, C) \tag{3}$$

$$\beta = arcTan\left(A/B\right) \tag{4}$$

where $\vec{v}$ is the vector normal to the plane; β is the angle between the horizontal projection of the normal vector and the cartesian *Y*-axis.

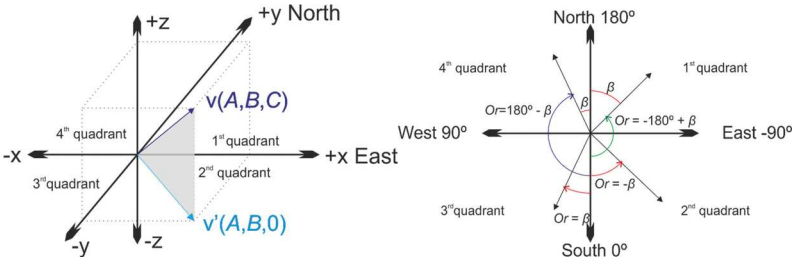

Figure 3. (**Left**) Quadrant determination from the components of the vector normal to the plane. (**Right**) Absolute orientation of the roof, denoted as "*Or*", from the angle between the projection of the vector on the horizontal plane and the cartesian *Y*-axis.

The tilt of the surface is calculated by a simple trigonometric process in a right-angled triangle where the normal vector is considered the hypotenuse and its projection on the horizontal plane ($Z = 0$) and C value the adjacent and opposite legs respectively (Figure 4) (Equations (5–7)).

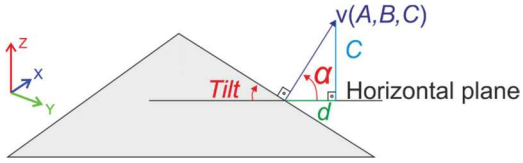

Figure 4. Tilt angle from the values of the normal vector of the plane.

$$d = \sqrt{A^2 + B^2} \tag{5}$$

$$\alpha = arcTan\left({}^{C}/_{d}\right) \tag{6}$$

$$Tilt = 90° - \alpha \tag{7}$$

where d is the module of the vector $\vec{v}$ projected on the horizontal plane ($Z = 0$); α is the angle between the horizontal plane and the normal vector of the surface; *Tilt* represents the tilt of the plane.

2.2.4. Geometric Analysis and Classification

Once the different planes of the roofs are detected and segmented, their areas, tilts and orientations are analyzed in order to perform their geometric classification. The roofs with an area smaller than required for the installation of solar panels and those with North orientation are discarded due to their inadequacy. The remaining roofs are classified in different groups according to their theoretical productivity as a function of their tilt and orientation, also taking into account the possibilities of either integrating the solar panels in the roof or installing them in configurable supports. The CTE (Technical Edification Code) sets the South orientation as the optimal position for these elements, with a tilt equal to the latitude where they are installed. However, the limits on the tilt can be computed according to the minimum efficiency allowed for the orientation of the surface using the method explained by the IDAE (Institute for Diversification and Saving of Energy) (Equations (8) and (9)) [9].

If $Tilt > 15°$

$$Solar\ energy\ losses(\%) = 100 \cdot [1.2 \cdot 10^{-4} \cdot (Tilt - \varphi + 10)^2 + 3.5 \cdot 10^{-5} \cdot Or^2] \quad (8)$$

If $Tilt < 15°$

$$Solar\ energy\ losses(\%) = 100 \cdot [1.2 \cdot 10^{-4} \cdot (Tilt - \varphi + 10)^2] \quad (9)$$

where Or is the Orientation of the plane and φ its latitude.

These limits allow the evaluation of the suitability of the surface under study and the computation of the ideal geometry of the support platforms if needed, taking into account that productivity losses cannot exceed the 20% if solar panels are installed directly over the roofs, consequently keeping the angle of solar incidence of the roof. However, productivity losses should be under 10% using the general method which implies the installation of solar panels in supports to modify the angle of solar incidence regarding the tilt of the roof.

2.2.5. Thermographic Refinement of Surfaces

Once the geometric classification is performed, the thermographic data enables the location of elements that constitute an obstacle for the installation of solar panels in order to avoid protrusions or shadows that could reduce their productivity, produced by both the elements of the roof surface and by nearby buildings. This identification of obstacles allows the analysis to find the optimal location within each roof. The existence of obstacles and anomalies in the roofs involves the presence of different materials and surfaces with different emissivity values, so the temperature detected by the thermographic images will be different even if the solar radiation received was the same. In addition, the existence of obstacles that prevent direct sunlight will be manifested by changes in the temperatures of the roof surfaces. These facts allow the location of those surfaces of the roofs affected by anomalies through the performance of a statistical study of the mean and the standard deviation of temperatures. A point will be considered as an obstacle when the difference between its temperature value and the mean temperature of the roof is higher than the standard deviation of the temperatures of the surface that is being analyzed. Considering the fact that the shadow produced by an obstacle will move following the path of the Sun, a perimeter defined by the user around each obstacle will be considered for further analysis. Although a self-occlusion analysis would be appropriate for the determination of the perimeter, the performance of this processing for each obstacle in large study areas would be a high computationally demanding task. Experimental analysis performed by the authors establishes 0.5 m as a recommendable value.

2.2.6. Location of the Most Suitable Zones

The existence of obstacles, detected by the thermographic refinement step, prevents the installation of solar panels covering the whole surface of those roofs classified by the geometric analysis as having the optimal geometry (orientation and tilt) for this purpose. Therefore, the development of a procedure to locate the optimal zones for panel installation inside optimal surfaces (Figure 5) is necessary. This task is addressed by analyzing the spatial distribution of those 3D points belonging to the optimal surfaces and not considered as obstacles. This approach is focused on four steps individually applied to each surface. (i) Projection of the point cloud to the horizontal plane in order to evaluate the surfaces in

a 2D environment, simplifying the process; (ii) Extraction of those points that describe the perimeter of the surface to evaluate (concave hull); (iii) Computation of the largest empty rectangles (no concave hull points inside); (iv) Re-projection of the largest empty rectangles to 3D. The concave hull can be defined as a set of points that enclose a concave region and define the perimeter of an unorganized set of points allowing any angle between consecutive edges. The area of the defined shape should be minimized without distorting the appearance of the point cloud.

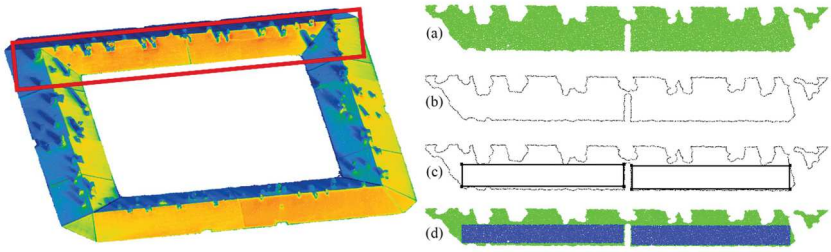

Figure 5. Procedure to locate optimal zones inside optimal surfaces. (**Left**) 3D surface selected (red rectangle) over the roof. (**Right**) From top to bottom: (**a**) surface under evaluation, without obstacles, projected to the horizontal plane; (**b**) concave hull that defines the perimeter of the surface; (**c**) largest empty rectangles inside the concave hull and (**d**) evaluated surface inliers of the largest empty rectangles re-projected to 3D.

The extraction of the points that describe the perimeter of the surface to evaluate is performed through the computation of their concave hull using an implementation of the "alpha shape" computational geometry approach based on the Delaunay triangulation [26]. The computation of the largest empty rectangles is performed through an iterative implementation presented in [27], restricting the orientation of the edges of the rectangles to the same orientation of the evaluated surface and its perpendicular vector on the horizontal plane. Finally, the largest empty rectangles are re-projected to the 3D space obtaining the georeferenced location of the optimal zones for the installation of solar panels in each roof, and their area.

2.2.7. Estimation of the Solar Irradiation

To introduce this section it will be useful to explain the differences between the terms "solar irradiance" and "solar irradiation". Solar irradiance describes the instantaneous radiant flux per unit area that is being delivered to a surface, usually expressed in W/m^2. It varies depending on the location of the surface, time and date, and atmospheric conditions, among other factors. Solar irradiation, also known as insolation and typically expressed in $kWh/m^2/a$, represents the amount of solar energy that can be collected on a surface per unit of area within a given time (*i.e.*, solar irradiance integrated over time). The use of georeferenced point clouds at this point is crucial given that solar irradiation is heavily influenced by day length and the position of the Sun (solar ephemeris), obtaining very different results for different locations on Earth. Solar irradiation may also significantly differ between building roofs in the same zone, depending on the orientation of the roof: a more favorable angle of a surface to the Sun

means better exposure and more solar energy. Two roof surfaces of the same size at the same location but different orientations (azimuth) and tilts, may drastically differ in their solar potential [28,29]. This solar irradiation value, complemented with the area of the optimal surface obtained in the previous step, allows the computation of the solar irradiation of a surface in kWh/a [6,30]. Therefore, we can say that solar irradiation on a roof surface is mainly derived of four essential geographic parameters (area, tilt, azimuth and geographic location) that may be defined as a function (Equation (10)):

$$I = \int ([\varphi, \lambda], \beta, \theta, A, [\omega]) \tag{10}$$

where I is the solar irradiation on a roof; φ is the latitude; λ is the longitude;β is the tilt of the surface; θ is the azimuth; A is the area and ω other components such as cloud cover.

Solar irradiance can be decomposed into three components [31,32]: direct irradiance, diffuse irradiance and reflected irradiance. These three components are important and significantly influence the total irradiance [33], so they have been analyzed separately in this approach. Direct and reflected irradiance and their adjustment for a tilted and oriented surface have been calculated as described in [34]. The estimation of the diffuse solar irradiance is more complex and must be adjusted to one of the several existing empirical models [35–37].

Therefore, solar irradiation can be estimated by integrating the solar irradiance over a period of time (Equation (11))

$$I = \sum_{i=start}^{end} E_i + \Delta t_i \tag{11}$$

where I is the solar irradiation; Δt_i is the length of the i^{th} time interval and E is the solar irradiance

The annual solar irradiation is calculated following the protocol used in the Solar3DCity [5,38] that includes the modeling of "real-sky" conditions through the integration of the historical EPW (Energy Plus Weather file format) weather data downloaded from the nearest weather station[39]. Solar ephemerides are from XEphem [40,41], which have been proven suitable for solar irradiation studies [42]. The computations use the empirical anisotropic irradiance model developed by [43], which was implemented in the solpy library [44]. The annual solar irradiation is then calculated for each roof surface by integrating the hourly irradiance values of the entire year. The computation of solar irradiation values can be extrapolated for every azimuth/tilt combination obtaining a function, usually called tilt-orientation-factors (TOF), which can be represented in a 3D diagram. This TOF function can be considered an additional product, since it represents the optimal tilt and orientation for a location, which is the main aim of several location-based studies [45,46].

3. Experimental Results

3.1. Study Case

The proposed methodology has been validated in a wide urban area in the city of Avila (Latitude 40°66'N, Longitude 4°70'W), with an extension of 237,250 m^2 in a rectangular shape of 365 m × 650 m, chosen due to the existence of roofs with different geometric characteristics, which is an interesting characteristic for testing the methodology.

Flight planning was performed considering the limitations of the thermographic sensor (Figure 6). Time between shots, in order to ensure properly overlapping, was stablished as 500 ms for the RGB sensor and 160 ms for the thermographic sensor, both for a flight speed of 50 km/h. Due to the speed flight, it was necessary to minimize the shutter opening time in order to avoid the motion blurring effect. This requirement needed several tests to find the optimal ISO, aperture and shutter speed configuration to ensure the correct exposure of the images minimizing the effect of any external factor that might damage the survey. As result, 409 images for the RGB sensor and 5312 images for the thermographic sensor were captured covering the whole study area. The flight altitude over the ground selected was 160 m, resulting on a GSD of 11 cm and 2 cm for the thermographic and RGB cameras, respectively.

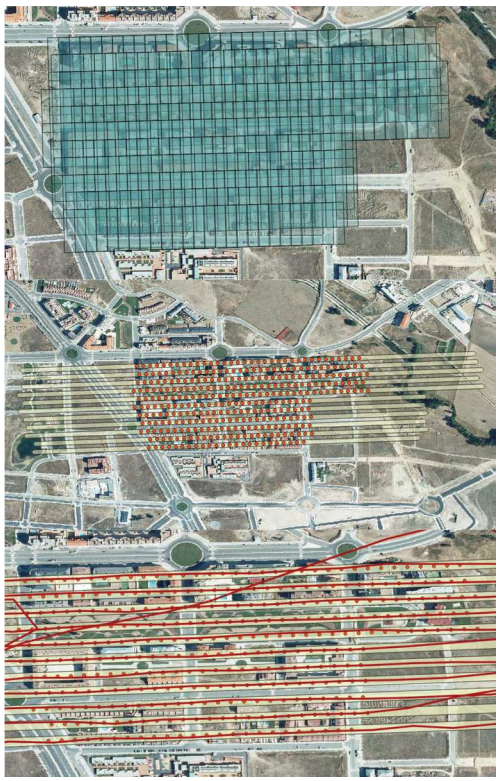

Figure 6. Flight planning: (**Top**) Areas captured by each image shot for the thermographic sensor. (**Middle**) Flight planning for the navigation of the aerial trike. (**Bottom**) GPS track after the aerial trike flight with the position of each image shot.

The full resolution RGB images were processed according to the photogrammetric and computer vision methodologies obtaining as result a point cloud of 24,858,863 points, implying an average resolution of 100 points/m^2 (≈1 point/GSD). The thermographic texture was projected over the point

cloud obtaining a hybrid 3D point cloud (Figure 7) with thermographic texture mapped over the points of the roofs.

Figure 7. Hybrid 3D point cloud generated from images captured with the RGB camera integrating thermographic texture mapped over the roofs. Areas shown in detail in consecutive figures are remarked in red.

The survey was designed in order to fulfill the conditions established by PNOA (Spanish National Plan of Aerial Orthophotography) [47]. These conditions state the required accuracy to the GSD value for the *X*, *Y* and *Z* point coordinates. In order to check compliance with these requirements, a topographic GPS survey was performed, consisting of 26 check points homogeneously distributed over the whole study area (Figure 8).

Figure 8. Check points homogeneously distributed over the whole study area.

This 3D point cloud with thermographic texture is the input of the algorithm developed. In the first step, ground, vegetation and façade points are removed using the pass through and conditional filters obtaining as result a point cloud of the roof with 8,930,030 points.

The point cloud of the roofs with thermographic texture is introduced into the segmentation process (Figure 9). The result of the Euclidean cluster segmentation is the extraction of 37 roofs that have been automatically segmented into 168 planar surfaces by the RANSAC algorithm and evaluated and classified regarding their geometrical suitability (location, area, orientation and tilt) for the installation of solar panels.

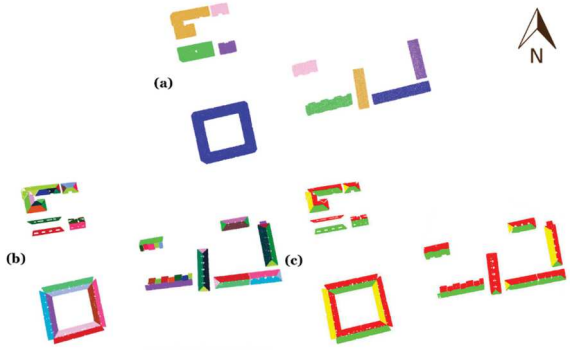

Figure 9. (**a**) Result of the extraction of each roof using the Euclidean cluster extraction algorithm. (**b**) Results of the extraction of each planar surface using the RANSAC algorithm. (**c**) Details of the previous point cloud segmented and classified by its suitability to install solar panels. (**Green**) Surfaces suitable to install solar panels without supports. (**Yellow**) Surfaces suitable to install solar panels using a support to modify the solar incidence angle. (**Red**) Surfaces not suitable for the installation of solar panels.

The radiometry of the thermographic images mapped on the 3D point cloud has been used as described in the methodology for the identification of possible obstacles (Figure 10). These obstacles have been taken into account for the location of the optimum zones for the installation of solar panels. This way, 67 zones (Figure 11) have been classified as optimal for the installation of solar panels, covering an area of 2230.77 m^2. Finally, all these data have been complemented with the estimation of the solar irradiation received by each optimal surface (Figure 12), quantifying an accumulated solar irradiation for the whole study area of 4.01×10^6 kWh/a.

The geometric and irradiation results are represented individually for each roof (Table 4). The geometric results show the azimuth (°) and tilt (°) of each surface and the area (m^2) of each optimal location. The irradiation results show the yearly solar irradiation for unit of area (kWh/m^2/a), computed from the azimuth and tilt values supported with the irradiation models and the atmospheric data, and the yearly total solar irradiation (kWh/a) of each optimal surface from its area. The area and the irradiation results of each optimal location for the installation of solar panels inside each roof surface are represented consecutively. The results of each segmented surface are recorded showing the total calculation of area and solar irradiation of the optimal areas in the whole surface.

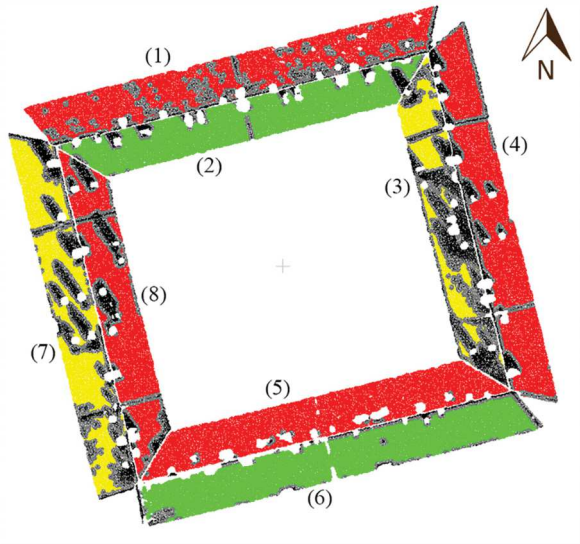

Figure 10. Detail of the point cloud segmented and classified after the thermographic analysis. (Black) Points removed by the statistical thermographic analysis. (Grey) Perimeter defined by a distance parameter around the obstacles detected to assist the optimal location of solar panels.

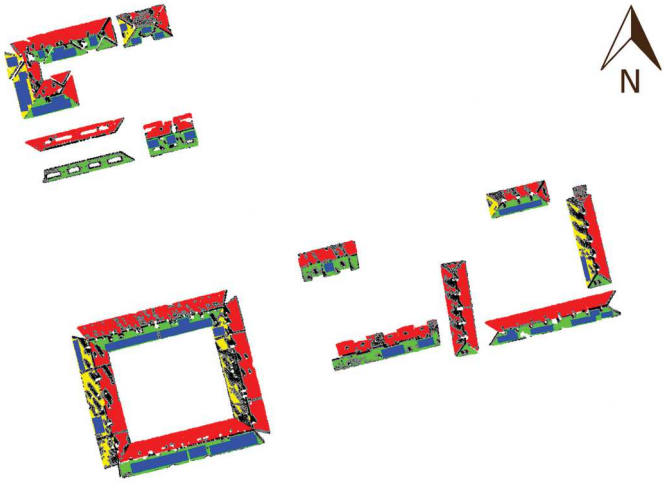

Figure 11. Georeferenced point cloud of the detail zones after the process. Optimal surfaces (rectangles) for the installation of solar panels are highlighted in blue. Roof ID's are used in Table 4.

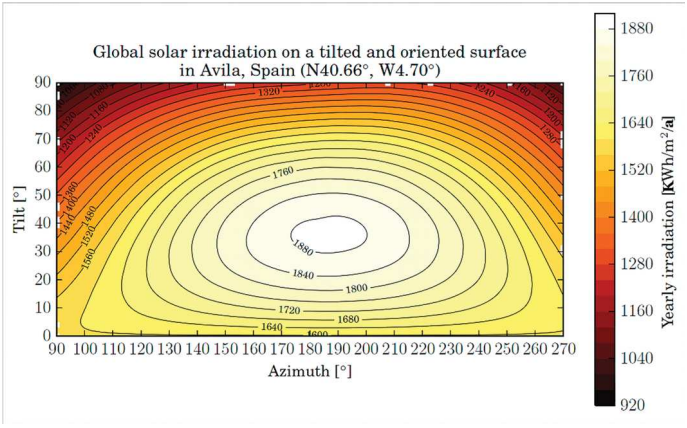

Figure 12. Tilt-orientation-factors (TOF) representation for Ávila (Spain) estimated by Solar 3D city.

Table 4. Example of the results after the processing of a roof of the dataset (roof and numbers in Figure 8).

Surface	Tilt (°)	Azimuth (°)	Yearly Solar Irradiation by m² (kWh/m²/a)	Area of Optimal Location (m²)	Yearly Total Solar Irradiation (kWh/a)
1	19.3568	346.0080	1295.011	--	--
2	19.4968	165.6463	1824.290	103.066	188,023
--	--	--	--	99.026	180,652
--	--	--	--	18.197	33,196.8
3	19.0947	156.1201	1651.910	22.938	37,891.8
4	19.3133	76.2060	1523.485	—	--
5	19.2929	346.1950	1295.834	--	--
6	19.5358	166.1320	1824.914	140.417	256,249.0
--	--	--	--	110.023	200,782.0
--	--	--	--	41.781	76,245.8
--	--	--	--	25.003	45,628.7
7	19.3667	156.0211	1652.508	38.410	63,472.9
8	19.2102	76.2400	1524.167	—	--
Total results for optimal locations of surface 2				220.289	401,871.8
Total results for optimal locations of surface 3				22.938	37,891.8
Total results for optimal locations of surface 6				317.224	578,905.5
Total results for optimal locations of surface 7				76.703	126,752.5
Total results for optimal locations of the roof				637.154	1,145,421.6

Those surfaces with North orientation have not been evaluated as not being candidates for the installation of solar panels by their geometry. For that reason, the "area of optimal location" and "yearly total solar irradiation" values of these surfaces are not available.

In order to evaluate the weaknesses and the reliability of the process, the roof planar surfaces of the study area have been analysed by visual inspection. Through this inspection 216 planar surfaces have been counted in the whole area under study. The difference of 48 planes existing between the reality and the result of the processing is distributed as follows. 42 planar surfaces have been correctly extracted by the algorithm but their evaluation has been discarded due to their minimum size that would make impossible the installation of solar panels. The 6 remaining surfaces match with roofs where the angle between their planar surfaces is next to 180° (Figure 13). In this case, RANSAC algorithm is not able to segment the roof in different planar surfaces obtaining as result of the interpolation a single horizontal plane that does not match with the reality of the roof. Surfaces whose tilt comes close to horizontal plane can be classified as non-optimal for installation of solar panels. For these reasons, it could be considered that the proposed approach is efficient enough for the location of the optimal zones to install solar panels, since it only misses 2.8% of the number of roofs of interest.

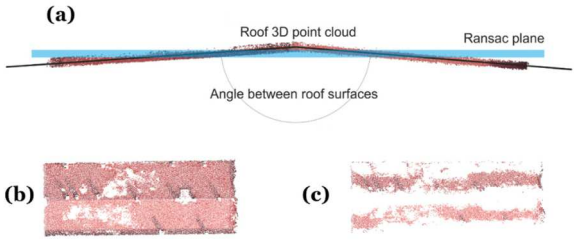

Figure 13. (**a**) Diagram of the RANSAC interpolation between two roof surfaces with an intersection angle next to 180°. (**b**) Top view of the evaluated roof. (**c**) Top view of the RANSAC algorithm results.

However, it must be emphasized that this algorithm only allows the automatic extraction of those surfaces which geometric approach can be interpreted and represented by a plane. Both curve and complex surfaces, where the installation of solar panels might be possible if complex support structures are used, are discarded.

3.2. Computing Efficiency Analysis

The machine used to perform the computation was a Microsoft Windows 8.1 workstation with 32 GB RAM, a 3.40 GHz Intel Core i5-3570K processor and an Nvidia Quadro 2000 GPU. The 3D dense point cloud generation was the most computationally demanding process investing a total of 13 h 20 min for the whole data set.

Regarding the algorithm developed for the automatic location of the best places for the installation of solar panels and the estimation of their incident solar irradiation, the execution time performed through a single thread algorithm was 26 min for the whole study area. However, multithreading computation is available, which would reduce the computation time proportionally to the number of concurrent running threads.

4. Conclusions

This article presents a methodology for the automatic processing of 3D point clouds with thermographic information for the automatic plane segmentation of the roof surfaces and their classification according to their theoretical productivity derived from their geometric characteristics (orientation, tilt and area). A refinement according to the thermographic radiometry allows the location of anomalies or obstacles that could prevent the installation of solar panels or reduce their productivity. This way, the location of the optimal zones for the installation of solar panels inside each surface is determined, avoiding obstacles detected in the thermographic refinement and allow the computation of the solar irradiation received on these zones. In particular, the hybrid product obtained provides complete thermographic and metric information of the different roof surfaces, which enables better detection, spatial location and interpretation of the suitability of each surface to harbor solar panels than traditional methods. In addition, the high level of automation of the procedure allows the evaluation of wide urban areas in a fast and accurate way, without the need to consult the technical documentation of each building.

The results of the application of the procedure are geo-referenced point clouds of the surfaces of the roofs with their geometric information (area, tilt, orientation), classified by their theoretical productivity regarding solar energy catchment. The computation has considered those elements that could reduce the productivity of the solar panels, as well as a perimeter zone potentially affected by the influence of the obstacles along the day. What is more, the procedure calculates the optimal tilt of the supports if they were necessary. In addition, results are combined in order to locate the optimal zones to install the solar panels inside each roof surface and complemented with the computation of the received solar irradiation. The latter, together with the technical characteristics of the panels to install, make possible the estimation of the productivity of the solar panels.

Thanks to that, the geometric information of the 3D point clouds has been preserved during all processing steps, enabling the performance of measurements directly on the point clouds of the segmented planes. As a result, the software developed could be used as a decision-making tool for those issues related with the dimension or type of solar panels that could be installed, calculating the actual productivity of the selected components.

In addition, the methodology proposed is valid for processing datasets captured with different airborne sensors such as LiDAR or any other RGB and thermographic sensors transported by any manned or unmanned aerial vehicle. This fact, supported with the existence of open access (public and free) LiDAR data [48] throughout the national territory, provides to this methodology and the developed software a direct applicability with minimum cost.

Regarding the efficiency of the approach developed, the methodology is applicable to the processing of entire towns or cities. Even assuming that the entire process of 3D reconstruction and the post-processing of point clouds for very large areas could imply some days of processing, the time required to perform the in-situ visual inspection (supported with technical documentation of the object) of large areas by human operators to achieve a similar result is not viable. It should also be noted that a human operator currently performs a subjective decision of the suitability of a roof to harbor solar panels (without generation of metric products and objective evaluation of obstacles). For this last reason, even in the case that a significant number of operators is available to perform the in-situ inspection in a “reasonable” period of time, the proposed approach is also an important breakthrough, especially since only an aerial

trike pilot and an expert operator are required to perform the survey and to oversee the processing and analyze the results, respectively.

The main drawback of the methodology proposed is the possibility of finding particular homogeneous surfaces on the roofs where either the photogrammetric approach or the LiDAR measurement fails. These could lead to the appearance of areas without points or too noisy that prevent the segmentation process.

This project opens new trends for future work both from a sensorial and methodological point of view. Concerning the first, the evolution of multimodal matching techniques which can be applied to the matching of RGB and thermographic images would allow the automatic registration between both data sets, avoiding the tedious manual identification of homologous points between them, in those cases where the accurate positioning of both cameras is not possible. From the methodological point of view, the integration of the Sun path enables the most accurate determination of the location of the shadow zones that could reduce the productivity of the solar panels. The procedure considers shadows produced both by obstacles located on the same roof and by adjacent buildings. Improving the latter through a self-occlusion analysis directly from the 3D geometric information, together with the incorporation of the possible surrounding orography occlusion effects will be the next milestone towards the increase of the reliability of the decision-making processes using as input the processing results obtained from this methodology.

Regarding the possibility to take advantage of the large amount of information derived from this methodology, it would be interesting to advance in the automatic generation of BIM (Building Information Modelling) and CIM (City Information Modelling), using gbXML or CityGML languages, respectively, for the representation of the 3D point cloud geometry of the segmented roofs and the inclusion of the solar irradiation estimation. Progress toward these systems will allow to work with lighter and more agile information that we can include as an additional layer on a GIS enabling the integration of this information with other data sources (cadastral information, demographic information, urban parameters, *etc.*) to perform urban energy management tasks.

Acknowledgments

Authors would like to give thanks to the Ministerio de Educación. Cultura y Deporte (Gobierno de España) for the financial support given through human resources programs (FPDI-2013-17516). Also, we thank the support given by the Ministerio de Economía y Competitividad through projects ENE2013-48015-C3-1-R.

Author Contributions

All authors conceived and designed the study. Luis López-Fernández implemented the methodology. All authors discussed the basic structure of the manuscript. Luis López-Fernández wrote the document and all authors read and approved the final manuscript.

Conflicts of Interest

The authors declare no conflict of interest

References

1. Agugiaro, G.; Remondino, F.; Stevanato, G.; De Filippi, R.; Furlanello, C. Estimation of solar radiation on building roofs in mountainous areas. In Procceedings of the ISPRS Conference, Munich, Germany, 5–7 October 2011; pp. 155–160.
2. Agugiaro, G.; Nex, F.; Remondino, F.; de Filippi, R.; Droghetti, S.; Furlanello, C. Solar radiation estimation on building roofs and web-based solar cadastre. *ISPRS Ann. Photogramm. Remote Sens. Spat. Inf. Sci.* **2012**, *1*, 177–182.
3. Hofierka, J.; Suri, M. The solar radiation model for open source gis: Implementation and applications. In Proceedings of the Open Source GIS-GRASS Users Conference, Trento, Italy, 11–13 September 2002; pp 1–19.
4. Nguyen, H.; Pearce, J.M. Estimating potential photovoltaic yield with r. Sun and the open source geographical resources analysis support system. *Sol. Energy* **2010**, *84*, 831–843.
5. Biljecki, F.; Heuvelink, G.B.M.; Ledoux, H.; Stoter, J. Propagation of positional error in 3D GIS: Estimation of the solar irradiation of building roofs. *Int. J. Geogr. Inf. Sci.* **2015**, doi:10.1080/13658816.2015.1073292.
6. Strzalka, A.; Alam, N.; Duminil, E.; Coors, V.; Eicker, U. Large scale integration of photovoltaics in cities. *Appl. Energy* **2012**, *93*, 413–421.
7. Christensen, C.; Barker, G. Effects of tilt and azimuth on annual incident solar radiation for united states locations. In Procceedings of the Solar Forum 2001: Solar Energy: The Power to Choose, Washington, DC, USA, 21–25 April 2001; pp. 225–232.
8. López, L.; Lagüela, S.; Picon, I.; González-Aguilera, D. Automatic analysis and classification of the roof surfaces for the installation of solar panels using a multi-data source and multi-sensor aerial platform. *Int. Arch. Photogramm. Remote Sens. Spat. Inf. Sci.* **2015**, *1*, 171–178.
9. IDAE. Available online: http://www.Idae.Es/uploads/documentos/documentos_5654_fv_pliego_condiciones_tecnicas_instalaciones_conectadas_a_red_c20_julio_2011_3498eaaf.Pdf (accessed on 12 January 2015).
10. Microlight Navigation. Available online: http://www.boe.es/diario_boe/txt.php?id=BOE-A-1986-11068 (accessed on 12 January 2015).
11. Premerlani, W.; Bizard, P. *Direction Cosine Matrix IMU: Theory*; DIY Drone: Washington, DC, USA, 2009.
12. Lagüela, S.; González-Jorge, H.; Armesto, J.; Herráez, J. High performance grid for the metric calibration of thermographic cameras. *Meas. Sci. Technol.* **2012**, *23*, doi:10.1088/0957-0233/23/1/015402.
13. Kraus, K; Waldhäusl, P. *Photogrammetry: Fundamentals and Standard Processes*; Dümmmler Verlag: Bonn, Germany, 1993.
14. Agarwal, S.; Furukawa, Y.; Snavely, N.; Simon, I.; Curless, B.; Seitz, S.M.; Szeliski, R. Building rome in a day. *Commun. ACM* **2011**, *54*, 105–112.
15. Lowe, D.G. Object recognition from local scale-invariant features. In Proceedings of the Seventh IEEE International Conference on Computer Vision, Kerkyra, Greece, 20–27 September 1999; pp. 1150–1157.

16. Luhmann, T.; Robson, S.; Kyle, S.; Harley, I. *Close Range Photogrammetry: Principles, Methods and Applications*; Whittles: Dunbeath, UK, 2006.
17. Deseilligny, M.P.; Clery, I. Apero, an open source bundle adjusment software for automatic calibration and orientation of set of images.In Procceedings of the International Archives of the Photogrammetry, Remote Sensing and Spatial Information Sciences, Trento, Italy, 2–4 March 2011; pp. 269–276.
18. Apero-Micmac. Available online: http://www.tapenade.gamsau.archi.fr/TAPEnADe/Tools.html (accessed on 18 June 2015).
19. Gehrke, S.; Morin, K.; Downey, M.; Boehrer, N.; Fuchs, T. Semi-global matching: An alternative to lidar for DSM generation. In Proceedings of the 2010 Canadian Geomatics Conference and Symposium of Commission I, Calgary, AB, Canada, 15–18 June 2010.
20. Hirschmuller, H. Accurate and efficient stereo processing by semi-global matching and mutual information. In Procceedings of the IEEE Computer Society Conference on Computer Vision and Pattern Recognition, San Diego, CA, USA, 20–25 June 2005; pp. 807–814.
21. Gonzalez-Aguilera, D.; Guerrero, D.; Hernandez-Lopez, D.; Rodriguez-Gonzalvez, P.; Pierrot, M.; Fernandez-Hernandez, J. Silver CATCON award, technical commission WG VI/2. In Proceeding of the XXII ISPRS Congress; Melbourne, Australia, 25 August–1 September 2012.
22. Rusu, R.B.; Cousins, S. 3D is here: Point cloud library (pcl). In Proceedings of the 2011 IEEE International Conference on Robotics and Automation (ICRA), Shanghai, China, 9–13 May 2011.
23. Gallo, O.; Manduchi, R.; Rafii, A. Cc-ransac: Fitting planes in the presence of multiple surfaces in range data. *Pattern Recognit. Lett.* **2011**, *32*, 403–410.
24. Hulik, R.; Spanel, M.; Smrz, P.; Materna, Z. Continuous plane detection in point-cloud data based on 3D hough transform. *J. Vis. Commun. Image Represent.* **2014**, *25*, 86–97.
25. Fischler, M.A.; Bolles, R.C. Random sample consensus: A paradigm for model fitting with applications to image analysis and automated cartography. *Commun. ACM* **1981**, *24*, 381–395.
26. Edelsbrunner, H.; Kirkpatrick, D.G.; Seidel, R. On the shape of a set of points in the plane. *IEEE Trans. Inf. Theory* **1983**, *29*, 551–559.
27. Orlowski, M. A new algorithm for the largest empty rectangle problem. *Algorithmica* **1990**, *5*, 65–73.
28. Yang, H.; Lu, L. The optimum tilt angles and orientations of pv claddings for building-integrated photovoltaic (BIPV) applications. *J. Sol. Energy Eng.* **2007**, *129*, 253–255.
29. Santos, T.; Gomes, N.; Freire, S.; Brito, M.; Santos, L.; Tenedório, J. Applications of solar mapping in the urban environment. *Appl. Geogr.* **2014**, *51*, 48–57.
30. Li, Z.; Zhang, Z.; Davey, K. Estimating geographical pv potential using lidar data for buildings in downtown san francisco. *Trans. GIS* **2015**, doi:10.1111/tgis.12140.
31. Šúri, M.; Hofierka, J. A new GIS-based solar radiation model and its application to photovoltaic assessments. *Trans. GIS* **2004**, *8*, 175–190.
32. Liang, J.; Gong, J.; Li, W.; Ibrahim, A.N. A visualization-oriented 3D method for efficient computation of urban solar radiation based on 3D–2D surface mapping. *Int. J. Geogr. Inf. Sci.* **2014**, *28*, 780–798.
33. Gulin, M.; Vašak, M.; Perić, N. Dynamical optimal positioning of a photovoltaic panel in all weather conditions. *Appl. Energy* **2013**, *108*, 429–438.

34. Masters, G.M. *Renewable and Efficient Electric Power Systems*; John Wiley & Sons Inc.: Hoboken, NJ, USA, 2013.
35. David, M.; Lauret, P.; Boland, J. Evaluating tilted plane models for solar radiation using comprehensive testing procedures, at a southern hemisphere location. *Renew. Energy* **2013**, *51*, 124–131.
36. Demain, C.; Journée, M.; Bertrand, C. Evaluation of different models to estimate the global solar radiation on inclined surfaces. *Renew. Energy* **2013**, *50*, 710–721.
37. Gulin, M.; Vašak, M.; Baotic, M. Estimation of the global solar irradiance on tilted surfaces. In Proceedings of the 17th International Conference on Electrical Drives and Power Electronics (EDPE 2013), Dubrovnik, Hrvatska, 2–4 October 2013; pp 334–339.
38. Solar3Dcity. Available online: https://github.com/tudelft3d/Solar3Dcity (accessed on 5 August 2015).
39. Energy Plus weather data. Available online: http://apps1.eere.energy.gov/buildings/energyplus/weatherdata_about.cfm (accessed on 5 August 2015).
40. XEphem. Available online: http://www.clearskyinstitute.com/xephem/ (accessed on 5 August 2015).
41. Meeus, J.H. *Astronomical Algorithms*; Willmann-Bell, Incorporated: Richmond, VA, USA, 1991.
42. Reda, I.; Andreas, A. Solar position algorithm for solar radiation applications. *Sol. Energy* **2004**, *76*, 577–589.
43. Perez, R.; Ineichen, P.; Seals, R.; Michalsky, J.; Stewart, R. Modeling daylight availability and irradiance components from direct and global irradiance. *Sol. Energy* **1990**, *44*, 271–289.
44. Solpy. Available online: https://github.com/nrcharles/solpy (accessed on 5 August 2015).
45. Šúri, M.; Huld, T.A.; Dunlop, E.D. Pv-gis: A web-based solar radiation database for the calculation of pv potential in europe. *Int. J. Sustain. Energy* **2005**, *24*, 55–67.
46. Rowlands, I.H.; Kemery, B.P.; Beausoleil-Morrison, I. Optimal solar-pv tilt angle and azimuth: An Ontario (Canada) case-study. *Energy Policy* **2011**, *39*, 1397–1409.
47. PNOA. Available online: https://contrataciondelestado.es/wps/wcm/connect/7050f80e-1d0c-4231-afad-5c8262529580/DOC20090605131632pdf.pdf?MOD=AJPERES (accessed on 16 August 2015).
48. LiDar Data. Available online: http://centrodedescargas.cnig.es/CentroDescargas/buscadorCatalogo.do?codFamilia=LIDAR (accessed on 12 August 2015).

Capítulo V

Automatización de procesos de inspección en plantas fotovoltaicas

5. Automatic evaluation of photovoltaic power stations from high-density RGB-T 3D point clouds

Este capítulo contiene el artículo "*Automatic evaluation of photovoltaic power stations from high-density RGB-T 3D point clouds*" publicado en la revista de alto impacto *Remote Sensing* en Junio del 2017.

5.1. Resumen

La publicación científica recogida en este capítulo representa el tercer hito establecido en la hoja de ruta de la línea de investigación. El objetivo principal es el desarrollo de una metodología que permita la automatización de las labores de inspección plantas fotovoltaicas, posibilitando estrategias de mantenimiento activo que permitan la detección precoz de patologías que limiten la productividad energética de la instalación, así como el asesoramiento en la toma de decisiones mediante la evaluación de la severidad de las patologías detectadas. En particular, el enfoque desarrollado presenta tres componentes: (1) definición de las técnicas geomáticas más adecuadas para la digitalización de plantas fotovoltaicas a gran escala desde un punto de vista cenital; (2) desarrollo de estrategias de detección y segmentación de paneles fotovoltaicos; (3) identificación y cuantificación de patologías, derivando la clasificación del panel fotovoltaico según su estado.

Dado que se propone la identificación de patologías en superficies fotovoltaicas, habitualmente de dimensión reducida, se ha elegido una plataforma aérea no tripulada (Unmanned aerial vehicle - UAV) que permita sobrevolar las plantas fotovoltaicas a escasa altura, garantizando así una resolución adecuada en las imágenes termográficas que posibilite la identificación de anomalías térmicas sobre las superficies fotovoltaicas. Debido a limitaciones en la capacidad de carga de la plataforma y las diferentes necesidades en cuanto a la altura de vuelo para el sensor RGB y

el sensor termográfico ha sido necesario realizar un vuelo independiente para cada sensor. Para este caso de estudio, se ha incorporado un sensor fotográfico compacto comercial, elegido por su versatilidad, calidad y peso. Dado que se propone la reconstrucción de superficies fotovoltaicas, caracterizadas por presentar una textura homogénea y con un patrón repetitivo sobre toda su superficie, se abordó una evaluación rigurosa del estado del arte en cuanto a los algoritmos involucrados en el proceso de reconstrucción fotogramétrica, como de técnicas de procesamiento de imágenes procedentes de otros ámbitos como, por ejemplo, la optimización de imágenes médicas [36,37]. Estas herramientas han sido implementadas en el software FME® (Feature Matching Evaluation) (ver apéndice B), desarrollado por los autores durante esta Tesis Doctoral para la evaluación y selección de las técnicas de preprocesamiento y optimización de imágenes digitales más adecuadas, que a posteriori serían incorporadas al flujo de trabajo fotogramétrico implementado en el software GRAPHOS® (ver apéndice B) mencionado anteriormente. Asimismo, se ha realizado un estudio previo de evaluación de la franja horaria y de posición solar óptimas para la detección de patologías en los paneles.

El proceso desarrollado ha sido validado con datos reales, contrastado frente a una verdad-terreno establecida en campo por un operario especializado. La metodología propuesta ha sido capaz de evaluar un área de estudio de 4000 m^2, detectando todas las patologías reflejadas en la verdad terreno sin incluir ningún falso positivo y reduciendo las discrepancias en la estimación del área dañada del 5%, obtenido por el operario experto a través de la inspección visual, al 2%. De este modo, se contrasta la viabilidad de la metodología propuesta.

Palabras clave: reconstrucción 3D; UAV; fotogrametría; visión computacional; termografía infrarroja; nube de puntos; energía fotovoltaica.

remote sensing
Article

Automatic Evaluation of Photovoltaic Power Stations from High-Density RGB-T 3D Point Clouds

Luis López-Fernández [1,*], Susana Lagüela [1,2], Jesús Fernández [1] and Diego González-Aguilera [1]

[1] Department of Cartographic and Land Engineering, University of Salamanca, Hornos Caleros, 50, 05003 Ávila, Spain; sulaguela@usal.es (S.L.); j.f.h@usal.es (J.F.); daguilera@usal.es (D.G.-A.)
[2] Applied Geotechnologies Research Group, University of Vigo, Rúa Maxwell s/n, Campus Lagoas-Marcosende, 36310 Vigo, Spain
* Correspondence: luisloez89@usal.es; Tel.: +34-920-353-500 (ext. 3820); Fax: +34-920-353-505

Received: 20 February 2017; Accepted: 13 June 2017; Published: 20 June 2017

Abstract: A low-cost unmanned aerial platform (UAV) equipped with RGB (Red, Green, Blue) and thermographic sensors is used for the acquisition of all the data needed for the automatic detection and evaluation of thermal pathologies on photovoltaic (PV) surfaces and geometric defects in the mounting on photovoltaic power stations. RGB imagery is used for the generation of a georeferenced 3D point cloud through digital image preprocessing, photogrammetric and computer vision algorithms. The point cloud is complemented with temperature values measured by the thermographic sensor and with intensity values derived from the RGB data in order to obtain a multidimensional product (5D: 3D geometry plus temperature and intensity on the visible spectrum). A segmentation workflow based on the proper integration of several state-of-the-art geomatic and mathematic techniques is applied to the 5D product for the detection and sizing of thermal pathologies and geometric defects in the mounting in the PV panels. It consists of a three-step segmentation procedure, involving first the geometric information, then the radiometric (RGB) information, and last the thermal data. No configuration of parameters is required. Thus, the methodology presented contributes to the automation of the inspection of PV farms, through the maximization of the exploitation of the data acquired in the different spectra (visible and thermal infrared bands). Results of the proposed workflow were compared with a ground truth generated according to currently established protocols and complemented with a topographic survey. The proposed methodology was able to detect all pathologies established by the ground truth without adding any false positives. Discrepancies in the measurement of damaged surfaces regarding established ground truth, which can reach the 5% of total panel surface for the visual inspection by an expert operator, decrease with the proposed methodology under the 2%. The geometric evaluation of the facilities presents discrepancies regarding the ground truth lower than one degree for angular parameters (azimuth and tilt) and lower than 0.05 m^2 for the area of each solar panel.

Keywords: 3D reconstruction; UAV; photogrammetry; computer vision; infrared thermography; point cloud; photovoltaic; solar energy; photovoltaic panel

1. Introduction

PV cells work under the photoelectric effect: when a light photon with appropriate frequency affects the cell surface, the silicon atoms are excited and an electron is ripped off them. In these conditions, each cell is converted into an electric generator that, grouped with the other cells of the PV module, produces the voltage and power supply to the external circuit. A single PV cell will overheat when it is inversely polarized or its connector is damaged. The reason is that all the energy circulates through a small part of the cell causing a significant temperature increase. Thus, regardless of the cause of the damage in the cell, the damaged surface will suffer a local overheating effect.

Thereby, heat transfer in solar energy conversion devices is one of the most important parameters to be studied for the determination of their state and their efficiency. In addition to other techniques mainly based on electrical properties [1,2], infrared thermography (IRT) has been proven as an adequate technique for the evaluation of solar energy installations [3]. The reason for the application of IRT is its capability to measure superficial temperature of objects from the radiation emitted in the thermal infrared band of the spectrum. Particularly, the detection of relative temperature differences allows de determination of thermal gradients and the detection of anomalous behaviors. Several thermographic techniques have been applied for the detection of pathologies and the evaluation of the productivity of the energy modules. These tests are mainly performed in laboratories, with limited sample size and mainly focused on the detection and precise characterization of pathologies at the level of PV cell with the aim at improving its design and performance [4–6]. In the cases where the thermographic studies were performed in-situ, two main aspects were analyzed. The first is the characterization and parameterization of the external factors that affect the absolute precision of the thermographic inspection for the performance of quantitative studies [7]. The second is the evaluation of energy facilities on small-scale communities [8].

Other pathologies that can reduce the productivity of the PV facilities are related to the geometric defects in the mounting. PV panel productivity depends directly on the incident solar radiation which is maximized when the solar rays strike orthogonally the photovoltaic surface. In this way, azimuth and tilt parameters of PV panels should be carefully defined according to the geographical location of the PV power station and validated after the construction process to confirm the fulfillment of the project guidelines.

The generation of 3D models from dense 3D point clouds is well-known in the scientific community [9–12]. These products present proven quality and applicability for the development of automatic segmentation and geolocation of elements of interest. The 3D models are generated through the segmentation and parameterization of the point clouds, using techniques that are usually based on initial pre-filtering strategies complemented with more sophisticated algorithms which take advantage of the geometric and radiometric information associated with each 3D point. Segmentation techniques can be focused on different strategies such as iterative search of basic primitives (planes, lines, etc.) [13–17]; evaluation of different sets of characteristics calculated from a point and its neighborhood [18–20]; or multiclass classification techniques based on supervised machine learning algorithms [21–23]. In this way, it is possible to locate different elements regardless the complexity of the scenario going from simple geometries such as roofs [24] or columns [25] to complex geometries such as trees [26,27], buildings [24,28,29] or vehicles [30].

The current procedure for monitoring PV stations is based on the thermographic inspection, panel-by-panel, performed in-situ by a human operator who tries to estimate the percentage of damaged panel that can affect its productivity. This procedure is not only slow and expensive but also dependent on the subjectivity and expertise of the operator. Some companies use unmanned aerial vehicles equipped with thermographic video cameras in a similar way as proposed in this studies [2,31,32], but the processing is performed manually through the visualization of the data recorded by a human operator. Thus, capture time is reduced but processing time and human subjectivity are still elements that affect the quality of the final product, although some researchers have tried to solve this subjectivity by using image processing algorithms [32]. An alternative to the use of thermographic cameras is the integration of RGB cameras in the UAV [33,34]; the main drawback of this option is that the type of defect detected depends on the flight conditions.

Both current established inspection protocols and more novel methodologies proposed by researchers are still affected by the subjectivity implicit in the inspection processes supervised by human operators. Although these novel methodologies present advances in data acquisition, they do not propose automatisms that allow speeding up the inspection processes. In addition, these novel methodologies do not provide a metric product that allows a geometric evaluation of the facilities in the inspection or construction processes. In order to improve the limitations of

the methodologies remarked above, we developed a methodology able to segment automatically individual PV panels from a precise dataset obtained with a low-cost aerial platform equipped with RGB cameras. The segmented individual panels are evaluated through the complementary thermographic information. Particularly, this methodology provides advances in the robustness and efficiency of the classical inspection and validation procedures, which performed by a human operator. Results are obtained through unsupervised detection techniques adding semantics to the geometry contained in the point cloud. This semantic information is accurately geo-referenced reaching centimeter accuracy. Thus, the inspection procedure becomes accurate, faster and not affected by human subjectivity.

The proposed methodology consists of three complementary segmentation strategies: (i) a geometrically-based segmentation process is used to extract points belonging to PV panel clusters; (ii) an intensity-based segmentation [35–37] is used to segment each individual PV panel through the detection of points belonging to their frames; and (iii) a thermographic-based segmentation is used for the detection and location of pathologies through a qualitative approach based on relative temperature differences. Thus, the computation of the thermophysical properties of PV modules or their precise absolute temperature is not necessary and the accurate location of the pathologies is performed through a custom 5D metric product. In this case, images from the RGB cameras are processed with photogrammetric and computer vision algorithms [38,39] for their orientation and generation of a 3D dense point cloud of the PV panels.

The data processing methodology is scalable to any other high-density aerial data sources such as LiDAR (Light Detection And Ranging) [40]. The use of geo-referenced 3D dense point clouds will allow the performance of accurate analysis of areas, azimuths and tilts of the PV panels which are parameters strictly linked to the productivity of PV installations [41–43].

The paper has been structured as follows: after this introduction, Section 2 includes a detailed explanation of the materials and methods used for data acquisition and processing towards the automatic segmentation of PV panels and their classification according to the existence of geometric or thermal irregularities. Section 3 is devoted to analyzing the methodology through the results of its application to a PV power station selected as case study. Finally, Section 4 establishes the most relevant conclusions of the approach. The selected case study is a PV power station located in Gotarrendura (center of Spain) (coordinates 40°42′N, 4°44′W), which is nationally well-known as pioneer in the implementation of new energy models based on the exploitation of renewable energy sources and on self-sufficiency.

2. Materials and Methods

2.1. Equipment

The acquisition of RGB imagery (Figure 1a) was performed following the photogrammetric principles using an Olympus E-PM1 camera (Table 1) equipped with a 14–42 mm lens. This camera was selected because of its relationship among versatility, quality and weight (390 g).

The thermographic data acquisition (Figure 1b) was performed with a camera Gobi 384 equipped with a thermographic lens with 10 mm focal length, providing a field of view of 51° × 40°. This camera was selected due to its compromise between lightweight and thermal resolution. Its sensor is a 384 × 288 uncooled microbolometer array able to acquire with a frame rate up to 50 fps (frames per second).

Table 1. Olympus E-PM1 camera characteristics.

Parameter	Value
Sensor Type	4/3 CMOS (Complementary Metal-Oxide Semiconductor) Sensor
Sensor size	17.3 mm × 13.0 mm
Effective Pixels	12.3 Mp
Lens	14–42 mm (crop factor = 2)

Remote Sens. **2017**, *9*, 631

Both imaging sensors are mounted on an unmanned aerial vehicle chosen with the requirements of high payload, low-cost and agility. The UAV used for the case study is an eight-propeller copter, a rotary-wing electric powered system specially designed for aerial photography. The copter has an onboard navigation system based on a GPS (Global Positioning System) receiver and an IMU (Inertial Measurement Unit). The system includes a gyrostabilized camera platform in which the sensors are mounted providing strength, anti-vibration and the possibility of making changes of orientation through digital servos. Thus, the camera can be kept in horizontal position, offsetting the motions of the equipment in flight.

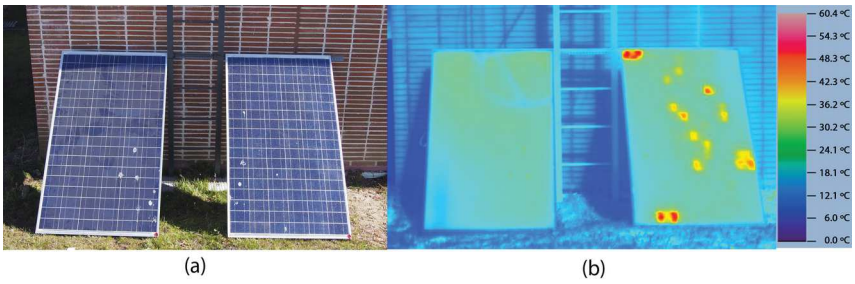

Figure 1. Example of the images generated by the different imaging sensors used: (**a**) RGB image; and (**b**) thermographic image with thermal values represented using a color map.

2.2. Methodology

The methodology proposed in this work consists of a linear workflow starting on the survey design and going to the generation of the final product (Figure 2). Survey design guidelines are proposed to obtain an imaging dataset that guarantees the correct execution of the process. RGB images are introduced in a Structure from Motion (SfM) process to obtain an accurate 3D point cloud. Information from IRT images is projected to the 3D point cloud to complement the visible spectrum radiometry associated to each 3D point. The point cloud is introduced into a geometric-based segmentation able to isolate points belonging to PV panel clusters. Isolated PV panel points clusters are processed using machine learning algorithms to perform the segmentation of each PV panel. Finally, IRT radiometry is used through a statistical approach to locate and quantify damages in the photovoltaic PV surfaces. Thus, metric information from the 3D point cloud is complemented with qualitative information from the IRT analysis, providing geometrical assembly parameters (tilt and azimuth), Thus, the 3D point cloud allows the accurate geolocation of the panels complemented with both their actual state and the location and extension of pathologies if detected.

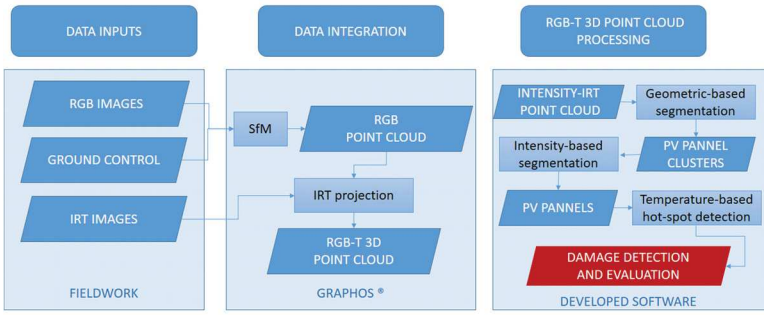

Figure 2. General workflow of the proposed methodology.

Remote Sens. **2017**, *9*, 631

2.2.1. Design of Thermographic Survey

Several external parameters influence the thermographic measurements, such as atmospheric attenuation, non-uniform heating of the object by solar incidence and reflections produced by the radiation emitted by surrounding elements and reflected on the surface under study [7]. The existence of these influential factors requires the establishment of a protocol for data acquisition with the aim of minimizing these effects and acquiring valid products for their processing and analysis.

The first rule is the adjustment of the ambient parameters in the camera for the atmospheric correction; that is, distance camera-object, ambient temperature and humidity, prior to data acquisition. This fact is essential when increasing the flying height, due to the higher quantity of atmosphere between camera and object and the consequent higher need for its correction.

The second rule is the acquisition of thermographic images with an angle of incidence of 20–25° between the normal to the object surface under study and the optical axis of the camera. Thus, the measurement of the radiation reflected from the unmanned aerial platform and other surrounding surfaces is minimized.

The third rule is the identification of the most suitable surveying conditions for the detection of the elements of interest (pathologies) and the minimization of false positives and false negatives. The survey should be performed in a period that ensures a high productivity level of the installation, preferably in the summer season. A thermographic monitoring test of the PV panels has been carried out to define these conditions. The test consisted of the thermographic monitoring of the panels with one-hour interval between sunrise and sunset. Each thermographic survey is composed by several thermograms from different points of view varying the distance between camera and object as well as the angle formed by the optical axis of the thermographic sensor and the surface under study. One set of results is shown in Figure 3 as example.

The monitoring results define the period between noon and an hour prior sunset as the valid time window for the detection of pathologies, considering that there is direct incidence of the Sun on the panels on the day of the inspection. Thus, the thermographic approach is "passive-active thermography", with the Sun acting as excitation source but no artificial heating involved [44]. Days with high cloudiness, where solar energy radiation will be limited and thus the heat transfer in the pathologies will not be enough for automatic detection, should be discarded. The central time zone of the day between noon and sun zenith angle of 23.5° should be discarded since it corresponds to the peak productivity of the PV panels and thus there is a high probability of registering as pathologies the overheated areas produced by overheating of the electronic components. Thus, the survey is proposed and performed between sun zenith angle of 23.5° and an hour prior to sunset in order to minimize the registration of false pathologies. The angle of 23.5° defines the angle of Sun declination in which solar irradiance presents a key reduction; the position of the Sun at this angle establishes summer and winter solstices. The same value of 23.5° is applied in this paper to define the zenith angle where solar radiation is at its top, with independence of the time of the year. It varies in a time frame of 1 or 2 h, depending of the time of the year and the location of the study, and can be determined using libraries such as SPA (Solar Position Algorithm) [45].

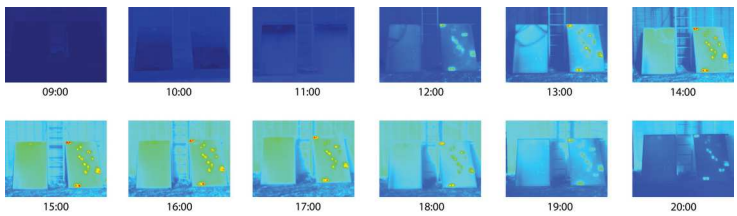

Figure 3. Thermographic monitoring of PV panels. The color palette applied is the same as in Figure 2 (from 0 to 60 °C).

Remote Sens. **2017**, *9*, 631

In order to avoid missing pathologies, attention was given to acquire thermographic images from the totality of the surface of each PV panel.

2.2.2. Flight Planning and RGB-IRT Image Acquisition

Proper flight planning is important to ensure the acquisition of high quality images and minimize acquisition time. Due to the different characteristics and purpose of the imaging sensors, different flights have been planned for the RGB and the thermographic survey. The flight planning for RGB imagery was carried out based on the classical principles of aerial photogrammetry [46] adapted to the new algorithms and strategies of Structure from Motion (SfM) [47]. The adaptation consists mainly on increasing the overlap between images (short baselines) in order to guarantee good results in dense matching. The thermographic flight planning was carried out based on the design guidelines of the thermographic survey and the desired target resolution, in such way that information acquired covers the totality of the object under study.

Thus, the flight height is determined by the characteristics of each camera (pixel size and focal length) and the geometric resolution desired for the images (known as Ground Sample Distance (GSD)), as determined by Equation (1):

$$\frac{f}{H} = \frac{pixelsize}{GSD} \quad (1)$$

where f (m) is the focal length of the sensor; H (m) is the flight height over the ground; "*pixelsize*" (m) is the size of the pixel in the sensor; and GSD (m) is the Ground Sample Distance.

2.2.3. 3D Point Cloud Reconstruction

The generation of dense 3D point clouds is performed through an image-based modeling technique consisting of the combination of digital image processing, photogrammetry and computer vision [38,48]. The procedure is carried out for the RGB images, since their higher spatial resolution in comparison to the thermographic images allows for more accurate results. Due to the homogeneous and repetitive texture of the surfaces to be reconstructed (PV panels), digital image processing algorithms are necessary to increase the radiometric information and ensure a dense reconstruction, uniform over the entire surface. RGB images are processed using a contrast preserving decolorization algorithm [49] to convert the multi-channel imagery to gray-scale images. Then, a Wallis filter [50] is applied for the radiometric equalization of the images. It performs a locally-adaptive (spatially-varying) contrast enhancement on a grey-scale raster data, as opposed to a global contrast filter, which applies the same level of contrast to the entire image. The resulting image contains greater detail in both low and high-level contrast regions, ensuring local enhancement (Figure 4). The suitability of both algorithms for this purpose is justified in several studies [51–53].

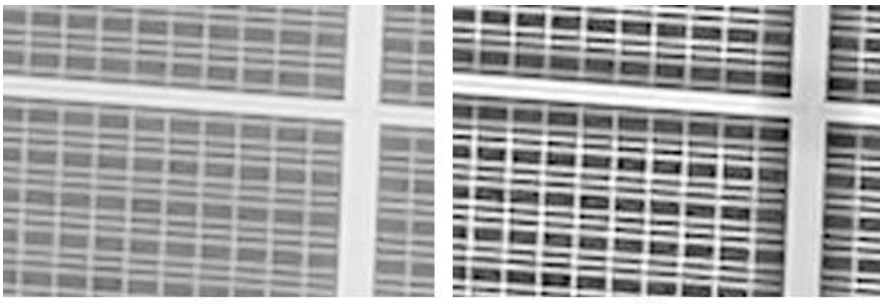

Figure 4. Image preprocessing filters: (**a**) contrast preserving decolorization algorithm; and (**b**) Wallis local contrast enhancement algorithm.

Once images are radiometrically optimized, the photogrammetric process consists of the following steps: local feature detection and matching to detect homologous tie points between images, relative image orientation to know the position of the camera in each acquisition, absolute image orientation to translate the camera positions to the global coordinate system and dense matching for the computation of the 3D coordinates of each image pixel. Further detail can be found in [38], as well as a description of GRAPHOS® software, an Open Source Photogrammetric Suite developed by the authors and used for this work.

With these steps, a dense 3D point cloud with radiometric information on the visible spectrum was obtained for the case study. This radiometric information is converted to its intensity value, represented as a digital level by the sum of the RGB channels normalized to 8 bits. The thermographic mapping of the 3D point cloud was solved through the interactive identification of homologous entities between each thermographic image and the 3D point cloud. The result obtained is a 5D point cloud (X, Y, Z, T, RGB-I) where each point (X, Y, Z) has a temperature (T) and an intensity (I) value associated. Each radiometric value is represented by the RGB conversion to a predefined color map according to intensity and temperature values, respectively (Figure 5).

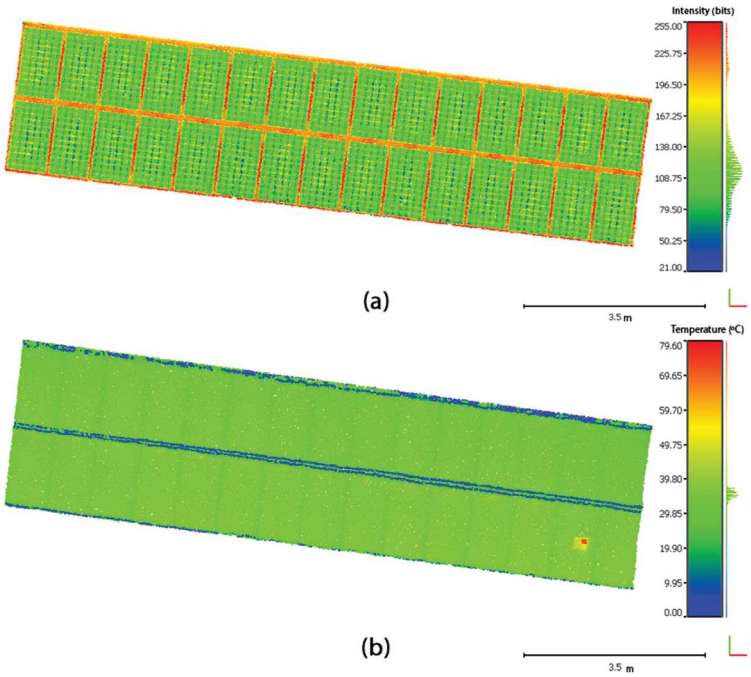

Figure 5. Multidimensional metric product: (**a**) hybrid 4D point cloud with intensity radiometry; and (**b**) hybrid 4D point cloud with thermographic radiometry.

2.2.4. Geometric-Based Segmentation of PV Panel Clusters

Once the 3D point cloud is generated from the RGB images and the thermographic texture is applied, the next procedure is the segmentation of the point cloud for the identification of individual PV panels. This is performed in several steps. First, a Voxel-Grid subsampling algorithm implemented by PCL (Point Cloud Library) [54] was used to down-sample and homogenize the density of the 3D point cloud, allowing the accurate evaluation of the spatial distribution of the points. This step allows a considerable acceleration of the processing due to the significant reduction of data volume,

and implies the creation of a "Voxel grid" (a set of tiny 3D boxes in space) over the input cloud data. Then, in each voxel (i.e., 3D box) all the points will be approximated (i.e., downsampled) by their centroid. This approach is slightly slower than their approximation to the center of the voxel, but entails a more accurate representation of the underlying surface. The result is a point cloud with homogeneous density in which the approximate quantification of areas is possible by counting points.

A progressive morphological filter is used to remove ground points by gradually increasing the evaluation window size and using elevation difference thresholds (more details about the filter can be found in [55]). An initial filtered surface is derived by applying an opening operation with a default window size to the raw point cloud. This operation is common in computer vision for object detection and background removal, and is based on a combination of dilation and erosion operations. An opening operation is then performed on the resulting surface to derive a second surface. The elevation difference of a cell between surfaces is compared to a threshold to determine if the point in this cell is a non-ground point. In the next iteration, the window size is increased, and another opening operation is applied to the filtered surface. These steps are repeated until the size of the filtering window is larger than the pre-defined largest size of non-ground objects (maximum dimension of PV panel clusters). The threshold is determined by the elevation difference and terrain slope [56].

Non-ground point clouds including the PV panels are segmented using Euclidean cluster segmentation. It consists of the evaluation of each cluster using Principal Component Analysis (PCA) to find the best-fit plane of the panel cluster based on the evaluation of the covariance matrix. This procedure is chosen because the values of the covariance matrix contain information that is suitable for the geometric characterization of each cluster of PV panels. Specifically, the eigenvector corresponding to the smallest eigenvalue contains information about the normal vector of the fitting plane, from which azimuth and tilt values can be computed as shown in [57]. The other two eigenvalues, and their corresponding eigenvectors, contain information about the direction of the principal dimensions of the cluster. Geometric outlier points are removed through the evaluation of the point-to-plane Euclidean distance.

2.2.5. Intensity-Based Segmentation of PV Panels

This step is based on the fact that PV modules are composed by two elements which are clearly distinguishable: (1) the frame that supports the panel, which is constituted by metallic profiles usually made from anodized aluminum; and (2) the PV surfaces, which are constituted by the encapsulation of diverse material layers, generally from glass, ethylene-vinyl acetate, polyvinylidene fluoride and the PV elements. Given the high contrast in the reflectance and absorbance properties between the metallic panel frames and the surface of the PV cells, the intensity attribute on the visible spectrum is used for the classification of frame/non-frame points. Assuming that the intensity distribution of reflective and non-reflective points follows a normal distribution, they can be fitted to a Gaussian Mixture Model (GMM) with two components [58]. Thus, the first component is assigned to a Gaussian distribution centered on a high intensity value (high-reflective points), while the second component is associated to the Gaussian distribution centered on a low intensity value, for non-reflective points. Thus, each point is assigned to one or the other component, as a function of their largest posterior probability.

Once high-reflective points are segmented, the detection of the points strictly belonging to the aluminum frames is performed. This step is necessary to filter out reflective points from the mounting or other surrounding elements. An iterative RANSAC (Random Sample Consensus) algorithm [59] is applied to detect lines parallel to the eigenvectors v_1 and v_2 that define the direction in each cluster of the principal dimensions of the panel as shown in Figure 6. Line directionality is complemented with geometric constraints to evaluate the continuity and length of the lines extracted. The intersections of the lines extracted projected over a horizontal reference plane are used to create a segmentation grid, used for the isolation of each PV panel of a cluster in an individual point cloud. The dimensions of each PV panel are calculated through the computation of the minimum bounding box of points

belonging to each isolated PV panel. This approach is also based on the previous results of the PCA analysis. Eigenvectors complemented with the centroid of each PV panel define a local reference coordinate system per PV panel where the minimum volume bounding box can be computed. Thus, the methodology is robust to the existence of PV panels with different dimensions in the study area.

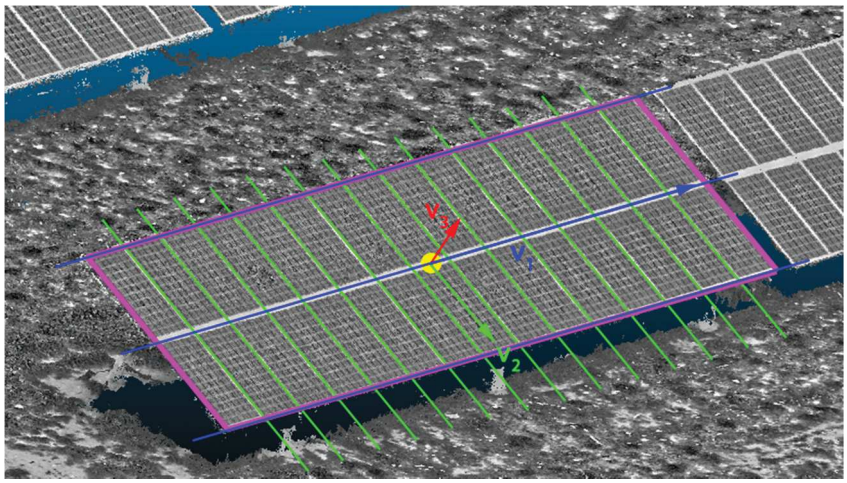

Figure 6. Distribution of RANSAC lines parallel to PCA v_1 and v_2 eigenvectors. Projection over plane $Z = 0$ is used as PV panel segmentation grid.

2.2.6. Temperature-Based Detection of Thermal Pathologies

Once each PV panel is clustered, the surface affected by significant pathologies is computed individually. In this case, the data used for segmentation are the temperature values acquired with the thermographic camera.

In this case, the median temperature of all the PV panels in a grid is computed as reference value. The median (M) is a measure of central tendency but offers the advantage of being very insensitive to the presence of outliers; thus, it was chosen as robust estimator of the central tendency of the temperatures of the PV panels, corresponding to non-damaged PV panel surface. This parameter is computed for all the panels in a grid with the aim of avoiding the use of an anomalous temperature from a defect as reference. Specifically, thermographic outliers are segmented using the Median Absolute Deviation (MAD) (Equation (2)), which is totally immune to the sample size.

$$MAD = b \times M_i\left(\left|x_i - M_j(x_j)\right|\right) \tag{2}$$

where x_j is a single sample, M_i is the median of the absolute deviation from the median of the series, $M_j(x_j)$ is the median of the n original samples and $b = 1.4826$, a constant linked to the assumption of normality of the data.

In addition, the rejection criterion of a value must be defined. As for the mean and standard deviation, it is necessary to define a level of decision, a. Miller, J. [60] proposes the following values for the level of decision: 3 (very conservative), 2.5 (moderately conservative) or 2 (poorly conservative). Points are considered as non-damaged inliers if the condition defined by equation (Equation (3)) is satisfied.

$$M - a \times MAD < x < M + a \times MAD \tag{3}$$

where, in this case study, x is the evaluated temperature value, M is the median of the temperature values and a is the level of decision selected as rejection criterion.

Remote Sens. 2017, 9, 631

Assuming that the surface of a PV panel is a perfect plane, each cluster of 4D points (geometry plus temperature) segmented as pathology is projected to a plane adjusted by least squares to enable the precise quantification of the surface affected and minimize deviations produced by the "noise" of this type of 3D products. Pathology points inside each PV panel are clustered as individual pathologies using the method based on the Euclidean distance between points explained in Section 2.2.4. The extraction of the points that describe the perimeter of each pathology cluster is performed through the computation of their concave hull using an implementation of the "alpha shape" computational geometry approach based on the Delaunay triangulation [61]. This perimeter is used to compute the area of the affected surface, obtaining the ratio of damaged surface per panel as the sum of the damaged areas divided by the total area of the panel.

3. Experimental Results

3.1. Study Case

The proposed methodology has been selected due to the knowledge of the existence of damaged PV panels, adequate for testing the methodology. The PV installations consist of 21 fixed PV panel clusters distributed in 8 equidistant lines. Each line is composed by 30 PV panels of the same type with dimensions of 1.5 m $\times$ 0.8 m. Temporal security regulations limited the inspection to the first 6 lines from south to north. The result was an aerial survey of 16 PV clusters with an extension of 4000 m^2 in a rectangular shape of 50 m $\times$ 80 m.

Regarding the RGB Flight planning (Figure 7a), time between shots was established as 2 s for an approximated flight speed of 10 km/h, ensuring image acquisition with minimum forward and side overlaps of 70% and 30%, respectively. The focal length of the RGB sensor was fixed to 14 mm and the flight altitude over the ground was 40 m, resulting on a GSD of 1 cm. As a result, 43 RGB images were acquired covering the whole study area.

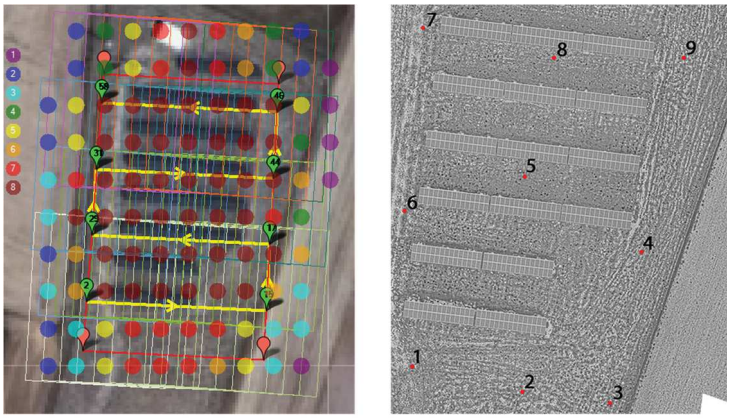

Figure 7. (**a**) Flight planning designed for acquisition of RGB imagery according to the requisites. Yellow lines represent the flight path. Green labels represent way points. Color points represent image redundancy through overlapping. In particular, the number of images with overlap are indicated in the legend with a number at the left of the image. (**b**) GCP (Ground Control Points) homogeneously distributed over the whole study area.

The full resolution RGB images were processed according to the photogrammetric and computer vision methodologies. RGB radiometry of each point was converted to its intensity value on the visible spectrum. The point cloud generated was preprocessed with the voxel grid algorithm to homogenize

point density, obtaining as result a point cloud of 39,194,155 points, implying an approximated average resolution of 10,000 points/m^2 (≈1 point/GSD^2).

In order to georeference the scene and perform the quality assessment of the survey, a topographic GNSS (Global Navigation Satellite System) survey was performed, consisting of nine GCP homogeneously distributed over the study area (Figure 7b). Because the absolute positioning accuracy of the scene should not be strict for this type of work, GCP were measured using RTK (Real Time Kinematics) positioning, ensuring that on-flight positioning precision provided by the equipment was better than 2 cm. Five of these GCP (points 1, 3, 5, 7 and 9) were used for the absolute georeferencing of the scene (Table 2) obtaining a final deviation of 0.012 m. The remaining points (points 2, 4, 6 and 8) were used as check points to perform the geometric quality assessment of the final product (Table 3) obtaining a final deviation of 0.033 m.

Table 2. Ground Control points. "*XY* error" is the root mean square error for *X* and *Y* coordinates for a GCP location, "*Z* error" is the error for *Z* coordinate for a GCP location, "RMSE" is the Root Mean Square Error for *X*, *Y*, *Z* coordinates for a GCP location and "Mean" implies averaging over all the GCP locations.

Point Label	*XY* Error (m)	*Z* Error (m)	RMSE (m)
1	0.013	−0.006	0.015
3	0.013	0.000	0.013
5	0.008	0.012	0.014
7	0.005	−0.002	0.005
9	0.008	−0.005	0.010
Mean	**0.010**	**0.007**	**0.012**

Table 3. Check points. "*XY* discrepancy" is the *X* and *Y* discrepancies obtained comparing the measurements provided by the GNSS system and the coordinates measured in the point cloud for a "Check point"; "*Z* discrepancy" is the *Z* coordinate discrepancy between coordinates measured with the GNSS system and the *Z* coordinate measured in the point cloud for a "Check point"; "Accuracy" is the root mean square discrepancy for *X*, *Y*, *Z* coordinates for a "Check point" and "Mean" implies averaging all the "Check points".

Point Label	*XY* Discrepancy (m)	*Z* Discrepancy (m)	Accuracy (m)
8	0.004	−0.014	0.015
2	0.024	−0.043	0.050
4	0.025	−0.030	0.039
6	0.011	−0.001	0.011
Mean	**0.018**	**0.027**	**0.033**

In the case of the IRT flight planning, time between shots and flight speed should be carefully correlated to ensure a high redundancy in the information to allow the supervised selection to discard blurred or radiometrically inconsistent imagery. Experience derived from previous surveys allows establishing an approximated flight speed of 10 Km/h as an appropriate parameter for the sensor used. Flight planning was designed through the definition of way points at the beginning and end of each line of PV panel clusters, guaranteeing that the vehicle overhangs the panels in the vertical of the terrain. Thermographic redundancy is guaranteed due to the high frame rate of the sensor, established in 50 fps. Flight altitude selected was 10 m over the ground, resulting on a GSD of 2.5 cm. In this case, 116 thermographic images were acquired and supervised by a human operator to select a total amount of 80 for the study of the study area. The thermographic texture was projected over the point cloud obtaining a hybrid RGB-I 3D point cloud with thermographic texture mapped over the points of the PV panels.

Remote Sens. **2017**, *9*, 631

The 5D point cloud with intensity and thermographic texture is the input of the algorithm developed. In the first step, ground points are removed using the progressive morphological filter, obtaining as result a point cloud of the PV panels with 2,524,058 points. In this first filtering process, only geometry (X, Y, Z) is required.

The point cloud of the PV panels without ground points is introduced into the geometric segmentation process resulting in the extraction of 16 PV panel clusters (Figure 8a) that have been automatically evaluated and classified regarding their geometric properties (azimuth and tilt) (Table 4) without finding any construction defect limiting the productivity of the installation. These clusters are processed with the intensity-based segmentation process, resulting in the segmentation of 480 PV panels (Figure 8b).

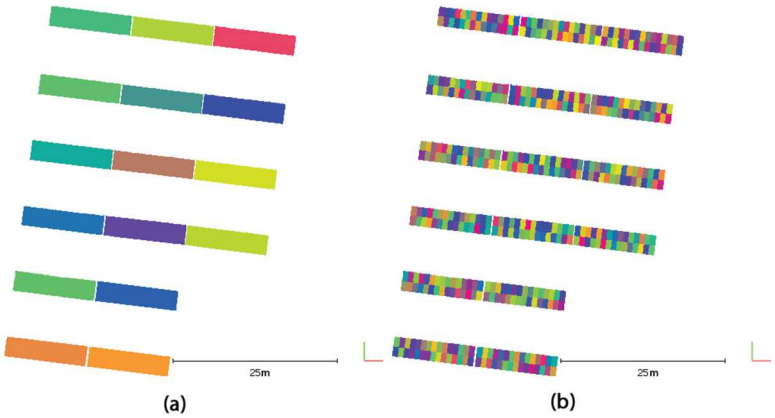

Figure 8. (**a**) Result of the extraction of PV panels cluster using the Euclidean cluster extraction algorithm. (**b**) Results of the extraction of each PV panel with the intensity-based algorithm.

Table 4. PV Cluster parameters: IDs are defined in ascendant order from north to south and from west to east.

ID	PV Cluster Parameters		PV Cluster Centroid Geolocation		
	Azimut (deg)	Tilt (deg)	X_{UTM} (m)	Y_{UTM} (m)	Height (m)
1	187.4	28.2	353,632.70	4,520,762.18	934.55
2	187.0	27.8	353,645.10	4,520,760.67	934.59
3	187.1	28.2	353,657.57	4,520,759.15	934.54
4	187.4	28.1	353,631.40	4,520,752.27	934.61
5	186.8	27.6	353,643.85	4,520,750.76	934.61
6	186.7	28.1	353,656.24	4,520,749.23	934.61
7	187.3	28.3	353,630.22	4,520,742.89	934.57
8	187.1	27.9	353,642.65	4,520,741.37	934.58
9	187.0	28.2	353,655.11	4,520,739.87	934.58
10	187.1	28.0	353,628.94	4,520,732.99	934.61
11	187.0	27.9	353,641.41	4,520,731.47	934.61
12	186.7	28.3	353,653.80	4,520,729.96	934.62
13	187.3	27.8	353,627.64	4,520,723.09	934.68
14	187.1	28.0	353,640.17	4,520,721.52	934.71
15	187.2	28.0	353,626.36	4,520,713.19	934.69
16	187.2	28.1	353,638.91	4,520,711.62	934.70
Mean	187.1	28.0			
Std. dev.	0.2	0.2			

Each individual PV panel is evaluated through temperature radiometry and classified regarding the existence of pathologies or damaged areas, quantifying the percentage of area affected (Figure 9). In total, nine damaged PV panels were detected (Table 5).

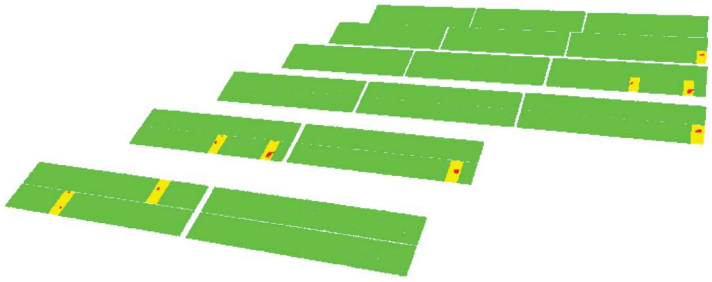

Figure 9. Result of the temperature-based detection of thermal pathologies applied to each single PV panel: (Green) Non-Damaged PV panels; (Yellow) Damaged PV panel; and (Red) Damaged surface.

Table 5. Damaged PV panel parameters: IDs are defined in ascendant order from north to south and from west to east.

ID	Damaged PV Panel Parameters		Damaged PV Panel Centroid Geolocation		
	Area (m^2)	Area (%)	X_{UTM} (m)	Y_{UTM} (m)	Height (m)
1	0.1036	8.4	353,661.82	4,520,747.87	934.25
2	0.1335	12.9	353,655.80	4,520,739.10	934.22
3	0.1362	11.9	353,659.83	4,520,738.55	934.21
4	0.0898	8.1	353,659.37	4,520,728.62	934.28
5	0.1747	13.9	353,628.32	4,520,722.30	934.30
6	0.1474	12.4	353,632.37	4,520,721.81	934.33
7	0.1180	9.6	353,644.85	4,520,720.24	934.32
8	0.0716	6.5	353,629.66	4,520,713.53	935.10
9	0.0349	2.9	353,623.83	4,520,712.81	934.31

The results are stored using both simple ASCII files and GIS Shapefiles, allowing the simple integration of the information derived from the proposed methodology with external data sources (Figure 10).

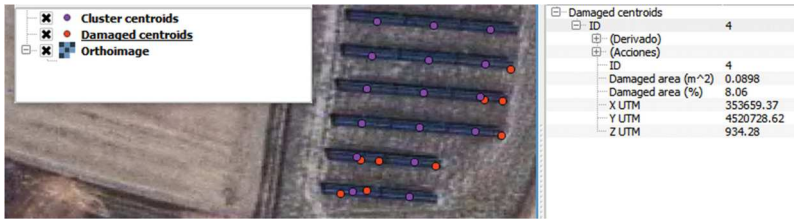

Figure 10. Result of the proposed methodology integrated with aerial orthophotography from a WMS (Web Map Service) using a GIS (Geographic Information System) client.

3.2. Accuracy Assessment

In order to perform an accuracy assessment of the proposed methodology, fieldwork has been carried out to acquire validation information that can be established as ground truth. Regarding the PV panel segmentation, the validation has consisted in a supervised monitoring of the segmentation

results. This process determines the high robustness of the segmentation process, with no lack or excess of segmentation: only the existing PV panels were segmented, with no appearance of new panels resulting from over-segmentation. The ground truth for the thermal pathologies was defined through a visual inspection. The whole case study was evaluated from the ground by an expert human operator aided with a thermographic camera. The human operator took note of all detected thermal pathologies, referencing the damaged PV panels through a predefined reference system based on their position within the facilities (line, cluster and number of panel). The proposed methodology was also able to detect all pathologies detected by the human operator in the field survey, without creating new (non-existent) ones. Regarding damaged areas of each PV panel, these were also measured by an expert operator following two different methodologies. The first, through a visual estimation of the damaged area (in percentage). This subjective approach is the usual methodology according to the established inspection protocols. The second, designed to obtain a ground truth less affected by the subjectivity of the operator and which will be used for comparison with the proposed methodology, was generated by measuring the damaged surfaces using a flexometer. Given the arbitrariness in the shape of pathologies, the areas of the thermal pathologies were calculated from their approximation to basic primitives such as rectangles (height and width measurements) and circumferences (diameter measurements), which are assumed to result in over-sized area values. The comparison between the results and the ground truth obtained (Table 6) manifests the effects of the subjectivity on the visual inspection, showing the tendency of the inspector to quantify the damaged surface by counting only the number of cells fully affected by overheating. This results in an under-sizing of the actual damaged surface because the productivity reduction by the overheating of adjacent cells is not taken into account. The comparison of the results of the proposed methodology with the ground truth established from the direct measurement of damage dimensions (with the flexometer) shows the accuracy of the proposed workflow with discrepancies lower than 2% of the panel area (1.22 m^2), corresponding to discrepancies smaller than 0.02 m^2 for the 480 solar panels evaluated.

Table 6. Verification of the damaged area per PV panel regarding ground truth: IDs are defined in ascendant order from north to south and from west to east.

Ground Truth		Compared Methodologies			
Flexometer Measurements		Visual Estimation		Proposed Workflow	
ID	Damaged Area (%)	Damaged Area (%)	Discrepancy (%)	Damaged Area (%)	Discrepancy (%)
1	9.7	5.0	4.7	8.4	1.3
2	13.6	10.0	3.6	12.9	0.7
3	13.6	10.0	3.6	11.9	1.7
4	9.0	5.0	4.0	8.1	0.9
5	15.3	10.0	5.3	13.9	1.3
6	14.1	10.0	4.1	12.4	1.7
7	11.2	5.0	6.2	9.6	1.6
8	7.1	5.0	2.1	6.5	0.6
9	3.1	2.0	1.1	2.9	0.2

Finally, regarding the geometric evaluation of the facilities, the accuracy of the azimuth and tilt of the PV clusters was tested through the comparison of the parameters extracted with the proposed methodology and the values defined as ground truth by the topographic survey (Table 7). In particular, the topographic survey was supported by the GCP and using a reflectorless total station, Trimble VX, whose precision for 3D point surveying without prism is 10 mm. Solar panels azimuth and tilt ground truth values were acquired making multiple angular and distance measurements in order to guarantee more precision and reliability. Discrepancies were lower than one degree for angular parameters, being these results completely acceptable due to the precisions established for the measurement of the GCPs used both for the absolute orientation of the point cloud and for the establishment of the reference system in the topographic survey.

Table 7. Geometric attributes verification regarding ground truth.

	Proposed Workflow		Ground Truth		Discrepancies	
ID	**Azimut (deg)**	**Tilt (deg)**	**Azimut (deg)**	**Tilt (deg)**	**Azimut (deg)**	**Tilt (deg)**
1	187.4	28.2	186.5	28.2	0.9	0.0
2	187.0	27.8	186.7	28.2	0.3	0.4
3	187.1	28.2	186.4	28.6	0.7	0.4
4	187.4	28.1	186.6	28.5	0.8	0.4
5	186.8	27.6	187.2	28.5	0.4	0.9
6	186.7	28.1	186.9	28.1	0.2	0.0
7	187.3	28.3	186.5	28.3	0.8	0.0
8	187.0	27.9	187.0	28.7	0.0	0.8
9	187.0	28.2	186.6	28.2	0.4	0.0
10	187.1	28.0	186.5	28.5	0.6	0.5
11	187.0	27.9	186.6	28.3	0.4	0.4
12	186.7	28.3	186.8	27.9	01	0.4
13	187.3	27.8	186.4	28.2	0.9	0.4
14	187.1	28.0	186.8	28.2	0.3	0.2
15	187.2	28.0	186.7	28.5	0.5	0.5
16	187.2	28.1	186.7	28.3	0.5	0.2

3.3. Computing Efficiency Analysis

The machine used to perform the computation was a Microsoft Windows 8.1 workstation with 32 GB RAM, a 3.40 GHz Intel Core i5-3570K processor and an Nvidia Quadro 2000 GPU. The dense point cloud generation was the most computationally demanding process investing a total of 17 min and 45 s for the whole data set.

Regarding the algorithm developed for the automatic classification of segmented PV panels, the execution time performed through a single thread algorithm was 2 min and 23 s for the whole study area. However, multithreading computation has been implemented, reducing computation time proportionally to the number of concurrent running threads.

4. Discussion

The advantages of using the proposed methodology for the evaluation of the state of PV panels from PV power stations include both efficiency and robustness against traditional thermographic inspection methods.

Whilst, in this study, the required data were acquired with an UAV, the proposed methodology is valid for processing datasets captured with different airborne sensors such as LiDAR or any other RGB and thermographic sensors transported by any manned or unmanned aerial vehicle that guarantees the required resolution and precision.

The quality of the product obtained with the proposed methodology relies on the factors mentioned below. The main problem is the complexity of the automation in the detection of pathologies minimizing the appearance of false positives, mainly due to the high number of factors to consider in the thermal imaging interpretation, such as environmental conditions, solar reflections, surface state of the element under study and emissivity. This problem can be solved through the election of an appropriate survey time window and the follow-up of the guidelines specified in Section 2.2.1 at the time of the thermographic acquisition. Geolocation accuracy is dependent on the quality of the ground control points used, in such way that the use of equipment and survey processes is necessary to guarantee the precision of the project.

The proposed methodology was able to detect 100% of the pathologies established in the ground truth, justifying the accuracy of the methodology for maintenance tasks. However, it is necessary to highlight that the use of the median as an estimator of the reference temperature value for non-damaged surfaces would not be a valid definition if the damages in a panel cluster cover more than one half of the surface. If this condition is fulfilled, the proposed methodology for the detection of thermal anomalies on the photovoltaic surface would set the temperature of damaged surfaces as the reference temperature value and therefore the entire surface would be classified as undamaged. However, if this

happened, the safety systems of the PV power station would generate warnings produced both by the existence of very high temperatures and by the low productivity of the system. Therefore, this is not a typical maintenance task and the proposed methodology is designed to avoid this situation, allowing the detection and resolution of incidences at an earlier stage.

Maximum discrepancies in the measurement of damaged surfaces descend from 5% for visual inspection to 2% using the proposed methodology. The geometric evaluation of the facilities presents discrepancies regarding the ground truth lower to one degree for angular parameters (azimuth and tilt). Although these accuracy improvements in the measurement of damaged areas cannot be considered as a decisive criterion for the replacement of current evaluation protocols for the proposed methodology, improvements in processing time and the metric qualities of the product are decisive to make more efficient inspection processes, especially in large PV power stations. Regarding land-based inspection methods, where the facilities are traversed by a human operator equipped with a thermographic camera and a GPS tracking system, our inspection method drastically reduces survey time reaching the day productivity of a human operator in just a few minutes of flight. In those cases where aerial vehicles are already used for the thermographic survey, the proposed unsupervised algorithm removes the tedious and manual process of thermographic interpretation and evaluation by a human operator, removing human errors and reporting metric and objective information from the evaluated facilities. In all cases, geolocation is highly improved reaching centimeter accuracy in the geolocation of pathologies. Thus, the inspection procedure becomes accurate, faster and not affected by human subjectivity.

Trying to compare the proposed methodology against other similar techniques, no similar strategies for the evaluation of large-scale PV power stations were found.

5. Conclusions

This paper presents a methodology for the automatic processing of 5D point clouds with geometric, intensity and thermographic information for the evaluation of the state of PV power stations through a completely automatic process, which allows the detection and evaluation of pathologies on the facilities. A combined geometric, radiometric (RGB intensity-based) and statistical process allows the identification of individual PV panels and the evaluation of construction inaccuracies, which could considerably limit the productivity of the facility by not taking full advantage of available solar resources. Individual clustered PV panels are evaluated again through a combined geometric, radiometric (temperature-based) and statistical approach, to detect and quantify surfaces affected by pathologies that can drastically reduce the production capacity of the element. The resulting hybrid product provides a complete and georeferenced, thermographic and metric information of the elements in the PV power station. This information enables faster and better detection of pathologies, their spatial location and interpretation of the real state of the facilities. The high-level of automation of the procedure allows the evaluation of wide PV power stations in a fast and accurate way, establishing as only limitations the capacity of payload and autonomy of the aerial platform as well as the operational capacities of the computer equipment where the process is executed.

This project opens new trends for future work both from a sensorial and methodological point of view. Concerning the first, the accurate registration of the thermographic sensor regarding the aerial platform, through the accurate relative orientation and timestamp synchronization between imaging sensors and navigation system, would allow the automatic registration between thermographic images and 3D point clouds. Robust integration of high density LiDAR sensors on UAV platforms is still a developing field. The use of these sensors will not only reduce processing time in the photogrammetric generation of 3D point clouds avoiding the difficulties related to the reconstruction of texture-less surfaces but will also provide a new radiometric value to integrate in the process, as the intensity of the returned signal is usually at near infrared wavelengths.

From a methodological point of view, regarding the possibility to take advantage of the large amount of information derived from this methodology, it would be interesting to advance in the definition of an universal data structure allowing to work with lighter and more agile information

that we can include as an additional layer on a GIS (Geographic Information System) enabling the integration of this information with other data sources (cadastral information, demographic information, urban parameters, etc.) to perform energy demand studies allowing the proper dimensioning of the installations.

Acknowledgments: Authors would like to thank the Ministry of Economy and Competitiveness, Government of Spain, for the financial support given through human resources grants (IJCI-2015-24492).

Author Contributions: All authors conceived and designed the study. L.L.F. implemented the methodology. All authors discussed the basic structure of the manuscript. L.L.F. wrote the document. All authors read and approved the final manuscript.

Conflicts of Interest: The authors declare no conflict of interest.

References

1. Ghanbari, T.; Hoseini, S.R.K. KF-based technique for detection of anomalous condition of the PV panels. *IET Gener. Transm. Distrib.* **2016**, *10*, 3698–3706. [CrossRef]
2. Hachana, O.; Tina, G.M.; Hemsas, K.E. PV array fault DiagnosticTechnique for BIPV systems. *Energy Build.* **2016**, *126*, 263–274. [CrossRef]
3. Buerhop, C.; Pickel, T.; Dalsass, M.; Scheuerpflug, H.; Camus, C.; Brabec, C.J. aIR-PV-check: A quality inspection of PV-power plants without operation interruption. In Proceedings of the IEEE 43rd Photovoltaic Specialists Conference (PVSC), Portland, OR, USA, 5–10 June 2016; pp. 1677–1681.
4. Breitenstein, O. Nondestructive local analysis of current–voltage characteristics of solar cells by lock-in thermography. *Sol. Energy Mater. Sol. Cells* **2011**, *95*, 2933–2936. [CrossRef]
5. Tsai, D.-M.; Wu, S.-C.; Li, W.-C. Defect detection of solar cells in electroluminescence images using Fourier image reconstruction. *Sol. Energy Mater. Sol. Cells* **2012**, *99*, 250–262. [CrossRef]
6. Isenberg, J.; Warta, W. Spatially resolved evaluation of power losses in industrial solar cells by illuminated lock-in thermography. *Prog. Photovolt. Res. Appl.* **2004**, *12*, 339–353. [CrossRef]
7. Krenzinger, A.; de Andrade, A.C. Accurate outdoor glass thermographic thermometry applied to solar energy devices. *Sol. Energy* **2007**, *81*, 1025–1034. [CrossRef]
8. Bazilian, M.D.; Kamalanathan, H.; Prasad, D.K. Thermographic analysis of a building integrated photovoltaic system. *Renew. Energy* **2002**, *26*, 449–461. [CrossRef]
9. Herrero-Huerta, M.; Felipe-García, B.; Belmar-Lizarán, S.; Hernández-López, D.; Rodríguez-Gonzálvez, P.; González-Aguilera, D. Dense Canopy Height Model from a low-cost photogrammetric platform and LiDAR data. *Trees* **2016**, *30*, 1287–1301. [CrossRef]
10. Fernández-Hernandez, J.; González-Aguilera, D.; Rodríguez-Gonzálvez, P.; Mancera-Taboada, J. Image-Based Modelling from Unmanned Aerial Vehicle (UAV) Photogrammetry: An Effective, Low-Cost Tool for Archaeological Applications. *Archaeometry* **2015**, *57*, 128–145. [CrossRef]
11. Chen, B.; Shi, S.; Gong, W.; Zhang, Q.; Yang, J.; Du, L.; Sun, J.; Zhang, Z.; Song, S. Multispectral LiDAR Point Cloud Classification: A Two-Step Approach. *Remote Sens.* **2017**, *9*, 373. [CrossRef]
12. Nevalainen, O.; Honkavaara, E.; Tuominen, S.; Viljanen, N.; Hakala, T.; Yu, X.; Hyyppä, J.; Saari, H.; Pölönen, I.; Imai, N.N.; et al. Individual Tree Detection and Classification with UAV-Based Photogrammetric Point Clouds and Hyperspectral Imaging. *Remote Sens.* **2017**, *9*, 185. [CrossRef]
13. Li, L.; Yang, F.; Zhu, H.; Li, D.; Li, Y.; Tang, L. An Improved RANSAC for 3D Point Cloud Plane Segmentation Based on Normal Distribution Transformation Cells. *Remote Sens.* **2017**, *9*, 433. [CrossRef]
14. Xu, B.; Jiang, W.; Shan, J.; Zhang, J.; Li, L. Investigation on the Weighted RANSAC Approaches for Building Roof Plane Segmentation from LiDAR Point Clouds. *Remote Sens.* **2016**, *8*, 5. [CrossRef]
15. Wu, T.; Hu, X.; Ye, L. Fast and Accurate Plane Segmentation of Airborne LiDAR Point Cloud Using Cross-Line Elements. *Remote Sens.* **2016**, *8*, 383. [CrossRef]
16. Arastounia, M.; Lichti, D.D. Automatic Object Extraction from Electrical Substation Point Clouds. *Remote Sens.* **2015**, *7*, 15605–15629. [CrossRef]
17. Rodríguez-Cuenca, B.; García-Cortés, S.; Ordóñez, C.; Alonso, M.C. Automatic Detection and Classification of Pole-Like Objects in Urban Point Cloud Data Using an Anomaly Detection Algorithm. *Remote Sens.* **2015**, *7*, 12680–12703. [CrossRef]

18. Li, Y.; Li, L.; Li, D.; Yang, F.; Liu, Y. A Density-Based Clustering Method for Urban Scene Mobile Laser Scanning Data Segmentation. *Remote Sens.* **2017**, *9*, 331. [CrossRef]
19. Yang, H.; Chen, W.; Qian, T.; Shen, D.; Wang, J. The Extraction of Vegetation Points from LiDAR Using 3D Fractal Dimension Analyses. *Remote Sens.* **2015**, *7*, 10815–10831. [CrossRef]
20. Aijazi, A.K.; Checchin, P.; Trassoudaine, L. Segmentation Based Classification of 3D Urban Point Clouds: A Super-Voxel Based Approach with Evaluation. *Remote Sens.* **2013**, *5*, 1624–1650. [CrossRef]
21. Zhang, J.; Lin, X.; Ning, X. SVM-Based Classification of Segmented Airborne LiDAR Point Clouds in Urban Areas. *Remote Sens.* **2013**, *5*, 3749–3775. [CrossRef]
22. Corcoran, J.; Knight, J.; Pelletier, K.; Rampi, L.; Wang, Y. The Effects of Point or Polygon Based Training Data on RandomForest Classification Accuracy of Wetlands. *Remote Sens.* **2015**, *7*, 4002–4025. [CrossRef]
23. Ni, H.; Lin, X.; Zhang, J. Classification of ALS Point Cloud with Improved Point Cloud Segmentation and Random Forests. *Remote Sens.* **2017**, *9*, 288. [CrossRef]
24. Awrangjeb, M.; Fraser, C.S. Automatic Segmentation of Raw LiDAR Data for Extraction of Building Roofs. *Remote Sens.* **2014**, *6*, 3716–3751. [CrossRef]
25. Díaz-Vilariño, L.; Conde, B.; Lagüela, S.; Lorenzo, H. Automatic Detection and Segmentation of Columns in As-Built Buildings from Point Clouds. *Remote Sens.* **2015**, *7*, 15651–15667. [CrossRef]
26. Zhang, C.; Zhou, Y.; Qiu, F. Individual Tree Segmentation from LiDAR Point Clouds for Urban Forest Inventory. *Remote Sens.* **2015**, *7*, 7892–7913. [CrossRef]
27. Weinmann, M.; Weinmann, M.; Mallet, C.; Brédif, M. A Classification-Segmentation Framework for the Detection of Individual Trees in Dense MMS Point Cloud Data Acquired in Urban Areas. *Remote Sens.* **2017**, *9*, 277. [CrossRef]
28. Yang, B.; Huang, R.; Li, J.; Tian, M.; Dai, W.; Zhong, R. Automated Reconstruction of Building LoDs from Airborne LiDAR Point Clouds Using an Improved Morphological Scale Space. *Remote Sens.* **2017**, *9*, 14. [CrossRef]
29. Gilani, S.A.N.; Awrangjeb, M.; Lu, G. An Automatic Building Extraction and Regularisation Technique Using LiDAR Point Cloud Data and Orthoimage. *Remote Sens.* **2016**, *8*, 258. [CrossRef]
30. Zhang, J.; Duan, M.; Yan, Q.; Lin, X. Automatic Vehicle Extraction from Airborne LiDAR Data Using an Object-Based Point Cloud Analysis Method. *Remote Sens.* **2014**, *6*, 8405–8423. [CrossRef]
31. Sharma, V.; Chandel, S.S. A novel study for determining early life degradation of multi-crystalline-silicon photovoltaic modules observed in western Himalayan Indian climatic conditions. *Sol. Energy* **2016**, *134*, 32–44. [CrossRef]
32. Aghaei, M.; Gandelli, A.; Grimaccia, F.; Leva, S.; Zich, R.E. IR real-time analyses for PV system monitoring by digital image processing techniques. In Proceedings of the 2015 International Conference on Event-Based Control, Communication, and Signal Processing (EBCCSP), Krakow, Poland, 17–19 June 2015; pp. 1–6.
33. Aghaei, M.; Dolara, A.; Leva, S.; Grimaccia, F. Image resolution and defects detection in PV inspection by unmanned technologies. In Proceedings of the IEEE Power and Energy Society General Meeting (PESGM), Boston, MA, USA, 17–21 July 2016; pp. 1–5.
34. Ortega-Farías, S.; Ortega-Salazar, S.; Poblete, T.; Kilic, A.; Allen, R.; Poblete-Echeverría, C.; Ahumada-Orellana, L.; Zuñiga, M.; Sepúlveda, D. Estimation of Energy Balance Components over a Drip-Irrigated Olive Orchard Using Thermal and Multispectral Cameras Placed on a Helicopter-Based Unmanned Aerial Vehicle (UAV). *Remote Sens.* **2016**, *8*, 638.
35. Riveiro, B.; Lourenço, P.B.; Oliveira, D.V.; González-Jorge, H.; Arias, P. Automatic Morphologic Analysis of Quasi-Periodic Masonry Walls from LiDAR. *Comput. Aided Civ. Infrastruct. Eng.* **2015**, *31*. [CrossRef]
36. Shen, Y.; Lindenbergh, R.; Wang, J. Change Analysis in Structural Laser Scanning Point Clouds: The Baseline Method. *Sensors* **2016**, *17*, 26. [CrossRef] [PubMed]
37. Vo, A.-V.; Truong-Hong, L.; Laefer, D.F.; Bertolotto, M. Octree-based region growing for point cloud segmentation. *ISPRS J. Photogramm. Remote Sens.* **2015**, *104*, 88–100. [CrossRef]
38. González-Aguilera, D.; López-Fernández, L.; Rodríguez-Gonzálvez, P.; Guerrero, D.; Hernandez-Lopez, D.; Remondino, F.; Menna, F.; Nocerino, E.; Toschi, I.; Ballabeni, A.; et al. Development of an all-purpose free photogrammetric tool. *Int. Arch. Photogramm. Remote Sens.* **2016**, *41*, 31–38. [CrossRef]
39. Remondino, F.; Spera, M.G.; Nocerino, E.; Menna, F.; Nex, F. State of the art in high density image matching. *Photogramm. Rec.* **2014**, *29*, 144–166. [CrossRef]

40. Roca, D.; Martínez-Sánchez, J.; Lagüela, S.; Arias, P. Novel Aerial 3D Mapping System Based on UAV Platforms and 2D Laser Scanners. *J. Sens.* **2016**, *2016*. [CrossRef]
41. Hussein, H.M.S.; Ahmad, G.E.; El-Ghetany, H.H. Performance evaluation of photovoltaic modules at different tilt angles and orientations. *Energy Convers. Manag.* **2004**, *45*, 2441–2452. [CrossRef]
42. Schuffert, S.; Voegtle, T.; Tate, N.; Ramirez, A. Quality Assessment of Roof Planes Extracted from Height Data for Solar Energy Systems by the EAGLE Platform. *Remote Sens.* **2015**, *7*, 17016–17034. [CrossRef]
43. Huang, Y.; Chen, Z.; Wu, B.; Chen, L.; Mao, W.; Zhao, F.; Wu, J.; Wu, J.; Yu, B. Estimating Roof Solar Energy Potential in the Downtown Area Using a GPU-Accelerated Solar Radiation Model and Airborne LiDAR Data. *Remote Sens.* **2015**, *7*, 17212–17233. [CrossRef]
44. Solla, M.; Lagüela, S.; Riveiro, B.; Lorenzo, H. Non-destructive testing for the analysis of moisture in the masonry arch bridge of Lubians (Spain). *Struct. Control Health Monit.* **2013**, *20*, 1366–1376. [CrossRef]
45. Reda, I.; Andreas, A. Solar position algorithm for solar radiation applications. *Sol. Energy* **2004**, *76*, 577–589. [CrossRef]
46. Tait, D.A. *Photogrammetry, vol. 1. Fundamentals and Standard Processes: Karl Kraus*; Ferdinand Dümmels Verlag: Bonn, Germany, 1993; p. 402, DM 58.00; ISBN 3-427-78681-1.
47. Agarwal, S.; Furukawa, Y.; Snavely, N.; Simon, I.; Curless, B.; Seitz, S.M.; Szeliski, R. Building Rome in a day. *Commun. ACM* **2011**, *54*, 105–112. [CrossRef]
48. Remondino, F.; El-Hakim, S. Image-based 3D modelling: A review. *Photogramm. Rec.* **2006**, *21*, 269–291. [CrossRef]
49. Lu, C.; Xu, L.; Jia, J. Contrast preserving decolorization. In Proceedings of the IEEE International Conference on Computational Photography (ICCP), Seattle, WA, USA, 28–29 April 2012; pp. 1–7.
50. Wallis, R. An approach to the space variant restoration and enhancement of images. In Proceedings of the Symposium on Current Mathematical Problems in Image Science, Monterey, CA, USA, 10–12 November 1976; pp. 329–340.
51. Remondino, F.; Zhang, L. Surface reconstruction algorithms for detailed close-range object modeling. In Proceedings of the ISPRS Commission III Symposium, Bonn, Germany, 20–22 September 2006; pp. 117–123.
52. Ohdake, T.; Chikatsu, H. 3D modelling of high relief sculpture using image-based integrated measurement system. *Int. Arch. Photogramm. Remote Sens. Spat. Inf. Sci.* **2005**, *36*, 6.
53. Seiz, G.; Baltsavias, E.P.; Gruen, A. Cloud mapping from the ground: Use of photogrammetric methods. *Photogramm. Eng. Remote Sens.* **2002**, *68*, 941–951.
54. Rusu, R.B.; Cousins, S. 3D is here: Point cloud library (pcl). In Proceedings of the 2011 IEEE International Conference on Robotics and Automation, Shanghai, China, 9–13 May 2011; pp. 1–4.
55. Zhang, K.; Chen, S.-C.; Whitman, D.; Shyu, M.-L.; Yan, J.; Zhang, C. A progressive morphological filter for removing nonground measurements from airborne LIDAR data. *IEEE Trans. Geosci. Remote Sens.* **2003**, *41*, 872–882. [CrossRef]
56. Zhang, K.; Whitman, D. Comparison of three algorithms for filtering airborne LiDAR data. *Photogramm. Eng. Remote Sens.* **2005**, *71*, 313–324. [CrossRef]
57. López-Fernández, L.; Lagüela, S.; Picón, I.; González-Aguilera, D. Large scale automatic analysis and classification of roof surfaces for the installation of solar panels using a multi-sensor aerial platform. *Remote Sens.* **2015**, *7*, 11226–11248. [CrossRef]
58. Soilán, M.; Riveiro, B.; Martínez-Sánchez, J.; Arias, P. Traffic sign detection in MLS acquired point clouds for geometric and image-based semantic inventory. *ISPRS J. Photogramm. Remote Sens.* **2016**, *114*, 92–101. [CrossRef]
59. Fischler, M.A.; Bolles, R.C. Random sample consensus: A paradigm for model fitting with applications to image analysis and automated cartography. *Commun. ACM* **1981**, *24*, 381–395. [CrossRef]
60. Miller, J. Short report: Reaction time analysis with outlier exclusion: Bias varies with sample size. *Q. J. Exp. Psychol.* **1991**, *43*, 907–912. [CrossRef]
61. Edelsbrunner, H.; Kirkpatrick, D.G.; Seidel, R. On the shape of a set of points in the plane. *IEEE Trans. Inf. Theory* **1983**, *29*, 551–559. [CrossRef]

Capítulo VI

Conclusiones y perspectivas futuras

6. Conclusiones y perspectivas futuras

En esta Tesis Doctoral se ha demostrado que las metodologías y procedimientos desarrollados contribuyen a la aplicación de las herramientas cartográficas de última generación, en combinación con sensores termográficos, en procedimientos de inspección enfocados al aprovechamiento de recursos energéticos. El producto híbrido derivado de las herramientas geomáticas, complementadas con información termográfica, permite automatizar la detección y evaluación de superficies de interés así como comportamientos anómalos sobre las mismas. Esta premisa permite su aplicación a diferentes ámbitos relacionados con el aprovechamiento de recursos energéticos, con especial atención al aprovechamiento del recurso solar. Las principales ventajas que nos ofrecen estos procedimientos son la aplicación de técnicas de inspección a gran escala, directamente inviables utilizando técnicas de inspección "in-situ" por operarios expertos o suponiendo un avance incomparable en cuanto a tiempos de ejecución. Por otro lado, se dota de una componente métrica de análisis dimensional, permitiendo el desarrollo de procesos automáticos para geolocalización y clasificación de elementos de interés en función de sus dimensiones y atributos térmicos, así como cuantificación de su efecto energético, añadiendo rigor a los procesos de inspección y eliminando la subjetividad de los métodos tradicionales de inspección visual.

A continuación, tras alcanzar de forma satisfactoria los objetivos propuestos en la línea de investigación, se desarrollan en detalle las conclusiones derivadas de cada una de las publicaciones científicas. Estas conclusiones son complementadas con un desglose de las líneas de trabajo futuras, abiertas durante el desarrollo del estudio realizado y basadas en la aplicación del mismo, que permitirán continuar avanzando en el uso de las herramientas geomáticas, en constante evolución, para un desarrollo energético sostenible.

6.1. Conclusiones

En relación a las herramientas geomáticas empleadas para la investigación, se concluye que las técnicas fotogramétricas complementadas con los más novedosos algoritmos de análisis de imágenes y visión computacional, implementados en software propio (GRAPHOS®), aplicadas a imágenes procedentes de cámaras convencionales embarcadas en diferentes plataformas de transporte aéreas, suponen una herramienta de bajo coste, rigurosa y eficaz para la documentación de escenarios de gran escala desde un punto de vista cenital. Una gran ventaja de estas herramientas reside en la capacidad de procesar imágenes procedentes de cualquier tipo de cámara, pudiendo incluso aplicar las metodologías a imágenes procedentes de sensores de baja calidad o estabilidad como los incluidos en dispositivos portátiles como "Smartphones" o "Tablets". Las estrategias de autocalibración ejecutadas durante el proceso fotogramétrico, eliminan la dependencia de procesos previos de calibración, lo que le atribuye una gran flexibilidad, acercando la tecnología a personal no cualificado. En cuanto a los sistemas de cartografiado móvil de interiores basados en sistemas de adquisición LiDAR, se contrasta su idoneidad para la documentación de escenarios interiores complejos, convirtiéndose en herramientas complementarias que aportan un gran valor añadido a los procesos de inspección energética, eliminando las limitaciones de los sistemas tradicionales de medición estática relacionadas con la necesidad de realizar numerosos estacionamientos para la documentación completa y continua de escenarios complejos, implicando tediosas tareas de registro que unifique el resultado. Suponen a mayores una amplia mejora respecto a las mediciones establecidas en los protocolos actuales, realizadas con distanciómetro y que implican una gran simplificación de la realidad constructiva, obviando la presencia de elementos que pueden ser clave en el estudio energético tales como vigas, columnas o variaciones en altura producidas por la existencia de falsos techos.

En cuanto al uso de técnicas termográficas, se ha validado su aplicabilidad para la detección de patrones térmicos anómalos sobre superficies homogéneas que permitan la detección, clasificación y cuantificación del efecto de elementos de interés. Más concretamente, se ha contrastado su aplicabilidad en diferentes escenarios y con diferentes objetivos. La primera publicación, recogida en el capítulo III, demuestra el potencial de

las mediciones termográficas para la detección y cuantificación de elementos de interés y patologías en envolventes de edificios que afecten directamente al consumo energético en labores de climatización, tales como fallos en aislamiento, presencia de humedades y filtraciones de aire, permitiendo un análisis exhaustivo del estado real del objeto de estudio de manera automática. La segunda publicación, recogida en el capítulo IV, demuestra la viabilidad de la tecnología para la detección de obstáculos que puedan impedir la instalación de paneles solares en coberturas urbanas o puedan producir sombras limitando su productividad. Para finalizar, la última publicación, recogida en el capítulo V, demuestra la viabilidad de las tecnologías geomática y termográfica para la detección automática y cuantificación de patologías en superficies fotovoltaicas que limiten la productividad energética de las instalaciones.

Toda la información resultante de los procesos desarrollados se presenta en formatos de intercambio estandarizados. Por un lado, se aporta el producto cartográfico tridimensional, en forma de nubes de puntos 3D, enriquecido con la semántica derivada del proceso. Análogamente, el producto es transformado a productos vectoriales interpretables por herramientas GIS (Geographic Information System), escalando el alcance de las metodologías propuestas, posibilitando no solo la aplicabilidad directa a escenarios similares a los casos de estudio, sino la generación de estudios de mayor complejidad mediante la integración directa con información procedente de recursos externos. De esta forma, la integración de información catastral, demográfica o de usos del suelo, entre otras, con la información derivada de los desarrollos resultantes de esta Tesis Doctoral, supone una sinergia de gran potencial, por ejemplo, para un escalado correcto de nuevas instalaciones de aprovechamiento de energía solar, en función de las necesidades energéticas de la construcción, derivadas de parámetros relacionados con su uso, el volumen de habitantes o la fecha de construcción/rehabilitación.

6.2. Perspectivas futuras

Tras el desarrollo de esta Tesis Doctoral se han abierto diferentes líneas de trabajo, enfocadas a mejorar o complementar las metodologías propuestas.

Principalmente, las líneas de trabajos venideras se presentan como un seguimiento de la evolución tecnológica en el campo de la geomática y las mediciones remotas. Son muchos los cambios experimentados en el contexto de las herramientas geomáticas durante los últimos meses. La evolución de los sistemas de medición LiDAR compactos, propulsada principalmente por los avances y necesidades derivadas del mundo de la automoción en la carrera por la conducción autónoma, ha supuesto el inicio de la integración de estos dispositivos de medición en plataformas aéreas no tripuladas. De esta forma, resulta de interés la evaluación del producto geomático derivado de la captura de datos con un sistema LiDAR de estas características integrado en una plataforma aérea de bajo coste para los procesos presentados en el capítulo IV y V de la presente Tesis Doctoral. Por otro lado, son numerosos y diversos los avances en los dispositivos enfocados al cartografíado móvil de escenarios interiores. En los últimos meses se ha presentado la comercialización de dispositivos de diferente índole, casi todos ellos impulsados por los avances en las estrategias software de posicionamiento y cartografíado simultáneo. En este ámbito, surgen plataformas de cartografíado portables basadas en las técnicas SLAM, fácilmente manejables por un operario humano, compuestas por un sensor LiDAR compacto mecanizado para dotar el instrumento de un eje de giro adicional, de forma similar a lo implementado habitualmente en los sistemas LiDAR estáticos. Por otro lado, son numerosas las compañías que distribuyen sus equipos integrados en una plataforma portable directamente a las espaldas de un operador humano (wereables MLS). Estos equipos cuentan ya con versiones que complementan la unidad central de medición LiDAR con sensores de percepción pasivos capturando información en diferentes bandas del espectro electromagnético. Todas estas nuevas tecnologías nacen enfocadas a mejorar la robustez, precisión y resolución de la generación anterior en cuanto a herramientas geomáticas enfocadas a la digitalización de escenarios interiores se refiere. De este modo resulta indispensable evaluar si estos nuevos productos suponen una mejora sustancial en los procesos resultantes de esta Tesis Doctoral.

Por otro lado, es necesario evaluar la aplicabilidad de otro tipo de sensores pasivos formadores de imagen existente, de gran impacto en la comunidad científica y muchos de ellos ya integrados en diferentes ámbitos de la ingeniería. La constante evolución de los sensores multiespectrales o

hiperespectrales, capaces de captar información procedente de diferentes bandas del espectro electromagnético, proporciona la oportunidad de establecer nuevas hipótesis de trabajo en el marco presentado en esta línea de investigación. De este modo, resulta de especial interés la evaluación de la respuesta de las superficies fotovoltaicas en diferentes bandas del espectro electrómagnetico, en un intento de detectar otras patologías que pueda condicionar su productividad y resulten indetectables en mediciones en el espectro visible o infrarrojo térmico, así como de permitir la caracterización de dichas patologías mejorando su diagnóstico. Estos instrumentos podrían suponer también una herramienta capaz de monitorizar el comportamiento de superficies fotovoltaicas para una detección prematura de las patologías.

En cuanto a la complementación de los resultados actuales con información procedente de recursos externos, se plantea la integración de factores demográficos y catastrales para un dimensionamiento adecuado de las instalaciones productoras de energía. En la actualidad el principal problema no reside en la producción de energía sino en su almacenamiento y transporte, implicando que esta deba ser consumida con la mayor celeridad posible. De este modo, un correcto dimensionamiento que adapte la producción energética a las necesidades reales de la comunidad parece un factor clave del proceso.

Asimismo, se plantea el uso de las herramientas geomáticas para la optimización o aprovechamiento de recursos energéticos renovables de otra naturaleza. Si bien la termografía, junto con los ultrasonidos, es una técnica estandarizada en procesos de inspección de diferentes componentes en aerogeneradores, es posible que la geometría derivada de las técnicas geomáticas de reconstrucción 3D puedan aportar valor añadido a estos procesos de inspección. Por otro lado, el uso de técnicas termográficas y geomáticas se encuentra en un estadio completamente experimental y en pleno desarrollo en campos como la geotermia. En este campo, disponemos de líneas de investigación activas, pendientes de ser financiadas por el proyecto de investigación MENInGEs presentado a la convocatoria Retos del MINECO (Ministerio de Economía, Industria y Competitividad) en la presente anualidad. Este proyecto propone evaluar, cuantificar y modelar el recurso geotérmico de muy baja y muy alta temperatura. Dado que la temperatura en los primeros metros de la corteza terrestre (de 1 a 3 metros) se ve afectada por factores como la acción solar,

la acumulación de calor en el entorno o las precipitaciones, los estudios recogidos en esta Tesis Doctoral en cuanto a la irradiación solar recibida por una superficie formarán parte del estudio del recurso geotérmico de muy baja temperatura.

La importancia de la realización de balances energéticos con conocimiento de la geometría se muestra también a través de sus aplicaciones biológicas, como en el caso del estudio realizado durante el desarrollo de la Tesis Doctoral, titulado "*Close-Range Photogrammetry and Infrared Imaging for Non-Invasive Honeybee Hive Population Assessment*" presentado para su publicación en la revista "Journal of Apicultural Research". Este trabajo aplica técnicas fotogramétricas complementadas con información termográfica para generación de un modelo 3D térmico de la envolvente de la colmena. A este modelo se le aplican correcciones relacionadas con las propiedades termofísicas de los materiales de la colmena para derivar la temperatura interior de la misma. De este modo, se posibilita la evaluación de la población de colmenas productoras de miel utilizando técnicas no invasivas, lo que permite conocer su estado sin una interacción intrusiva que podría suponer la extinción de la misma por una caída brusca de la temperatura.

Referencias

Referencias

1. Paquete Europeo de Energía y Cambio Climático http://www.mapama.gob.es/es/cambio-climatico/temas/el-proceso-internacional-de-lucha-contra-el-cambio-climatico/la-union-europea/. Consultado el 16 de Julio de 2017.

2. Marco de Políticas de Energía y Cambio Climático 2021-2030 https://ec.europa.eu/clima/policies/strategies/2030_es. Consultado el 16 de Julio de 2017.

3. UNFCCC, 2015. Paris Agreement to the United Nations on Climate Change. UN Doc FCCC/CP/2015/L.9, Dec. 12, 2015.

4. IPCC (Intergovernmental Panel on Climate Change). Climate Change 2014 Synthesis Report, Ginebra. 2014.

5. The World Bank - Fossil fuel energy consumption (% of total) http://data.worldbank.org/indicator/EG.USE.COMM.FO.ZS. Consultado el 16 de Julio de 2017

6. Winde, F.; Brugge, D.; Nidecker, A.; Ruegg, U. Uranium from Africa--An overview on past and current mining activities: Re-appraising associated risks and chances in a global context. *J. African Earth Sci.* 2017, *129*, 759–778.

7. Wada, T.; Nemoto, Y.; Shimamura, S.; Fujita, T.; Mizuno, T.; Sohtome, T.; Kamiyama, K.; Morita, T.; Igarashi, S. Effects of the nuclear disaster on marine products in Fukushima. *J. Environ. Radioact.* 2013, *124*, 246–254.

8. Yasumura, S.; Goto, A.; Yamazaki, S.; Reich, M. R. Excess mortality among relocated institutionalized elderly after the Fukushima nuclear disaster. *Public Health* 2013, *127*, 186–188.

9. Baker, R. J.; Chesser, R. K. The Chornobyl nuclear disaster and subsequent creation of a wildlife preserve. *Environ. Toxicol. Chem.* 2000, *19*, 1231–1232.

10. Rocha, M., Parra, P.Y., Sferra, F., Schaeffer, M., Roming, N., Ancygier, A., Ural, U., Hare, B. A stress test for coal in Europe under the Paris Agreement. *New York Clim. Anal.* 2017.

11. Chazan, G. Eon and RWE pursue radical restructurings. *Financ. Times* 2016, *18*, 2016.

12. Eurostat Propuesta de Directiva del Parlamento Europeo y del Consejo relativa al fomento del uso de energía procedente de fuentes renovables (refundición). 2015.

13. Agency, I. E. *Key world energy statistics*; International Energy Agency, 2007.

14. Hesse, C.; Kutterer, H. A mobile mapping system using kinematic terrestrial laser scanning (KTLS) for image acquisition. In *Proceedings of the 8th Conference on Optical*; 2007.

15. El-Hakim, S. F.; Boulanger, P. Mobile system for indoor 3-D mapping and creating virtual environments 1999.

16. Oliensis, J. A critique of structure-from-motion algorithms. *Comput. Vis. Image Underst.* 2000, *80*, 172–214.

17. Naikal, N.; Kua, J.; Zakhor, A. *Image augmented laser scan matching for indoor localization*; 2009.

18. Zarchan, P.; Musoff, H. Fundamentals of Kalman Filtering: A practical Approach vol. 232: American Institute of Aeronautics and Astronautics 2009.

19. Bailey, T.; Durrant-Whyte, H. Simultaneous localization and mapping (SLAM): Part II. *IEEE Robot. Autom. Mag.* 2006, *13*, 108–117.

20. Maini, R.; Aggarwal, H. A comprehensive review of image enhancement techniques. *arXiv Prepr. arXiv1003.4053* 2010.

21. Verhoeven, G.; Karel, W.; Stuhec, S.; Doneus, M.; Trinks, I.; Pfeifer, N. Mind your Grey Tones-Examining the Influence of Decolourization Methods on Interest Point Extraction and Matching for Architectural Image-Based Modelling. *Int. Arch. Photogramm. Remote Sens. Spat. Inf. Sci.* 2015, *40*, 307.

22. Apollonio, F. I.; Ballabeni, A.; Gaiani, M.; Remondino, F. Evaluation of feature-based methods for automated network orientation. *Int. Arch. Photogramm. Remote Sens. Spat. Inf. Sci.* 2014, *40*, 47.

23. Hartmann, W.; Havlena, M.; Schindler, K. Recent developments in large-scale tie-point matching. *ISPRS J. Photogramm. Remote Sens.* 2015.

24. Agarwal, S.; Snavely, N.; Seitz, S. M.; Szeliski, R. Bundle adjustment in the large. In *Computer Vision–ECCV 2010*; Springer, 2010; pp. 29–42.

25. Wu, C.; Agarwal, S.; Curless, B.; Seitz, S. M. Multicore bundle adjustment. In *Computer Vision and Pattern Recognition (CVPR), 2011 IEEE Conference on*; 2011; pp. 3057–3064.

26. Remondino, F.; Spera, M. G.; Nocerino, E.; Menna, F.; Nex, F. State of the art in high density image matching. *Photogramm. Rec.* 2014, *29*, 144–166.

27. Martín, M. R.; Lopez, S. L.; Aguilera, D. G.; Vilariño, L. D. Termografía Activa, Parte 1: Enfoque Teórico de la Captación Infrarroja, Proesamiento de Datos y Clasificación. *Dyna* 2015, *90*, 456–460.

28. Lee, J. H.; Choi, J.-S.; Jeon, E. S.; Kim, Y. G.; Le, T. T.; Shin, K. Y.; Lee, H. C.; Park, K. R. Robust pedestrian detection by combining visible and thermal infrared cameras. *Sensors* 2015, *15*, 10580–10615.

29. Ring, E. F. J. Progress in the measurement of human body temperature. *IEEE Eng. Med. Biol. Mag.* 1998, *17*, 19–24.

30. Bitar, D.; Goubar, A.; Desenclos, J. C.; others International travels and fever screening during epidemics: a literature review on the effectiveness and potential use of non-contact infrared thermometers. *Euro Surveill* 2009, *14*, 19115.

31. Kylili, A.; Fokaides, P. A.; Christou, P.; Kalogirou, S. A. Infrared thermography (IRT) applications for building diagnostics: A review. *Appl. Energy* 2014, *134*, 531–549.

32. Jadin, M. S.; Taib, S. Recent progress in diagnosing the reliability of electrical equipment by using infrared thermography. *Infrared Phys. Technol.* 2012, *55*, 236–245.

33. Martín, M. R. Termografía activa y fotogrametría de objeto cercano para la detección, medición y evaluación de defectos e imperfecciones en uniones soldadas. 2015.

34. 2020, H. Secure, Clean and Efficient Energy https://ec.europa.eu/programmes/horizon2020/en/h2020-section/secure-clean-and-efficient-energy. Consultado el 16 de Julio de 2017.

35. 2020, H. Climate Action, Environment, Resource Efficiency and Raw Materials https://ec.europa.eu/programmes/horizon2020/en/h2020-

section/climate-action-environment-resource-efficiency-and-raw-materials. Consultado el 16 de Julio de 2017.

36. Kimori, Y. Morphological image processing for quantitative shape analysis of biomedical structures: effective contrast enhancement. *J. Synchrotron Radiat.* 2013, *20*, 848–853.

37. Sundaram, M.; Ramar, K.; Arumugam, N.; Prabin, G. Histogram based contrast enhancement for mammogram images. In *Signal Processing, Communication, Computing and Networking Technologies (ICSCCN), 2011 International Conference on*; 2011; pp. 842–846.

Apéndice A

Indexación y factor de impacto de las publicaciones

Publicación I

- *Thermographic and mobile indoor mapping for the computation of energy losses in buildings*

Journal:	**Indoor and Built Evironment**
Editorial	**SAGE Publications LTD**
ISSN:	**1420-326X**
Impact factor (2016):	**1.181**
Ranking:	**32/61**
Quartile:	**Q3**

INDOOR AND BUILT ENVIRONMENT

ISSN: 1420-326X

SAGE PUBLICATIONS LTD
1 OLIVERS YARD, 55 CITY ROAD, LONDON EC1Y 1SP, ENGLAND
ENGLAND

Titles
ISO: Indoor Built Environ.
JCR Abbrev: INDOOR BUILT ENVIRON

Categories
CONSTRUCTION & BUILDING TECHNOLOGY - SCIE;
ENGINEERING, ENVIRONMENTAL - SCIE;
PUBLIC, ENVIRONMENTAL & OCCUPATIONAL HEALTH - SCIE;

Languages

6 Issues/Year;
Suppressed in 2012

Key Indicators

Year	Total Cites Graph	Journal Impact Factor Graph	Impact Factor Without Journal Self Cites Graph	5 Year Impact Factor Graph	Immediacy Index Graph	Citable Items Graph	Cited Half-Life Graph	Citing Half-Life Graph	Eigenfacto Score Graph	Article Influence Score Graph	% Articles in Citable Items Graph	Normalize Eigenfacto Graph	Average JIF Percentile Graph
2016	1,069	1.181	0.994	1.318	0.172	99	5.9	9.9	0.00164	0.284	94.95	0.18838	30.934
2015	893	0.943	0.750	1.076	0.118	85	6.5	9.9	0.00150	0.260	98.82	0.17047	31.133
2014	835	1.225	0.718	1.280	0.152	92	5.2	9.0	0.00125	0.230	96.74	0.14013	44.723
2013	836	1.716	0.723	1.494	0.179	84	4.5	9.2	0.00119	0.226	98.81	0.13089	63.057
2011	668	2.000	0.449	1.418	0.385	65	4.1	8.0	0.00103	0.187	98.46	Not A...	72.308
2010	430	0.634	0.473	0.756	0.286	63	5.4	>10.0	0.00123	0.215	96.83	Not A...	27.552
2009	328	0.698	0.543	0.695	0.145	55	4.7	7.9	0.00118	0.200	100.00	Not A...	28.575
2008	317	0.629	0.427	0.716	0.140	57	4.9	>10.0	0.00120	0.191	89.47	Not A...	24.553
2007	235	0.500	0.250	0.584	0.153	59	4.4	8.0	0.00083	0.139	98.31	Not A...	20.830

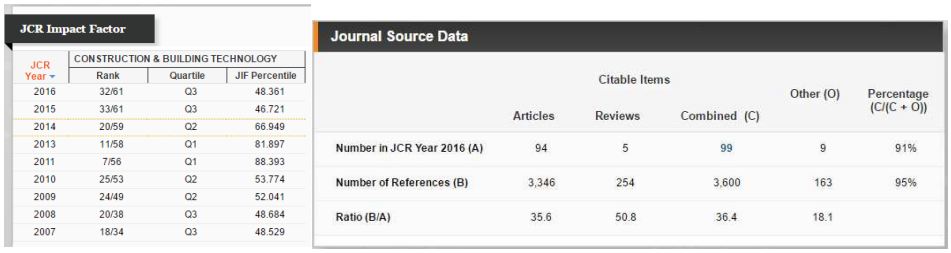

JCR Impact Factor

JCR Year	CONSTRUCTION & BUILDING TECHNOLOGY		
	Rank	Quartile	JIF Percentile
2016	32/61	Q3	48.361
2015	33/61	Q3	46.721
2014	20/59	Q2	66.949
2013	11/58	Q1	81.897
2011	7/56	Q1	88.393
2010	25/53	Q2	53.774
2009	24/49	Q2	52.041
2008	20/38	Q3	48.684
2007	18/34	Q3	48.529

Journal Source Data

	Citable Items			Other (O)	Percentage (C/(C + O))
	Articles	Reviews	Combined (C)		
Number in JCR Year 2016 (A)	94	5	99	9	91%
Number of References (B)	3,346	254	3,600	163	95%
Ratio (B/A)	35.6	50.8	36.4	18.1	

Journal Impact Factor

Cites in 2016 to items published in: 2015 =76, 2014 =133, Sum: 209

Number of items published in: 2015 =85, 2014 =92, Sum: 177

$$\text{Calculation} = \frac{\text{Cites to recent items}}{\text{Number of recent items}} = \frac{209}{177} = \mathbf{1.181}$$

Impact Factor Without Journal Self Cites

The tables show the contribution of the journals self cites to its impact factor. This information is also represented in the cited journal graph.

Total Cites	1069	Self Cites	165(15.435% of 1069)
Cites to Years Used in Impact Factor Calculation	209	Self Cites to Years Used in Impact Factor Calculation	33(15.789% of 209)
Impact Factor	1.181	Impact Factor without Self Cites	0.994

5-Year Journal Impact Factor

Cites in 2016 to items published in: 2015 =76, 2014 =133, 2013 =125, 2012 =81, 2011 =115, Sum: 530

Number of items published in: 2015 =85, 2014 =92, 2013 =84, 2012 =76, 2011 =65, Sum: 402

$$\text{Calculation:} \frac{\text{Cites to recent items}}{\text{Number of recent items}} = \frac{530}{402} = \mathbf{1.318}$$

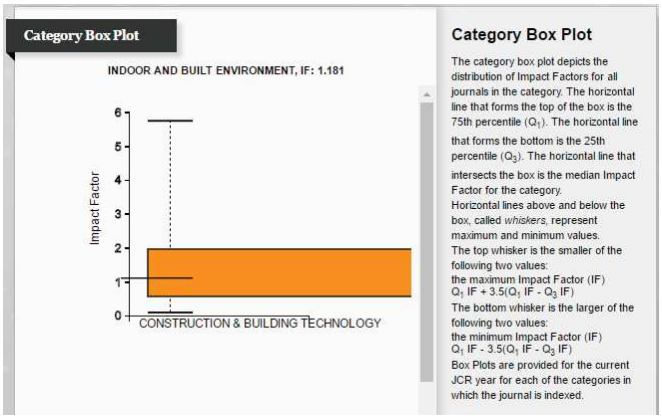
Category Box Plot
INDOOR AND BUILT ENVIRONMENT, IF: 1.181
Impact Factor
6
5
4
3
2
1
0
CONSTRUCTION & BUILDING TECHNOLOGY
Category Box Plot
The category box plot depicts the distribution of Impact Factors for all journals in the category. The horizontal line that forms the top of the box is the 75th percentile (Q_1). The horizontal line that forms the bottom is the 25th percentile (Q_3). The horizontal line that intersects the box is the median Impact Factor for the category.
Horizontal lines above and below the box, called *whiskers*, represent maximum and minimum values.
The top whisker is the smaller of the following two values:
the maximum Impact Factor (IF)
Q_1 IF + 3.5(Q_1 IF - Q_3 IF)
The bottom whisker is the larger of the following two values:
the minimum Impact Factor (IF)
Q_1 IF - 3.5(Q_1 IF - Q_3 IF)
Box Plots are provided for the current JCR year for each of the categories in which the journal is indexed.

Publicaciones II y III

- *Large scale automatic analysis and classification of roof surfaces for the installation of solar panels using a multi-sensor aerial platform*
- *Automatic evaluation of photovoltaic power stations from high-density RGB-T 3D point clouds*

Journal:	**Remote Sensing**
Editorial	**MDPI AG**
ISSN:	**2072-4292**
Impact factor (2016):	**3.244**
Ranking:	**7/29**
Quartile:	**Q1**

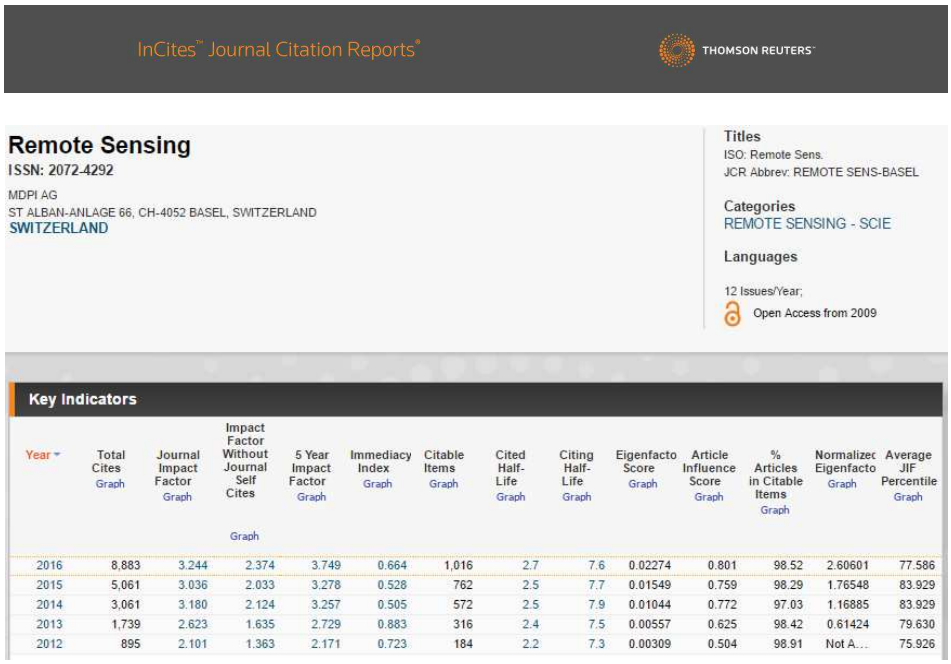

InCites™ Journal Citation Reports®

THOMSON REUTERS™

Remote Sensing
ISSN: 2072-4292

MDPI AG
ST ALBAN-ANLAGE 66, CH-4052 BASEL, SWITZERLAND
SWITZERLAND

Titles
ISO: Remote Sens.
JCR Abbrev: REMOTE SENS-BASEL

Categories
REMOTE SENSING - SCIE

Languages

12 Issues/Year;
Open Access from 2009

Key Indicators

Year	Total Cites	Journal Impact Factor	Impact Factor Without Journal Self Cites	5 Year Impact Factor	Immediacy Index	Citable Items	Cited Half-Life	Citing Half-Life	Eigenfacto Score	Article Influence Score	% Articles in Citable Items	Normalizec Eigenfacto	Average JIF Percentile
	Graph	Graph	Graph	Graph	Graph	Graph	Graph	Graph	Graph	Graph	Graph	Graph	Graph
2016	8,883	3.244	2.374	3.749	0.664	1,016	2.7	7.6	0.02274	0.801	98.52	2.60601	77.586
2015	5,061	3.036	2.033	3.278	0.528	762	2.5	7.7	0.01549	0.759	98.29	1.76548	83.929
2014	3,061	3.180	2.124	3.257	0.505	572	2.5	7.9	0.01044	0.772	97.03	1.16885	83.929
2013	1,739	2.623	1.635	2.729	0.883	316	2.4	7.5	0.00557	0.625	98.42	0.61424	79.630
2012	895	2.101	1.363	2.171	0.723	184	2.2	7.3	0.00309	0.504	98.91	Not A...	75.926

JCR Impact Factor

JCR Year	REMOTE SENSING		
	Rank	Quartile	JIF Percentile
2016	7/29	Q1	77.586
2015	5/28	Q1	83.929
2014	5/28	Q1	83.929
2013	6/27	Q1	79.630
2012	7/27	Q2	75.926

Journal Source Data

	Citable Items			Other (O)	Percentage (C/(C + O))
	Articles	Reviews	Combined (C)		
Number in JCR Year 2016 (A)	1,001	15	1,016	21	97%
Number of References (B)	52,136	2,677	54,813	447	99%
Ratio (B/A)	52.1	178.5	54.0	21.3	

Journal Impact Factor

Cites in 2016 to items published in: 2015 =2112, 2014 =2215, Sum: 4327

Number of items published in: 2015 =762, 2014 =572, Sum: 1334

$$\text{Calculation} = \frac{\text{Cites to recent items}}{\text{Number of recent items}} = \frac{4327}{1334} = \mathbf{3.244}$$

Impact Factor Without Journal Self Cites

The tables show the contribution of the journals self cites to its impact factor. This information is also represented in the cited journal graph.

Total Cites	8883	Self Cites	2129(23.967% of 8883)
Cites to Years Used in Impact Factor Calculation	4327	Self Cites to Years Used in Impact Factor Calculation	1160(26.808% of 4327)
Impact Factor	3.244	Impact Factor without Self Cites	2.374

5-Year Journal Impact Factor

Cites in 2016 to items published in: 2015 =2112, 2014 =2215, 2013 =1520, 2012 =951, 2011 =592, Sum: 7390

Number of items published in: 2015 =762, 2014 =572, 2013 =316, 2012 =184, 2011 =137, Sum: 1971

$$\text{Calculation:} \frac{\text{Cites to recent items}}{\text{Number of recent items}} = \frac{7390}{1971} = \mathbf{3.749}$$

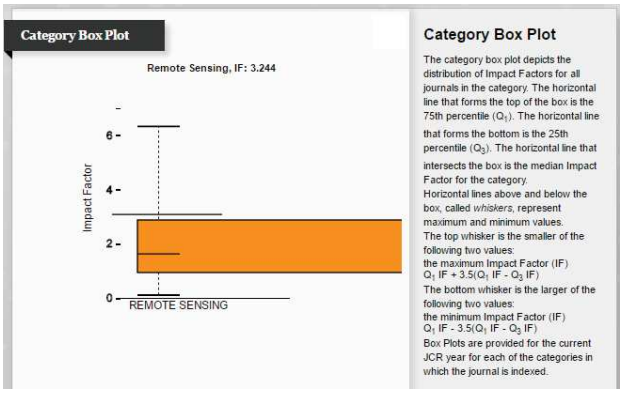
Category Box Plot
Remote Sensing, IF: 3.244
Impact Factor
6
4
2
0
REMOTE SENSING
Category Box Plot
The category box plot depicts the distribution of Impact Factors for all journals in the category. The horizontal line that forms the top of the box is the 75th percentile (Q_1). The horizontal line that forms the bottom is the 25th percentile (Q_3). The horizontal line that intersects the box is the median Impact Factor for the category.
Horizontal lines above and below the box, called *whiskers*, represent maximum and minimum values.
The top whisker is the smaller of the following two values:
the maximum Impact Factor (IF)
Q_1 IF + 3.5(Q_1 IF - Q_3 IF)
The bottom whisker is the larger of the following two values:
the minimum Impact Factor (IF)
Q_1 IF - 3.5(Q_1 IF - Q_3 IF)
Box Plots are provided for the current JCR year for each of the categories in which the journal is indexed.

Apéndice B

Desarrollo de software

FME®

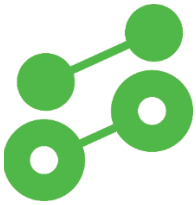

FME® – Feature Matching Evaluation

Tipo: Registro de propiedad intelectual

Referencia: SA-163-16

Universidad: Universidad de Salamanca

Códigos UNESCO:

- 2209.17 Fotografía
- 2209.90 Tratamiento digital de imágenes
- 2214.02 Metrología

Resumen:

FME® (Figura Ap.B.1) es una herramienta enfocada a la evaluación de algoritmos de visión computacional para la extracción, descripción y emparejamiento de puntos de interés en imágenes. La herramienta recoge una amplia selección de algoritmos en cada uno de los apartados, completamente compatibles entre sí, proporcionando un amplio abanico de flujos de trabajo diferentes completamente configurables por el usuario. El dato de entrada será un par estereoscópico de imágenes, pudiendo proceder estas tanto de sensores con diferentes resoluciones como de distintos rangos espectrales. La herramienta permite también incorporar al flujo de trabajo la homografía real entre ambas imágenes a modo de "Verdad-terreno", permitiendo la verificación de los resultados.

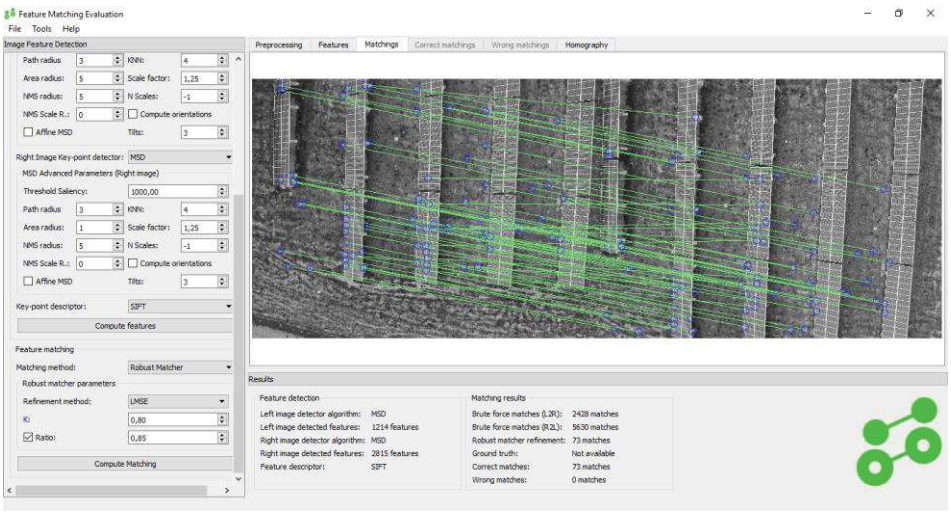

Figura Ap.B.1: Captura de pantalla de la interfaz gráfica mostrando el producto final más destacable.

Por otro lado, y no menos importante, la herramienta supone un gran instrumento tanto a nivel docente e investigador como para empresas relacionadas con el sector de la visión computacional y la robótica, proporcionando una herramienta eficiente, eficaz e intuitiva para la generación de flujos de trabajo y la evaluación y comparación de los resultados según las necesidades del usuario.

Autores:

- Luis López Fernández
- Manuel Gesto Díaz
- Diego Guerrero Sevilla
- Pablo Rodríguez Gonzálvez

Datos de entrada/requisitos:

- Imágenes digitales

Resultados:

- Puntos homólogos
- Homografía

GRAPHOS®

GRAPHOS® – inteGRAted PHOtogrammetric Suite

Tipo: Registro de propiedad intelectual

Referencia: SA-162-16

Universidad: Universidad de Salamanca

Códigos UNESCO:

- 2209.17 Fotografía
- 2209.90 Tratamiento digital de imágenes
- 2214.02 Metrología

Resumen:

GRAPHOS® (Figura Ap.B.2) es una plataforma de procesamiento fotogramétrico que permite integrar, bajo una interfaz intuitiva, diferentes algoritmias propias de la fotogrametría y la visión computacional a fin de permitir la reconstrucción 3D de objetos con un alto grado de automatización. La precisión, facilidad de uso y robustez de los productos obtenidos son otros de los aspectos más destacables de GRAPHOS®.

Figura Ap.B.2: Captura de pantalla de la interfaz gráfica mostrando el producto final más destacable.

Tomando como dato de entrada un conjunto de imágenes del objeto de estudio, GRAPHOS® es capaz de realizar el proceso completo de reconstrucción 3D con una interacción mínima por parte del usuario. La herramienta incluye una interfaz intuitiva capaz de guiar en todo el proceso a cualquier usuario no especializado, complementado por una configuración avanzada donde usuarios especializados podrán encontrar diferentes algoritmos de preprocesado de imágenes digitales; un amplio abanico de flujos de trabajo en cuanto a la detección, descripción y emparejamiento de puntos homólogos; diferentes modelos de autocalibración del sensor, estrategias de aerotriangulación, georreferenciación y ajuste del bloque fotogramétrico; y varias estrategias de densificación como punto final al proceso.

La herramienta resulta de gran interés para empresas que trabajen con modelos 3D de cualquier elemento, ya sea para aplicaciones ligadas a la geomática o arquitectura utilizando modelos de terreno, entornos urbanos o edificaciones, o para aplicaciones ligadas al ámbito de la ingeniería donde los modelos 3D generados suponen una aproximación inicial de precisión para procesos de ingeniería inversa. También es de gran interés para la comunidad científica permitiendo abordar la potencialidad y aplicabilidad de estos modelos 3D en innumerables campos.

Autores:

- Luis López Fernández
- Pablo Rodríguez Gonzálvez
- Diego Guerrero Sevilla
- David Hernández López
- Diego González Aguilera

Datos de entrada/requisitos:

- Imágenes digitales

Resultados:

- Parámetros intrínsecos del sensor
- Parámetros de distorsión del sensor
- Imágenes corregidas de distorsión
- Orientación absoluta de las imágenes
- Nubes de puntos 3D de alta resolución

SOLEMAP®

SOLEMAP® – SOLar Energy MAPping

Tipo: Registro de propiedad intelectual

Referencia: SA-159-16

Universidad: Universidad de Salamanca

Códigos UNESCO:

- 3305.06 Ingeniería Civil
- 3305.14 Viviendas
- 3322.03 Generación de energía
- 1206.01 Energía Solar
- 2209.09 Radiación infrarroja

Resumen:

SOLEMAP® (Figura Ap.B.3) es una herramienta para el análisis fotovoltaico de grandes áreas urbanas donde el análisis de cada cubierta de forma individual, ya sea mediante la visita in-situ de un técnico especializado o mediante el análisis de la documentación técnica de cada construcción, sería lento, impreciso e inviable económicamente. Esta herramienta permite la localización de las zonas óptimas para la instalación de paneles solares sobre cubiertas tomando como entrada modelos 3D de alta resolución con información termográfica capturados con cualquier tipo de plataforma aérea. Esta evaluación arrojará información tanto sobre la técnica óptima de instalación de los paneles como de su productividad, permitiendo la detección de obstáculos que impidan la instalación de paneles solares o puedan producir sombras que limiten su productividad, así como identificando zonas con humedades, etc.

Figura Ap.B.3: Captura de pantalla de la interfaz gráfica mostrando el producto final más destacable.

SOLEMAP® está alineado con uno de los retos más importantes de nuestra sociedad: reducir la elevada dependencia energética y garantizar la sostenibilidad del ecosistema reduciendo la contaminación y las emisiones de CO_2. Tareas claramente destacadas dentro de los desafíos que la Unión Europea se plantea para su futuro más inmediato e incluidos en el tratado 20-20-20 donde, entre otras cuestiones, se plantea que al menos el 20% del consumo energético en el año 2020 provenga de energías renovables.

Por otro lado, y no menos importante, las soluciones propuestas son un inestimable instrumento tanto para la administración pública en cuanto a labores de planificación y desarrollo de planes de actuación, como para las empresas relacionadas con el sector, proporcionando una herramienta eficiente y eficaz que para la auditoría energética de grandes áreas urbanas.

Autores:

- Luis López Fernández

- Susana Lagüela López
- Diego González Aguilera
- Pablo Rodríguez Gonzálvez
- David Hernández López
- Diego Guerrero Sevilla

Datos de entrada/requisitos:

- Nube de puntos 3D con radiometría termográfica

Resultados:

- Superficies de los tejados clasificadas según su productividad fotovoltaica

SOLFIN®

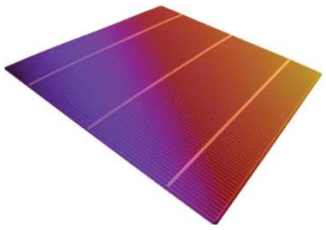

SOLFIN® – SOLar Farm INspection

Tipo: Registro de propiedad intelectual

Referencia: SA-157-16

Universidad: Universidad de Salamanca

Códigos UNESCO:

- 3305.06 Ingeniería Civil
- 3322.03 Generación de energía
- 1206.01 Energía Solar
- 2209.09 Radiación infrarroja

Resumen:

SOLFIN® (Figura Ap.B.4) es una herramienta para la inspección automática de instalaciones fotovoltaicas. Esta herramienta permite la identificación, cuantificación y geolocalización precisa de patologías en paneles solares fotovoltaicos tomando como entrada modelos 3D de alta resolución con información termográfica capturados con cualquier tipo de plataforma aérea. Esta evaluación arrojará información tanto cualitativa (existencia de daños) como cuantitativa (superficie dañada) de cada panel, permitiendo la detección de patologías que limiten su productividad y la planificación de forma eficaz de las labores de mantenimiento y reparación.

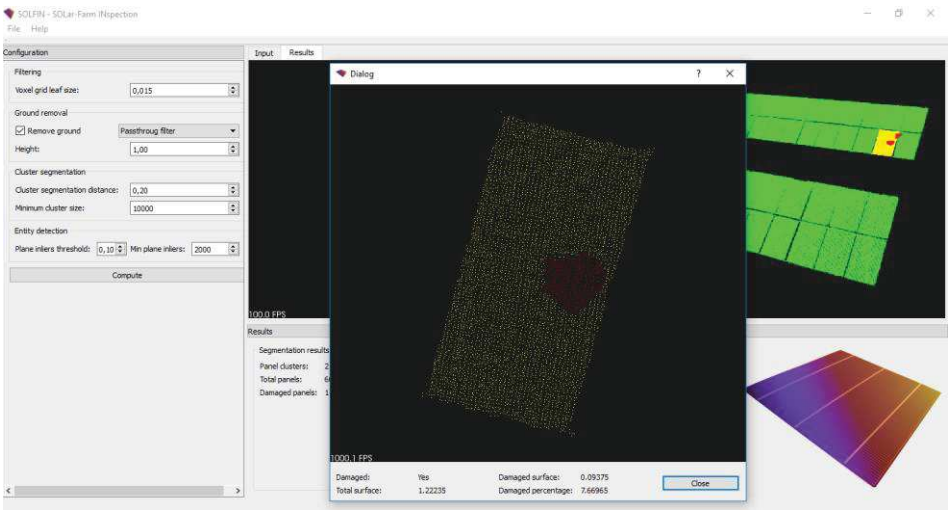

Figura Ap.B.4: Captura de pantalla de la interfaz gráfica mostrando el producto final más destacable.

SOLFIN® posibilita un mantenimiento activo de las plantas fotovoltaicas, permitiendo la ejecución de inspecciones con una mayor periodicidad. De esta forma, podrá optimizarse el aprovechamiento del recurso solar, detectando de forma precoz cualquier patología que pueda condicionar la productividad de la instalación.

Las soluciones propuestas resultan de gran interés para empresas que trabajen en la instalación y mantenimiento de elementos fotovoltaicos, ya sea para la verificación certificación del estado inicial de una instalación fotovoltaica o para la evaluación, planificación y gestión de labores de mantenimiento.

Autores:

- Luis López Fernández
- Susana Lagüela López
- Jesús Fernández Hernández
- Diego González Aguilera
- Pablo Rodríguez Gonzálvez

Datos de entrada/requisitos:

- Nube de puntos 3D con radiometría termográfica

Resultados:

- Superficie de los paneles fotovoltaicos clasificada según la existencia de patologías.
- Datos geométricos de las patologías detectadas.